Templex: A bridge between homologies and templates for chaotic attractors

Gisela Charó, Christophe Letellier, Denisse Sciamarella

Chaos

Templex: a bridge between homologies and templates for chaotic attractors

Gisela D. Charó,[1, 2, a)] Christophe Letellier,[3, b)] and Denisse Sciamarella[4, 2, c)]
[1)] *CONICET – Universidad de Buenos Aires. Centro de Investigaciones del Mar y la Atmósfera (CIMA), C1428EGA CABA, Argentina*
[2)] *CNRS – IRD – CONICET – UBA. Institut Franco-Argentin d'Études sur le Climat et ses Impacts (IRL 3351 IFAECI), C1428EGA CABA, Argentina.*
[3)] *Rouen Normandie University — CORIA, Campus Universitaire du Madrillet, F-76800 Saint-Etienne du Rouvray, France*
[4)] *CNRS – Centre National de la Recherche Scientifique, 75016 Paris, France.*

(Dated: July 5, 2022 to submit to *Chaos*)

The theory of homologies introduces cell complexes to provide an algebraic description of spaces up to topological equivalence. Attractors in state space can be studied using Branched Manifold Analysis through Homologies: this strategy constructs a cell complex from a cloud of points in state space and uses homology groups to characterize its topology. The approach, however, does not consider the action of the flow on the cell complex. The procedure is here extended to take this fundamental property into account, as done with templates. The goal is achieved endowing the cell complex with a directed graph that prescribes the flow direction between its highest dimensional cells. The tandem of cell complex and directed graph, baptized templex, is shown to allow for a sophisticated characterization of chaotic attractors and for an accurate classification of them. The cases of a few well-known chaotic attractors are investigated — namely the spiral and funnel Rössler attractors, the Lorenz attractor, the Burke and Shaw attractor and a four-dimensional system. A link is established with their description in terms of templates.

Cell complexes can be traced back to Poincaré's papers of 1900, and the study of chaotic attractors using cell complexes to the nineties. Since then, algebraic topology is seen as the mathematical formalism holding promise for a description of chaos beyond three dimensions – there where templates, developed in the eighties to extract the knot content of attractors, cannot go. The advent of computational methods with a firm ground in topology has given a new thrust to this initiative, which is often applied blindly, without a sound comprehension of the information contained in a cell complex. In this work, cell complexes are shown to be enhanced as descriptors of the topology of chaotic attractors, when endowed with a directed graph that carries the information of the flow direction in terms of allowed or forbidden cell connections in a complex. This two companion objects are combined in one which is termed "templex", a word resulting from the contraction between template and complex. Indeed, the description offered by a complex is as complete and precise as the one obtained with a template, without the burden of dimensionality restrictions.

I. INTRODUCTION

The fact that some dynamical systems may present complex solutions whose description resists analysis was recognized long ago with the three-body problem.[1] Once Henri Poincaré understood the inherent complexity combined with a sensitivity to initial conditions of its solutions,[2] he developed the *Analysis Situs*,[3] while knot theory was maturating.[4–8] In his investigation of the solutions to the three-body problem, Poincaré was already thinking in terms of manifolds, leading to the concept of homoclinic orbit and the inextricable entanglement which was finally sketched by Melnikov.[9] Using a representation based on isopleths, Lorenz provided the first interpretation of a solution to a dynamical system in terms of what is now called a branched manifold.[10] Slightly later, the concept of branched manifold was formally introduced by Williams[11] who later made a link with knot theory.[12] Templates were then used to describe the solution to dynamical systems.[13–15] Templates are viewed as a knot-holder.[12,16] Indeed, due to the richness of their structure, chaotic attractors (or "strange" in the sense of Ruelle and Takens,[17] that is, not regular or not described by a simple manifold) require a sophisticated approach to capture their specificities and to classify them accurately.[18–20]

Homological algebra started in the 19th century, with the work of Riemann (1857) and Betti (1871).[3,21–28] In 1895, Poincaré introduced the notion of homology numbers and in 1925, Emmy Noether shifted the attention to the "homology groups" of a space.[29] The basic building blocks in theory of homologies are called cells and are assembled into complexes. A cell complex is hence a sort of layered structure, built up of cells of various dimensions.[30] Such a complex can be constructed from a cloud of points in an arbitrary number of dimensions:

[a)] Electronic mail: gisela.charo@cima.fcen.uba.ar
[b)] http://www.atomosyd.net/spip.php?article1; Electronic mail: christophe.letellier@coria.fr
[c)] Electronic mail: denisse.sciamarella@cima.fcen.uba.ar

the cloud is replaced with a set of glued patches, from which a cell complex can be built.[31] The computation of Betti numbers using this approach was applied to regular attractors, that is, to quasi-periodic regimes.[32] A few years later, the approach was extended to handle clouds of points obtained from time-delay embeddings of experimental time series[33] as well as clouds of points obtained by integrating nonlinear dynamical systems related to simple branched manifolds.[34] In these two works, the cell complex can be non-simplicial (facilitating its construction) and the description is enriched, going beyond Betti numbers. The extended algorithm identifies the k-generators of the homology groups and introduces orientability chains.[33,34] More recent applications of this approach, now called BraMAH (Branched Manifold Analysis through Homologies), incorporate the extraction of *weak boundaries*,[35,36] enabling a more precise description of four-dimensional manifolds. Note also that Conley index was used for constructing a symbolic dynamics for thick first-return map.[37]

Templates can only be constructed for two-dimensional branched manifolds, while homology groups are defined without dimensional restrictions. The description in terms of templates limits the topological analysis of chaotic attractors to those whose embedding dimension is 3. Since there are many higher-dimensional attractors, it is of primary interest to extend the topological analysis to higher-dimensional attractors. An attempt to extend templates beyond three dimensions by using simplicial complexes was proposed but left without achievements.[38,39] There is no doubt that the most promising approach is based on homology groups, and before attacking high-dimensional attractors, it is necessary to develop an approach based on complexes and homology groups which provides a description of chaotic attractors at the accuracy offered by templates. This is what will be developed in this paper with two key steps: orienting the cells of the complex taking into account the flow direction and associating a directed graph or digraph to it. To the best of our knowledge, no previous approach has ever considered a cell complex endowed with a directed graph, carrying the information of the flow direction in terms of allowed cell connections. To accurately consider the rich structure of chaotic attractors in terms of cell complexes, it therefore appeared as a requirement to introduce a mathematical object that will hereafter be termed "templex". We will thus extend the numerical procedure initially based on a sole complex, to a procedure based on a complex endowed with a digraph, allowing to derive subtemplexes (parts of the original templex) which will play the role of strips in templates.

The aim of this paper is to show how a templex bridges the gap between the descriptions of chaotic attractors by homologies and templates. A brief introduction to templates and homology groups is provided in Section II with an introduction to the specific concepts required in our sophisticated strategy. In Section III, four attractors produced by strongly dissipative systems, namely the Rössler, the Lorenz, the Burke and Shaw and a four-dimensional system, are extensively treated. Section V gives a conclusion.

II. TOPOLOGICAL BACKGROUND

A. Templates as knot-holders for chaotic attractors

A chaotic attractor is an invariant set under the action of the flow ϕ_t which can be bounded by a semi-permeable surface.[40] Consequently, chaotic attractors can be bounded by genus-g tori whose holes are most often associated with singular points circled by the flow.[41,42] As we shall see, these holes are not holes in the sense of homologies, that is, they are not necessarily equivalent to generators of the homology groups. They are of two types: (i) those of the focus type which are circled by the flow as a periodic orbit circles a focus point and (ii) those which are associated with a tearing of the flow, splitting the attractor in strips with boundaries. It can be shown that there is always a hole of the saddle type between two holes of the focus type.[42] A few simple bounding tori are drawn in Fig.1. The periphery of the attractor is easily defined from the bounding torus and it can be naturally oriented according to the flow. Once the bounding torus is identified, the next step is to construct a Poincaré section and to compute a first-return map to it. The non trivial result from these bounding tori is that, when $g > 2$, a Poincaré section is made of $g-1$ components[42] which must be oriented from the center to the periphery to remove some degeneracy among the first-return maps.[43] A bounding torus is thus a manifold which can be naturally oriented according to the flow.

For strongly dissipative systems, the first-return map is one-dimensional and the number of monotone branches provides the number N_s of strips required to construct the corresponding template.[44] The critical points of the map — defining the partition of the map into N_s branches — discriminate the different paths followed by the flow ϕ_t determining the (fictive) boundaries between the different strips. Typically, a strip is defined between a splitting chart [Fig. 2(a)] and a joining chart [Fig. 2(b)] where the strips are fictively split to allow an easily readable representation of them and where the strips are joined (squeezed) into a single strip, respectively. According to the standard insertion convention introduced by Tufillaro,[16] the strips are merged from the back to the front and from the left to the right [Fig. 11(b)]. Typically, all the non-trivial dynamical processes are captured between the splitting chart where the template is split into strips and the joining chart where the strips are merged into a single one. The joining chart is ended by a joining line which corresponds to a Poincaré section [thick line in Fig. 2(b)].

Between these two charts, the strips can present local

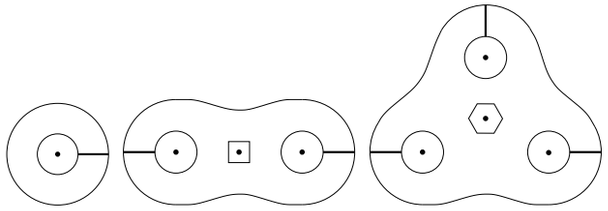

(a) $g = 1$ (b) $g = 3$ (c) $g = 4$

Figure 1: Bounding tori of various genus g ($g \leqslant 4$). The $g - 1$ components of the Poincaré section are plotted as thick lines. Case (a) applies for the Rössler attractor and (b) for the Lorenz attractor. Cases (c) may correspond to the 3-fold covers of the proto-Lorenz system.[45,46]

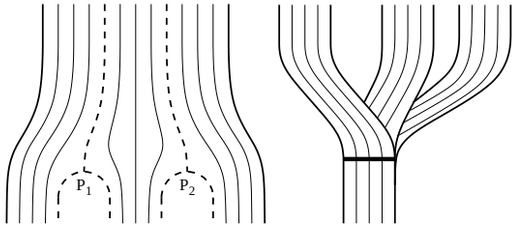

(a) Splitting chart (b) Joining chart

Figure 2: An ingoing strip is split into three outgoing strips according to the two critical points P_1 and P_2 (a) which are then joined into a single outgoing strip (b). In (a), true boundaries are in solid thick lines and fictive boundaries are in dashed thick lines. The very thick line (b) represents the joining line (branch line).

torsion and can be permuted. The template is closed by connecting the joining chart with the splitting chart with a trivial strip as drawn in the example of Fig. 3. At the joining chart, there is a joining line[14] (corresponding to the joining locus in the next section) at which, by definition, the flow cannot be reversed without violating uniqueness. The dynamics is described by the template in terms of charts and strips. According to a theorem due to Birman and Williams, the link of periodic orbits $\mathcal{L}_\phi$ of the flow ϕ_t is in bijective correspondence (under an ambient isotopy) with the link of periodic orbits $\mathcal{L}_\mathrm{T}$ of the corresponding template T.[47]

Each strip can be labelled with an integer using the natural order from the center to the periphery and whose parity is defined by the parity of the local torsion: in the case of Fig. 3, we have thus $0 < 1 < 2$ (note that one could have used also $2 < 5 < 8$). When the Poincaré section has $N_\mathrm{c} = g - 1$ components (joining lines) as for an attractor bounded by a torus with a genus $g > 2$, it is still possible to define a *total order* $\lhd$ for ordering the different strips spread in them.[14] This total order is used to compute the first-return map as it will be explained in the case of the Lorenz attractor (see Section III A).

A template can be described using an $N_\mathrm{s} \times N_\mathrm{s}$ linking matrix L_{ij} such that L_{ii} is the local torsion of the ith

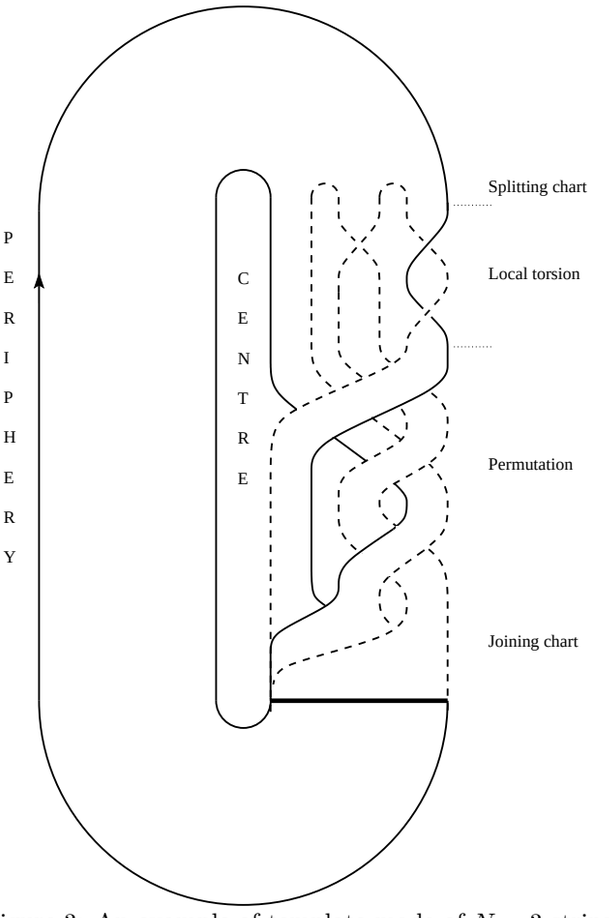

Figure 3: An example of template made of $N_\mathrm{s} = 3$ strips and $N_\mathrm{loc} = 1$ joining line. This template corresponds to an attractor bounded by a genus-1 torus. True boundaries are in solid line and fictive boundaries are in dashed line. The thick line represents the joining line. The arrow indicates the direction of the flow ϕ_t.

strip and L_{ij} is the permutation between the ith and the jth strips ($i \neq j$).[16,44] The linking matrix is thus symmetric. When there is a single component to the Poincaré section ($N_\mathrm{c} = 1$), an $N_\mathrm{c} \times N_\mathrm{s}$ joining matrix states the order with which the strips are joined, from the bottom to the top.[15] In the case of the template T drawn in Fig. 3, the linking matrix is

$$L_{ij} = \begin{bmatrix} 0 & -1 & -1 \\ -1 & -1 & -2 \\ -1 & -2 & -2 \end{bmatrix} \tag{1}$$

and the joining matrix is

$$J_{ij} = \begin{bmatrix} 1 & 1 & 1 \end{bmatrix}, \tag{2}$$

which is, in this example, trivial and is commonly omitted. Since the links of periodic orbits $\mathcal{L}_\phi$ and $\mathcal{L}_\mathrm{T}$ are equivalent under an ambient isotopy, the linking numbers are equal for both. Linking numbers are defined

as[48]

$$L_{\mathrm{k}} = (\mathcal{O}_1, \mathcal{O}_2) = \frac{1}{2} \sum_{\mathcal{O}_1 \cap \mathcal{O}_2} \epsilon_i \tag{3}$$

where $\epsilon_i = \pm 1$ is the sign of the ith crossing and $\mathcal{O}_1 \cap \mathcal{O}_2$ denotes the crossings between an orbit $\mathcal{O}_1$ and an orbit $\mathcal{O}_2$ in some regular representation. By definition, $L_{\mathrm{k}}(\mathcal{O}_1, \mathcal{O}_2) \in \mathbb{Z}$.

B. Homology groups

Topological data analysis through homologies starts with the construction of a complex from a finite set of points in some multidimensional space. In nonlinear dynamics, this set of points can proceed, for instance, from the integration of a system of ordinary differential equations, or from an embedding of a dataset. There are different rules for constructing a complex. For instance, a Čech complex is a complex built on a set of points such that, for balls of a certain radius defined around all the points in the set, there is a cell for every finite subset of balls with nonempty intersection.[49] In the case of BraMAH, the rules to construct the cell complex consider the set of points in a multidimensional state space which lies locally on a branched κ-manifold ($\kappa \in \mathbb{N}$), and uses subsets of points that can be locally approximated by κ-disks to construct κ-cells [whose boundaries have as many $(\kappa-1)$-cells as necessary], and glues them together in a complex of dimension κ. A BraMAH complex is a cell complex built in this manner. By construction, the dimension of a BraMAH complex coincides with the local dimension of the manifold on which an attractor lies. Further details on the construction of a BraMAH complex from a cloud of points are given in Appendix A. For strongly dissipative dynamical systems as considered in this work, the data points are recorded from the invariant set and they lie on a branched 2-manifold (an algorithmic procedure to construct a BraMAH complex of dimension 2 from a cloud of points in three or four dimensions is proposed in Refs. 33–36, and 50). The present paper focuses, not on this construction, but on the extraction of the topological properties from a BraMAH complex.

Before defining homology groups, let us first introduce the class of spaces for which they are defined, which is the class of all polyhedra.[31] A polyhedron is a space that can be built from "building blocks" as line segments, polygons, polyhedra, and their higher dimensional analogues, by "gluing them together" along their faces. A k-cell is defined as a set whose interior is homeomorphic to a k-dimensional disc with the additional property that its boundary must be divided into a finite number of $(k-1)$-cells, called the faces of the k-cell. So, a 0-dimensional cell is a point, a 1-cell is a line segment, a 2-cell is a polygon, a 3-cell is a solid polyhedron with polygons, edges, and vertices as faces. Thus, the endpoints of a 1-cell are 0-cells, the boundary of a 2-cell consists of 1-cells, etc. A finite number of cells glued together is said to form a cell complex K as long as the following two conditions hold: if σ and τ are k-cells in K, then all $(k-1)$-cells of σ and τ are elements of K, and $\mathrm{Int}(\sigma) \cap \mathrm{Int}(\tau) = \varnothing$, where Int(A) denotes the interior of A. The dimension κ of a cell complex is defined by the dimension of its highest-dimensional cells.

A complex K is much more than a set of points or a tessellation: it is a layered construction equipped with a structure of cells of various dimensions. To track all the cells from a complex and how they are glued together, we must also consider the directions of any edges glued together. A complex K of dimension $\kappa = 2$ is said to be oriented if each 1-cell is given a direction (from initial point to terminal point) and each 2-cell is given a direction (clockwise or counterclockwise). Note that the choices of directions for 1-cells and 2-cells are *a priori* arbitrary. For oriented complexes K of dimension κ, a k-chain C_k is defined as

$$C_k = \sum_i a_i \, \sigma_k^i \tag{4}$$

where $a_i \in \mathbb{Z}$ and σ_k^i is a k-cell ($\forall i \in \mathbb{N}$). The group of all k-chains $\mathcal{C}_k$ ($k = 1, \cdots, \kappa$) in K is an abelian group. Two k-cells are adjacent if they share a $(k-1)$-cell. Thus, a boundary operator

$$\partial_k : \mathcal{C}_k \to \mathcal{C}_{k-1}$$

is introduced in such a way that, for instance, the boundary of an oriented 2-cell is the chain formed by the 1-cells on its border, with a positive sign if the orientation of an edge is consistent with the direction of the 2-cell, and with a negative sign otherwise. By construction, the boundary operator satisfies

$$\partial_k \circ \partial_{k+1} \to 0_{k+1,k-1} \, ,$$

where 0 denotes the trivial group, that is, the constant map sending every element of $\mathcal{C}_{k+1}$ to the group identity in $\mathcal{C}_{k-1}$. One can show that ∂_k is a homomorphism for any complex K. Stating that "the boundary of a boundary is trivial" is equivalent to stating that $\mathrm{im}(\partial_{k+1}) \subseteq \ker(\partial_k)$, where $\mathrm{im}(\partial_{k+1})$ designates the image of the boundary operator and $\ker(\partial_k)$ its kernel. The elements of the group $\mathcal{B}_k(K) = \mathrm{im}(\partial_{k+1})$ are called k-boundaries, and the elements of $\mathcal{Z}_k(K) = \ker(\partial_k)$ are called k-cycles. Note that a k-cycle C_k in $\mathcal{C}_k$ is such that $\partial_k(C_k) = 0$, that is, a k-cycle has no boundary. Among the k-cycles, one can distinguish those that are the boundaries of some $(k+1)$-cells (they are thus k-boundaries), and they constitute the group $\mathcal{B}_k$.

The groups $\mathcal{C}_k$, $\mathcal{Z}_k$, and $\mathcal{B}_k$ depend on the particular complex that is built. To excerpt the main properties of the topology of the underlying cloud of points, an equivalence relation is introduced on chains.

Theorem 1 *Let $C_k^{\alpha_1}$ and $C_k^{\alpha_2}$ be two k-chains $\in \mathcal{C}_k$. They are said to be* `homologous` *— noted $C_k^{\alpha_1} \sim C_k^{\alpha_2}$ — if and only if there exists a boundary of a $(k+1)$-chain C_{k+1} such that $\partial_{k+1}(C_{k+1}) = C_k^{\alpha_1} - C_k^{\alpha_2}$.*

Since the chain group $\mathcal{C}_k$ is abelian, all its subgroups are normal. It is thus possible to introduce the quotient group

$$\mathcal{H}_k := \ker(\partial_k)/\mathrm{im}(\partial_{k+1}) = \mathcal{Z}_k/\mathcal{B}_k\,,$$

called the kth homology group of K made of homology classes over cycles. We denote a homology group in terms of its generators, that is, as $\mathcal{H}_k = [g_1, ..., g_q]$, with $q \in \mathbb{N}$. The cardinal q of $\mathcal{H}_k$ corresponds to the kth Betti number β_k. Notice that the k-generators g_i of a homology group $\mathcal{H}_k$ are homologically independent, that is, they cannot be deformed into each other by a continuous transformation (an isotopy). The homology groups thus cancel out unnecessary information for characterizing the underlying object. In each dimension, $\mathcal{H}_k(K)$ gives a piece of information related to the properties determined by that dimension. Thus, (i) the group $\mathcal{H}_0(K)$ measures the connectivity of the complex, and the rank of β_0 refers to the number of connected components, (ii) the group $\mathcal{H}_1(K)$ identifies non-trivial loops around the complex through the 1-generators, (iii) the group $\mathcal{H}_2(K)$ identifies the 2-generators of $\mathcal{H}_2$ which identify the enclosed cavities of the complex K.

The number of k-generators (the Betti numbers β_k) do not depend on the particular complex that is built, and allow to easily distinguish some topologically non equivalent manifolds. Even if the generators are necessarily written in terms of the labelled cells of the particular complex, identifying and locating them in the complex is highly relevant, since their relative intertwining offers information about how the underlying object is structured.

It is however important to remark that there is much more information contained in a cell complex than that encoded by the Betti numbers and the explicit generators of the homology groups. Additional properties can be extracted if all the cells in the complex are oriented in the same way, or, in other words, if the complex is uniformly oriented.[33,34] Two cells are said to have the same orientation if they are oriented so that the common edges are canceled when summing the borders of the two cells. Assigning a uniform orientation to a complex is simple if the underlying manifold is Haussdorff. A space is Hausdorff if, for any two distinct points in space, there exist two open sets (one for each point) which do not intersect. Let us assume that this is the case. One can hence start by assigning the same orientation to all the 2-cells of a 2-complex K ($\kappa = 2$). This is done by choosing an orientation for one 2-cell (e.g. clockwise) and propagating it across the rest of the 2-cells, till they are all oriented in the same manner. This yields a uniformly oriented complex K^u.

Now, let $\Gamma = \sum_i \sigma_2^i$ where σ_2^i are all the 2-cells in K^u. Let us write

$$\partial(\Gamma) = \underbrace{\sum_j a_j \sigma_1^j}_{\text{boundaries}} + \underbrace{\sum_j b_j \sigma_1^j}_{\text{torsions}}\,,$$

where $a_j = \pm 1$, $b_j \neq \pm 1$, and σ_1^j are 1-cells in K^u. The first term refers to the boundary of the manifold underlying the uniformly oriented complex, and the second term to some torsion elements. If the first term is null, the manifold approximated by the complex is said to have no boundary, as for a sphere, a torus or a Klein bottle. On the other hand, the underlying manifold is said to be non-orientable if the second term is non zero, that is, if $\partial\Gamma(K^u)$ contains torsion elements.

Table I lists some of the topological properties (Betti numbers β_i, existence of boundaries b or torsions elements t) for some common surfaces. The important message here is that a finer description can be obtained when one is working with a uniformly oriented complex.[36]

Table I: Betti numbers β_k, existence of torsion elements t or boundaries b for some 2-dimensional manifolds.

	β_0	β_1	β_2	t	b
Disk	1	0	0	No	Yes
Cylinder	1	1	0	No	Yes
Möbius band	1	1	0	Yes	Yes
Torus	1	2	1	No	No
Genus-g torus	1	$2g$	1	No	No
Klein bottle	1	1	0	Yes	No

Branched manifolds are mathematical objects which are not Hausdorff. In order to endow the corresponding complex with a uniform orientation that is compatible with the flow, one must decompose the complex in sub-units, as a template must be decomposed into strips. This decomposition leads us to the concept of *templex* as introduced in the next section.

C. Templex

State space is a ubiquitous concept that is especially relevant in chaos and nonlinear dynamics.[51] A cloud of points in an attractor is plotted in space, but each point in this particular space represents a state at a given time. When one attempts to describe such sets of points with a cell complex, an important piece of information is missing. This information concerns the flow. Templates are in fact constructed taking the flow information into account. In order to bridge the gap between cell complexes and templates, we need a mathematical object going beyond a cell complex. According to the flow, from a given κ-cell of the complex, it is only possible to go towards a few other κ-cells. These connections can be expressed in terms of a directed graph or digraph, whose nodes denote the highest dimensional cells of a complex, and whose directed edges denote allowed transitions between them. This combination of a cell complex and a digraph will be useful to encode all the information contained in a template, and will be therefore baptized with the term

"templex".

Step 0: BRAMAH *complex* In order to construct a templex, let us start from a BRAMAH complex obtained from a set of points associated with an attractor in a state space. The orientation of the cells at this stage is not necessarily uniform: any orientation is valid. Let us assume that our attractor lies in a branched 2-manifold, so that the dimension of the BRAMAH complex is $\kappa = 2$. We will use the Lorenz attractor as an example.

Step 1: Locating the joining locus The particularity of a branched 2-manifold as underlying a chaotic attractor is to present a joining chart at which more than two 2-cells share a 1-cell. The first step is to locate the 1-cells shared by at least three 2-cells (joining 1-cells). The 1-chain of these 1-cells is called the *joining locus*.

Step 2: Re-orienting the complex A 2-cell with one 1-cell at the periphery of the complex is arbitrarily chosen: this 1-cell is oriented according to the flow. For the complex in Fig. 4(a), say, for instance, that the 2-cell γ_2 is chosen: the peripheral 1-cell is thus oriented along the flow and, consequently, the 2-cell is clockwise.

The other 2-cells are oriented by a simple propagation of this orientation up to the joining locus. Indeed, one of the specificities of a templex is that the 2-cell orientation should not be propagated across a joining locus (it may happen that two ingoing cells are oriented in two opposite ways). If there are still 2-cells which have not yet been re-oriented (because they are located across a joining locus with respect to the initially chosen 2-cell), the procedure is repeated from another arbitrarily chosen 2-cell not yet re-oriented, and so on, up to the stage where all 2-cells are re-oriented. A complex that is oriented according to this rule will be said to be a **flow-oriented complex**.

In our example, the flow-oriented complex $K_1(\mathrm{L})$ drawn in Fig. 4(a) for the Lorenz attractor is obtained from two starting 2-cells (for instance, γ_2 and γ_{12}).

Step 3: Constructing a digraph A digraph related to the way 2-cells are visited by the flow is constructed as follows. Two nodes i and j are connected as $i \to j$ when the flow provides a path from γ_i to γ_j. This naturally leads to the introduction of the notion of *templex*.

Definition 1 *A* **templex** $T \equiv (K, G)$ *is made of a complex* K *of dimension* $dim(K) = \kappa$ *and a digraph* $G = (N, E)$ *whose underlying space is a branched* κ*-manifold associated with a dynamical system, such that (i) the nodes* N *are the* κ*-cells of* K *and (ii) the edges* E *are the connections between the* κ*-cells allowed by the flow.*

An example of templex $T_1(\mathrm{L}) = (K_1(\mathrm{L}), G_1(\mathrm{L}))$ for the Lorenz attractor is drawn in Figs. 4(a) and 4(b).

Step 4: Splitting the joining locus Let us designate as the *outgoing* 2-cells, the 2-cells which are visited by the flow just after crossing one of the joining 1-cells belonging to the joining locus. Each joining 1-cell must be oriented according to the outgoing 2-cell from which it is an edge. If there is a change in direction within a connected set of joining 1-cells — as the 0-cell $\langle 2 \rangle$ in Fig. 4(a) — then there is a *splitting* 0-cell which divides this connected set into two different connected sets of joining 1-cells. The existence of such a splitting 0-cell is induced by our convention for orienting the 2-cells according to the flow. This is strongly related to the convention for orienting the components of the Poincaré section from the centre to the periphery to avoid different descriptions of the same dynamics.[43] Once this is completed, each connected set of 1-cells sharing the same direction corresponds to one component of the Poincaré section. Each component is denoted by J_i where $i \in \mathbb{N}$.

In the flow-oriented complex K_1 of Fig. 4(a), the joining locus is split in two chains $J_1 = \langle 0,1 \rangle + \langle 1,2 \rangle$ and $J_2 = -\langle 2,3 \rangle - \langle 3,4 \rangle$. Here, $\langle 0,1 \rangle$ denotes the 1-cell starting in the 0-cell $\langle 0 \rangle$ and finishing in the 0-cell $\langle 1 \rangle$. Further details concerning notation are given in appendix B. The joining locus of the complex K_1 has thus two different components, J_1 and J_2. The 0-cell $\langle 2 \rangle$ is a *splitting* 0-cell.

Step 5: Removing superfluous joining 0-cells For each chain J_i of the joining locus, let us remove the 0-cells that are not its boundaries. This induces a simplified flow-oriented complex, with a minimal structure for the joining locus. For instance, the two joining 1-cells $\langle 0,1 \rangle$ and $\langle 1,2 \rangle$ are merged into a single one ($\langle 1,2 \rangle$), by removing the 0-cell $\langle 1 \rangle$. These two 1-cells are merged, and so the 2-cells attached to it. Notice that this suppression can only be done if the 2-cells share the 1-cell whose boundary includes the 0-cell that will be suppressed. After this simplification, the complex has only one outgoing 2-cell per component of the joining locus [Fig. 4(c)]. This so-reduced flow-oriented complex and its associated digraph $G_2(\mathrm{L})$ is what we shall call a *generating templex*. Here "generating" refers to the generating partition induced by the first-return map. In a generating templex, the number of components of the joining locus is equal to N_{loc}, each joining locus being made of a single 1-cell. There are N_{loc} outgoing 2-cells, one per component of the Poincaré section. We have thus $N_{\mathrm{loc}} = N_{\mathrm{c}}$, a number which cannot be reduced further.

Definition 2 *A* **generating templex** $T^{\mathrm{g}} \equiv (K^{\mathrm{g}}, G^{\mathrm{g}})$ *is a templex composed by a flow-oriented complex* K^{g} *associated with a digraph* G^{g} *such that there is only one outgoing 2-cell per component of the joining locus.*

By propagating this removal of 0-cells to the higher-dimensional 1-cells, the 2-cells γ_1 and γ_2 are merged in a single one, and similarly for the pair γ_7-γ_8, γ_9-γ_{10}, γ_{11}-γ_{12}, γ_{17}-γ_{18}, and γ_{19}-γ_{20}. This leads to the complex $K_2(\mathrm{L})$ drawn in Fig. 4(c). The resulting complex $K_2(\mathrm{L})$ has a joining locus with two components as expected, since the Poincaré section of the Lorenz attractor has two components. Trajectories in the attractor can cross

the joining locus from four ingoing 2-cells, namely γ_6, γ_7, γ_{13}, and γ_{14}. Each joining locus has two ingoing 2-cells and one outgoing 2-cell. For instance, J_1 has γ_6 and γ_{14} as ingoing 2-cells, and γ_1 as outgoing 2-cell. Notice that the total number of ingoing 2-cells is equal to the number N_s of strips in the corresponding template (4 for the Lorenz template as discussed in Section III A).

A generating templex is not unique and the number of 2-cells (or nodes) that do not share a joining 1-cell remains arbitrary.

Step 6: Computing stripexes Let us now compute the cycles of the generating digraph [Fig. 4(d)]. Due to the construction of the digraph, it is efficient to compute the cycles from the outgoing nodes (underlined) of the joining loci. From the generating digraph $G_2(\mathrm{L})$, there are three cycles

$$c_1 \equiv \underline{1} \to 2 \to 4 \to 6 \to \underline{1}$$

$$c_2 \equiv \underline{8} \to 9 \to 11 \to 13 \to \underline{8}$$

and

$$c_3 \equiv \underline{1} \to 3 \to 5 \to 7 \to \underline{8} \to 10 \to 12 \to 14 \to \underline{1}$$

Let us imagine another generating complex $K_2'(\mathrm{L})$ with more numerous 2-cells than $K_2(\mathrm{L})$, the 2-cells γ_2 and γ_4 being split in two, leading to the addition of γ_2' and γ_4', respectively. The corresponding digraph $G_2'(\mathrm{L})$ is drawn in Fig. 4(e). There is the additional cycle

$$c_1' \equiv \underline{1} \to 2' \to 4' \to 6 \to \underline{1}\,.$$

By construction, the cycles c_1 and c_1' are equivalent because their 2-chains visit the same ingoing and outgoing 2-cells. Note that in terms of template, they would belong to the same strip. Consequently, among the set of cycles of the digraph G, if there is more than one cycle visiting a given ingoing and a given outgoing nodes, only one is retained. From the digraph $G_2'(\mathrm{L})$, the cycle c_1' (for instance) would be discarded.

Let us now introduce the order p of cycle as the number of ingoing nodes. For the digraph $G_2(\mathrm{L})$, there two order-1 cycle (c_1 and c_2) and one order-2 cycle (c_3). The latter is in fact degenerated and shall be considered as the union of two weak cycles, namely

$$c_{3_1} \equiv \underline{1} \to 3 \to 5 \to 7 \to \underline{8}$$

and

$$c_{3_2} \equiv \underline{8} \to 10 \to 12 \to 14 \to \underline{1}\,.$$

In the Lorenz attractor, the weak cycles c_{3_1} and c_{3_2} are the images of each other under the action of the rotation symmetry. They are weak as boundaries are weak when they have to be travelled more than once to become actual boundaries.

With each cycle of the generating digraph G^g, there is an associated chain of 2-cells which forms a sub-templex.

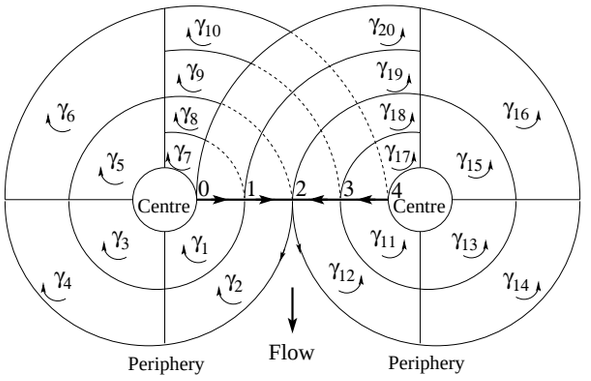

(a) Flow oriented complex $K_1(\mathrm{L})$

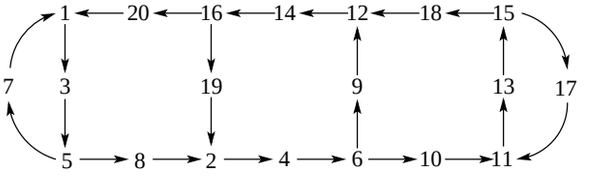

(b) Associated digraph $G_1(\mathrm{L})$

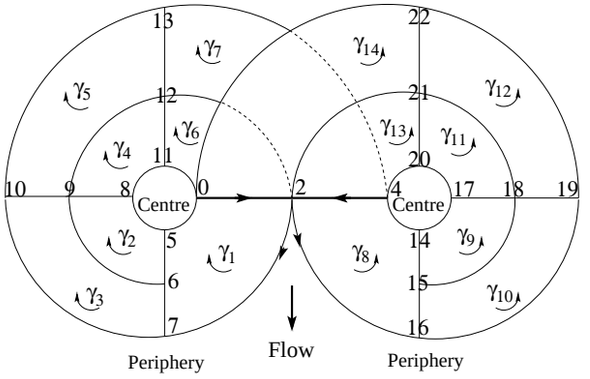

(c) Generating complex $K_2(\mathrm{L})$

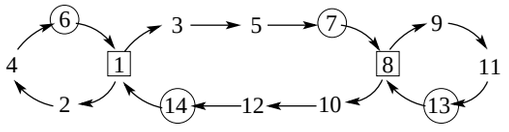

(d) Generating digraph $G_2(\mathrm{L})$

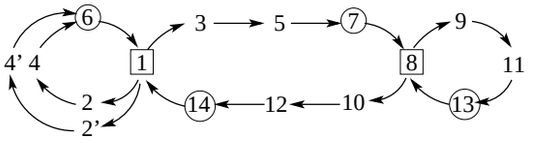

(e) Generating digraph $G_2'(\mathrm{L})$

Figure 4: (a-b) Templex $T_1(\mathrm{L}) = (K_1(\mathrm{L}), G_1(\mathrm{L}))$ and (c-d) generating templex $T_2(\mathrm{L}) = (K_2(\mathrm{L}), G_2(\mathrm{L}))$ for the Lorenz attractor. In (e), digraph $G_2'(\mathrm{L})$ corresponding to another generating complex $K_2'(\mathrm{L})$ — not shown — for the Lorenz attractor. Ingoing and outgoing nodes are squared and circled, respectively.

Definition 3 *Each cycle from the generating digraph G^{g} associated with its subcomplex forms a subtemplex that is called* **generatex** $\mathcal{G}$*. A generatex is said to be of order p with $p \in \mathbb{N}$, $p \geq 1$, if its cycle has p distinct ingoing nodes.*

A generatex is said to be *simple* if $p = 1$, and *degenerated* if $p > 1$.

The union of all equivalent sub-templexes (associated with equivalent cycles from the generating digraph) is a unit which plays a fundamental role in the characterization of branched manifolds. As we only retain a single representative for each group of equivalent cycles, we only save the representative generatexes.

Definition 4 *A* **stripex** $\mathcal{S}_i$ *is a subtemplex associated to a cycle or to a weak cycle of a generatex.*

By construction, each stripex is a subtemplex of T^{g}. A stripex is the analog of a strip from a template. Each strip is closely related to the structure of the first-return map to the Poincaré section.

In $T_2(\mathrm{L})$, for instance, there are four stripexes: $\mathcal{S}_1$ associated to c_1, $\mathcal{S}_2$ associated to c_2, $\mathcal{S}_3$ associated to c_{3_1} and $\mathcal{S}_4$ associated to c_{3_2}.

Step 7: Computing local twists The two free edges of the complex in stripex $\mathcal{S}_i$ are defined as the two disconnected 1-chains of the associated sub-complex K_i that result from applying the boundary operator ∂_2 to the sum of all the cells in K_i but the 1-cells from the joining locus.

Definition 5 *A stripex $\mathcal{S}_i = (K_i, G_i)$ is said to have a* **local twist** *if the free edges of K_i change their relative positions with respect to the orientation from the center to the periphery.*

Note that in the correspondence with templates, uneven local torsions in a strip correspond to a local twist. Strips with no local torsion or with even parity local torsions correspond to non twisted stripexes.

In $T_2(\mathrm{L})$, the 2-cells in stripex $\mathcal{S}_3$ $(\gamma_1, \gamma_3, \gamma_5, \gamma_7)$ and in $\mathcal{S}_4$ $(\gamma_8, \gamma_{10}, \gamma_{12}, \gamma_{14})$ have a local twist. For each of them, the free edge starting in the center ends at the periphery, and *vice versa*.

Step 8: Drawing the templex The standard representation of the different strips in a template introduces crossings to indicate local torsions and a certain order to organize the position of the strips, namely, which one is on top of the other and how they permute.

The graphical representation used in Figure 4 is a sort of 'semi-planar' diagram that keeps the shape of the butterfly for reference, giving an idea of how the complex is attached to the Lorenz attractor. Drawing a complex in this manner requires knowing which 2-cell is at the top of the other at the joining locus. For instance, when cells γ_6 and γ_{14} are considered, one should be able to determine which one is at the top of the other. Since we are in a three-dimensional space, it is important to locally orientate the direction of the top. To do this, we use the orientation of the flow and of the joining 1-cell. For a clockwise flow (counter-clockwise), we use the right (left) trihedron with the triplet flow-periphery-top as sketched in Fig. 5(a) [Fig. 5(b)]. According to this, in $T_2(\mathrm{L})$, γ_{14} should be drawn at the top of γ_6 and γ_{13} at the top of γ_7.

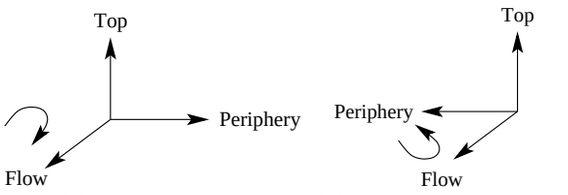

(a) Clockwise flow (b) Anti-clockwise flow

Figure 5: Orientation of the normal to a 2-cell to define relative top (and bottom). This is required for determining the order with which 2-cells are joined at a joining locus (see below).

Correspondence with templates To sum up, templexes enable to bridge the gap in the description of chaotic attractors offered by cell complexes and templates. The topological properties of an attractor are encoded by a generating templex. For a branched 2-manifold, the description provided by the generating templex is organized in terms of a number of layered properties:

- Splitting 0-cells are a particular case of critical points, appearing between two different components of the Poincaré sections.
- Joining 1-cells in the generating complex are the analogs of the components of the Poincaré section.
- Joining 2-cells are the analogs of the joining charts in a template.
- Stripexes are the analog of strips in a template: each stripex corresponds to a period-1 orbit in the template.

III. CHARACTERIZATION OF 3D CHAOTIC ATTRACTORS

We partly addressed the case of the Lorenz attractor when introducing the concept of templex. Let us now describe its template to exhibit its equivalence with the constructed templex. The cases of the Rössler attractor, the Burke-and-Shaw attractor and a four-dimensional attractor are then treated.

A. The Lorenz attractor

Template

The Lorenz attractor [Fig. 6(a)] produced by the Lorenz system[10]

$$\begin{cases} \dot{x} = -\sigma x + \sigma y \\ \dot{y} = Rx - y - xz \\ \dot{z} = -bz + xy \end{cases} \tag{5}$$

is bounded by a genus-3 torus which has three holes, two of the focus type which are associated with the center of each wings, and one, located in the rotation axis, which is a saddle type.[52] The first two ones can be easily detected because there are circled by the attractor. This is not so obvious for the hole of the saddle type, as drawn in Fig. 7(a), because it is bounded by trajectories issued from each of the two wings, that is, from different components of the Poincaré section.

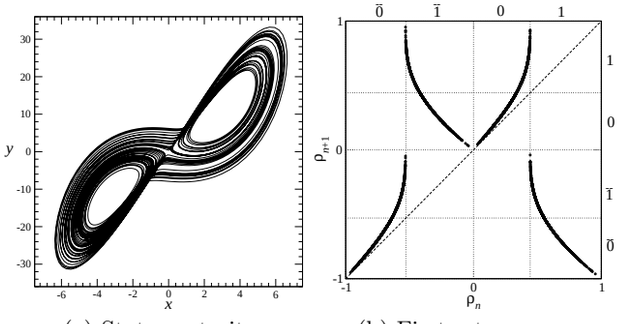

(a) State portrait (b) First-return map

Figure 6: Chaotic attractor produced by the Lorenz system (5) when the symbolic dynamics is nearly complete. Parameter values: $R = 28$, $\sigma = 10$, and $b = \frac{8}{3}$.

Let us first show how the Lorenz template is unveiled. The first step is to start from a view of the Lorenz attractor in the x-y plane and not in the x-z plane or in the y-z plane as commonly done. The template for the Lorenz attractor is drawn in Fig. 7(a). As suggested by the first-return map, it should be decomposed into four different strips. Two are the strips 0 and $\bar{0}$ [Fig. 7(a)] and one is the strip corresponding to the union of strips 1 and $\bar{1}$ [Fig. 7(b)].

There is another possibility to represent the template of the Lorenz attractor: it results mostly from a projection of the attractor in the x-z plane or in the y-z plane (Fig.8). In that particular representation, the Poincaré section may appear as being formed from a single component but there are a few characteristics which imposes to split it in two different components. Moreover, it is needed to orient the Poincaré section from the center of the attractor to its periphery. Typically, the center of an attractor is associated with the focus point around which trajectories circle. Consequently, the center of the attractor is different for each wing: the center of the left wing

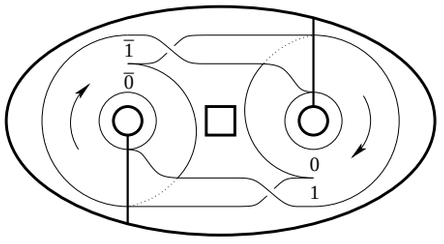

(a) Template and genus-3 bounding torus

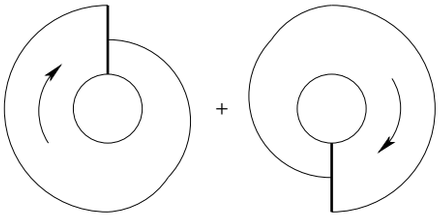

(b) Strips 0 and $\bar{0}$

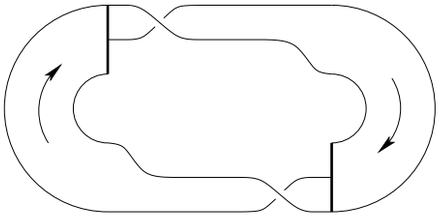

(c) Union of strips 1 and $\bar{1}$

Figure 7: Template and genus-3 bounding torus (thick lines) (a) for the Lorenz attractor and its decomposition into strips. The union of strips 1 and $\bar{1}$ (c) is degenerated since it crosses twice the joining 1-line.

is at the left of the Poincaré section and the center of the right wing is at the right of the Poincaré section. This means that the Poincaré section has necessarily two components which are oriented in opposed directions. Thus the point V_3 in Fig. 8 necessarily splits the Poincaré section in two components. This points results from the action of the rotation axis — the z-axis — at which the transverse flow is necessarily null.[53] The point V_3 thus splits the template issued from the joining line in two parts, one being associated with the left wing, the other one with the right wing.

The template for the Lorenz attractor [Fig. 7(a)] is described by the linking matrix

$$L_{ij} = \begin{bmatrix} 0 & 0 & 0 & 0 \\ 0 & +1 & 0 & 0 \\ 0 & 0 & 0 & 0 \\ 0 & 0 & 0 & +1 \end{bmatrix} \tag{6}$$

and the joining matrix

$$J_{ij} = \begin{bmatrix} 1 & \cdot & \cdot & 1 \\ \cdot & 1 & 1 & \cdot \end{bmatrix}. \tag{7}$$

Templex

The construction of a Lorenz templex was described

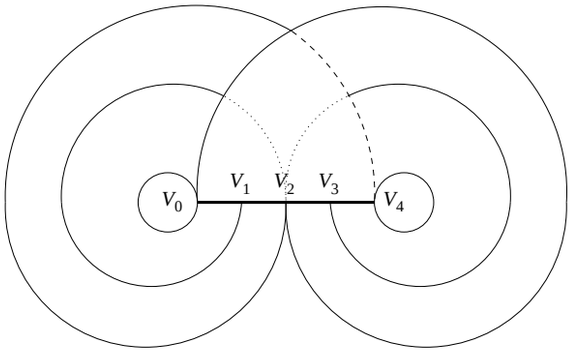

Figure 8: Decomposition of the template for the Lorenz attractor in four strips from an x-z view.

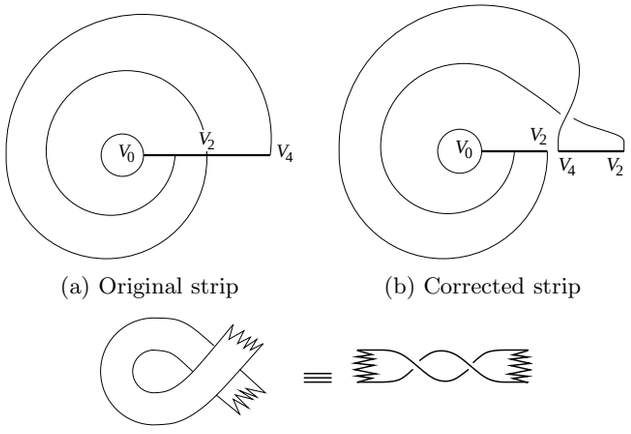

(a) Original strip (b) Corrected strip

(c) Third Reidemeister move

Figure 9: Strip $\bar{1}$ as originally seen (a) and as corrected when the right component of the Poincaré section is correctly oriented. The third Reidemeister move explains the origin of the π-twist.

in detail in section II C: the generating complex and its digraph in $T_2(\mathrm{L})$ are sketched in Figs 4(c-d). If we analyze $K_2(\mathrm{L})$ as a standard complex, one finds a single 0-generator, $\mathcal{H}_0 = [< 0 >]$, which speaks of a single connected component. There are two 1-generators:

$$\mathcal{H}_1(K_2(\mathrm{L})) = [[\langle 4,14\rangle - \langle 4,20\rangle + \langle 14,17\rangle + \langle 17,20\rangle, \langle 0,5\rangle - \langle 0,11\rangle + \langle 5,8\rangle + \langle 8,11\rangle]]$$

which identify and locate the two focus-type holes in the attractor. There are no 2-generators (no enclosed cavities): $\mathcal{H}_2 = \varnothing$.

What does the generating templex add to this description? It unveils a joining locus made of two-components, indicating the existence of a bipartite Poincaré section. This yields three generatexes and four stripexes $\mathcal{S}_i$ ($i = 1, ...4$) which are equivalent to the four strips in the template, two of them have local twists ($\mathcal{S}_3$ and $\mathcal{S}_4$). The three generatexes can be easily recognised in the decomposition of the template shown in Figs 7(b) and 7(c): in the latter, the stripexes $\mathcal{S}_3$ and $\mathcal{S}_4$ are weak since only their union defines a generatex.

B. The Rössler attractor

Template

The topologically simplest chaotic attractor (Fig. 10) is produced by the Rössler system[54]

$$\begin{cases} \dot{x} = -y - z \\ \dot{y} = x + ay \\ \dot{z} = b + z(x - c)\,. \end{cases} \tag{8}$$

It is characterized by a smooth first-return map to a Poincaré section [Fig. 10(b)].[44] Since the map is smooth and unimodal, the typical route to this chaotic attractor is a period-doubling cascade. This attractor was labelled as $\mathrm{C^1T^1}$ according to the nomenclature introduced in the taxonomy of chaos.[55] It is bounded by a trivial torus (1,1).

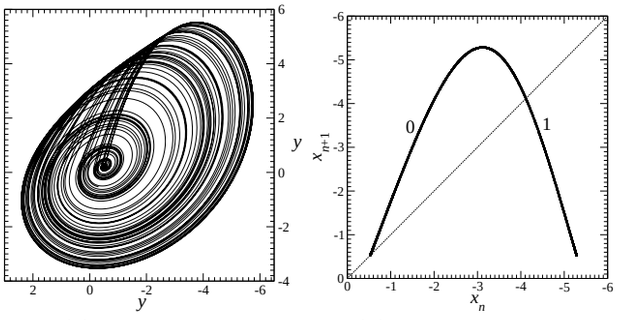

(a) State portrait (b) First-return map

Figure 10: Chaotic attractor produced by the Rössler system (8) when the symbolic dynamics is nearly complete. Parameter values: $a = 0.43295$, $b = 2$, and $c = 4$.

The Rössler attractor is described by the template drawn in Fig. 11(c). It should be decomposed into two strips, namely a normal band [Fig. 11(a)] and a Möbius band [Fig. 11(b)].[56] A direct template can be drawn directly from the y-x plane projection [note that the y-axis in Fig. 10(a) is inverted for a better equivalence with the template drawn in Fig. 11(a)]. The strips are encoded with the same integers as the branches of the first-return map: an even (odd) integer is used for a strip with an even (odd) local torsion. The natural order $0 < 1$ is drawn from the center to the periphery of the attractor [Fig. 11(b)]. The standard template is described by the linking matrix

$$L_{ij} = \begin{bmatrix} 0 & -1 \\ -1 & -1 \end{bmatrix}. \tag{9}$$

Templex

Let us now describe this attractor using a generating templex. As described in section II C, the first step is to

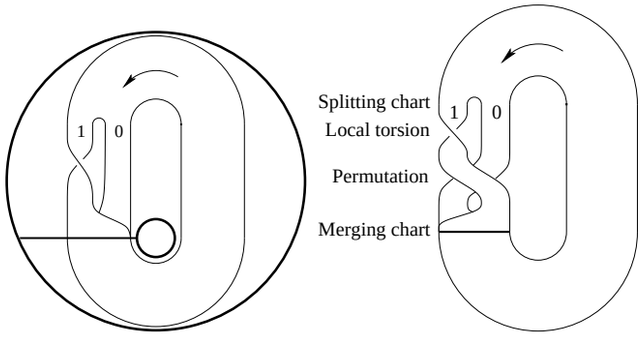

(a) Direct template (b) Standard template

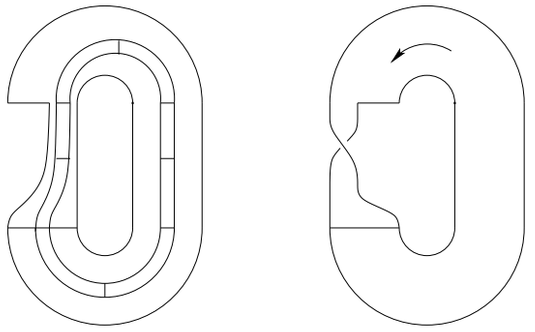

(c) Strip 0 (d) Strip 1

Figure 11: Direct (a) and standard (b) template for the Rössler attractor plotted in Fig. 10. The genus-1 bounding torus is drawn in (a) as thick circles. An example of 2-cycle is drawn in the strip 0 (c).

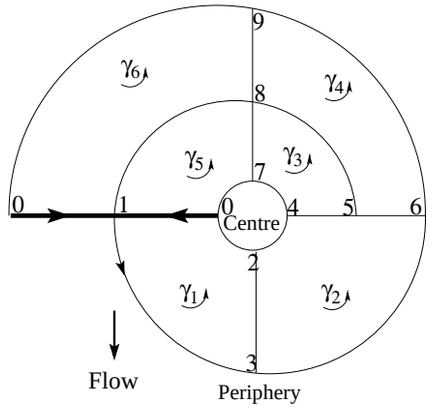

(a) Generating complex

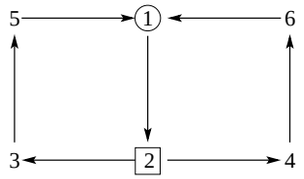

(b) Generating digraph

Figure 12: Generating templex $T(\mathrm{R})$ for the Rössler attractor made of the generating complex $K(\mathrm{R})$ shown as a planar diagram in (a) and the generating digraph $G(\mathrm{R})$ (b). The thick line indicates the joining 1-cell $\langle 0,1\rangle$.

construct a BraMAH complex. This is performed algorithmically, handling a set of points in the state space. The complex is next endowed with a digraph which reproduces the structure of the flow along the branched 2-manifold, till a generating templex is obtained. The result of the whole procedure is sketched in Fig. 12 where the complex $K(\mathrm{R})$ is drawn unfolded, that is, in a planar diagram, as is customary in homology theory. In planar diagrams, gluing instructions require some cells to be drawn twice with the same labels and direction. This is the case for the joining 1-cell $\langle 0,1\rangle$ in $K(\mathrm{R})$, which is drawn twice in Fig. 12(a). Flow-orienting this complex is achieved by propagating the orientation from γ_1 according to our convention [it is obvious in the planar representation shown in Fig. 12(a)].

The complex $K(\mathrm{R})$ has a single 0-generator, $\mathcal{H}_0(K(\mathrm{R})) = [< 0 >]$, that is, it has a single connected component. The single 1-generator of $K(\mathrm{R})$ is

$$\mathcal{H}_1(K(\mathrm{R})) = [[\langle 0,2\rangle - \langle 0,7\rangle + \langle 2,4\rangle + \langle 4,7\rangle]]$$

which identifies the focus-type hole in the attractor. There are no 2-generators (no enclosed cavities): $\mathcal{H}_2(K(\mathrm{R})) = \varnothing$. Notice that, homologically, $K(\mathrm{R})$ is a cylinder: fortunately, the generating templex tells us much more about its structure.

The generating templex $T(\mathrm{R}) = (K(\mathrm{R}), G(\mathrm{R}))$ has the following properties. There is one joining 2-cell (γ_1). Since there is a single joining 1-cell, the joining locus has a single component (as expected for an attractor bounded by a genus-1 torus) and there is no splitting 0-cell. There are two stripexes $\mathcal{S}_1$ and $\mathcal{S}_2$ associated with the cycles

$$c_1 \equiv \underline{1} \to 2 \to 4 \to 6 \to \underline{1}$$
$$c_2 \equiv \underline{1} \to 2 \to 3 \to 5 \to \underline{1}$$

The associated generatexes are simple ($p = 1$) and correspond to strips 0 and 1, respectively. The stripex $\mathcal{S}_1$ is a Möbius band – it has some torsion elements ($b_1 = 2$ for $\sigma_1^1 = \langle 0,1\rangle$ in $\partial\Gamma$) — while K_2 is a cylinder or normal band (without torsion).

The stripex $\mathcal{S}_1$ has a local twist which is sketched in Fig. 13. According to our convention for the top, the 2-cell γ_6 is at the top of the cell γ_5.

C. The three-strips Rossler attractor

Template

When the parameter a of the Rössler system is set to 0.492, the first-return map to a Poincaré section has three branches (Fig. 14)[44] and the template is drawn in Fig. 3. This attractor is labeled R_3.

Templex

A classical homological analysis of $K(\mathrm{R}_3)$ yields the following results: there is, as usual, one 0-generator (one

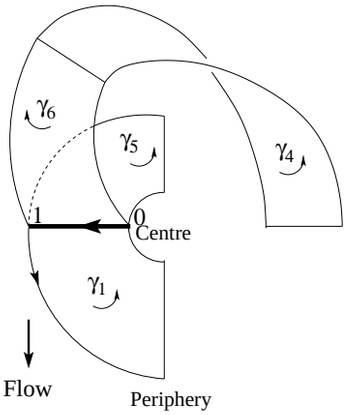

Figure 13: The three 2-cells (γ_1, γ_5, and γ_6) sharing the joining 1-cell. The 2-cell γ_4 is added to show the local twist of the stripex $\mathcal{S}_1$.

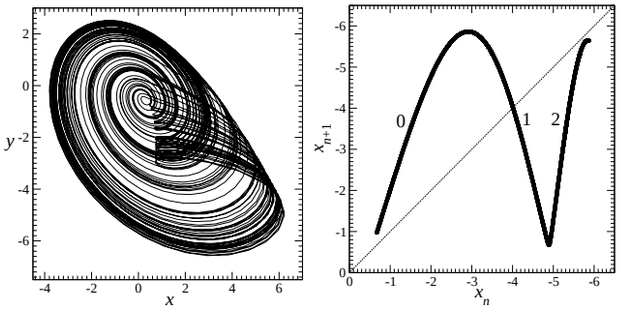

(a) State portrait (b) First-return map

Figure 14: Chaotic attractor with three branches as produced by the Rössler system (8). Parameter values: $a = 0.492$, and other parameter values as in Fig. 10.

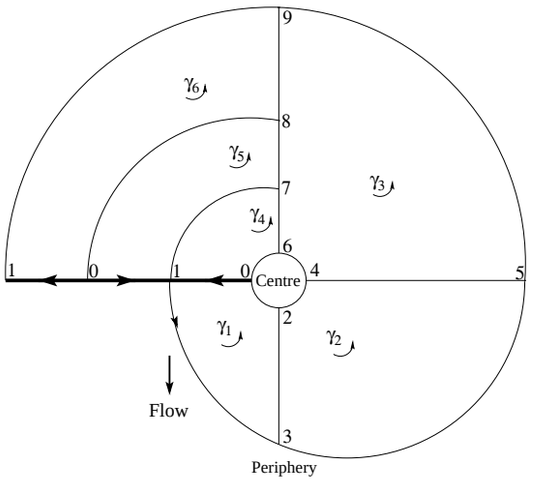

(a) Generating complex $K(\mathrm{R}_3)$

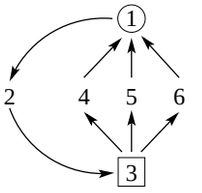

(b) Generating digraph $G(\mathrm{R}_3)$

Figure 15: Generating templex $T(\mathrm{R}_3) = (K(\mathrm{R}_3), G(\mathrm{R}_3))$ for the three-strip Rossler attractor. Parameter values: $a = 0.492$, $b = 2$ and $c = 4$. In the digraph, ingoing and outgoing nodes are squared and circled, respectively.

connected component). The 1-generator (corresponding to the hole of the focus type) is given by: $\mathcal{H}_1(K(\mathrm{R}_3)) = [[\langle 0,2\rangle - \langle 0,6\rangle + \langle 2,4\rangle + \langle 4,6\rangle]]$ which identifies the focus-type hole in the attractor. No 2-generators are found (there are no cavities enclosed).

A templex for the three-strips Rössler attractor $T(\mathrm{R}_3) = (K(\mathrm{R}_3), G(\mathrm{R}_3))$ is proposed in Fig. 15. The joining locus has one component and it is made of the 1-cell $\langle 0,1\rangle$. The 2-cell γ_1 is the unique outgoing joining 2-cell, and γ_4, γ_5, and γ_6 are the three ingoing joining 2-cells.

As expected, three generatexes and three stripexes $\mathcal{S}_{1,2,3}$ are found ($N_\mathrm{s} = 3$). They are associated with the three cycles

$$c_1 \equiv \underline{1} \to 2 \to 3 \to 4 \to \underline{1}$$
$$c_2 \equiv \underline{1} \to 2 \to 3 \to 5 \to \underline{1}$$
$$c_3 \equiv \underline{1} \to 2 \to 3 \to 6 \to \underline{1}$$

which are indeed non-equivalent because they are associated with different ingoing nodes. Of the the three stripexes, only $\mathcal{S}_2$ has a local twist, corresponding to the intermediate strip of the template in Figure 3. $\mathcal{S}_1$ corresponds to the strip with no local torsion and $\mathcal{S}_3$ to the strip with an even parity.

D. The Burke and Shaw attractor

Template

There is a Lorenz-like system which produces a quite common attractor: this is the Burke and Shaw system[57,58]

$$\begin{cases} \dot{x} = -ax - ay \\ \dot{y} = -y - axz \\ \dot{z} = b + axy\,. \end{cases} \tag{10}$$

As the Lorenz system (5), this system is equivariant under a rotation symmetry $\mathcal{R}_z(\pi)$. Close to the original parameter values,[57] there is a specific attractor which is encountered in many Lorenz-like systems.[59] Indeed, for $a = 10$ and $b = 2.271$, the attractor plotted in Fig. 16(a) is characterized by a four-branches first-return map [Fig. 16(b)]. It has four branches and a possible natural order between the integers used for labelling them is $\bar{1} < 0 < 1 < 2$.[58] This attractor is bounded by a genus-1 torus as sketched around the template drawn in Fig. 17(a). As a consequence, the Poincaré section should have a single component. Nevertheless, as shown in Fig.

16(a), there are two foldings located in the neighborhood of the rotation axis, leading to two joining charts.

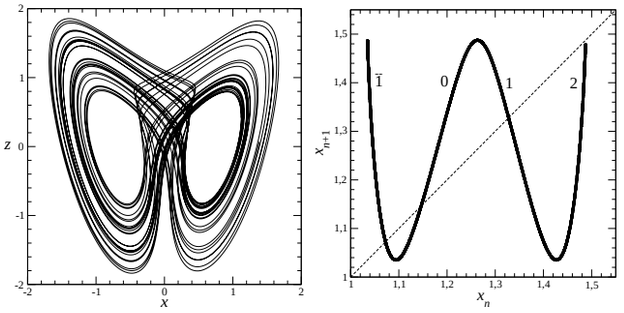

(a) State portrait (b) First-return map

Figure 16: Chaotic attractor produced by the Burke and Shaw system (10) when the symbolic dynamics is nearly complete. Parameter values: $a = 10$, and $b = 2.271$.

It is actually possible to sketch the topology of the attractor as the product of two mixers [each of them being located between one splitting chart and one joining chart as drawn in Figs. 17(a) and 17(b)]. As exhibited in the Lorenz attractor with the third Reidemeister move [Fig. 9(c)], there is a global torsion (a global torsion differs from a local one in the sense that it is applied to all the strips of the attractor, the latter being applied to a single strip, by definition) between a sequence of one joining chart followed by one splitting chart. With the help of the Reidemeister moves, each global torsion can be moved in one of the two mixers, to get the reduced double template shown in Fig. 17(b). In this representation, the rotation symmetry is obvious.

It is possible to conjugate these two mixers into a single one. In this case, the two strips of the first (say the left) mixer are spread into the two strips of the second (right) mixer to form four strips. Propagating permutations and local torsions using Reidemeister moves leads to the reduced template drawn in Fig. 17(c): it is described by the linking matrix L_{ij} (see Appendix C)

$$L_{ij} = \begin{bmatrix} 3 & 2 & 2 & 3 \\ 2 & 2 & 2 & 3 \\ 2 & 2 & 3 & 3 \\ 3 & 3 & 3 & 4 \end{bmatrix} \tag{11}$$

For a more direct correspondence with templexes, it is useful to redraw the direct template as shown in Fig. 18: it is topologically equivalent to the template drawn in Fig. 17.

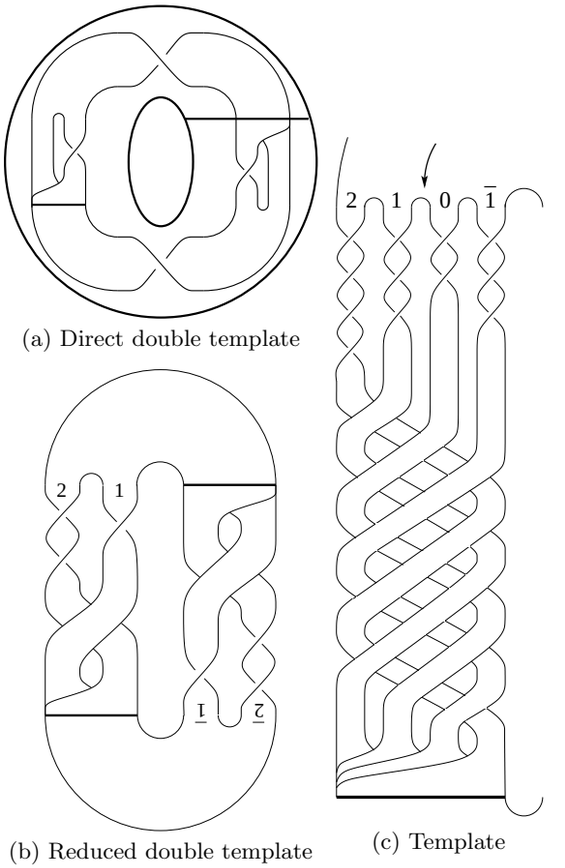

(a) Direct double template (b) Reduced double template (c) Template

Figure 17: Double template and genus-1 bounding torus (a) for the Burke & Shaw attractor plotted in Fig. 16(a). Direct double template (a), reduced double template (b) and reduced template (c).

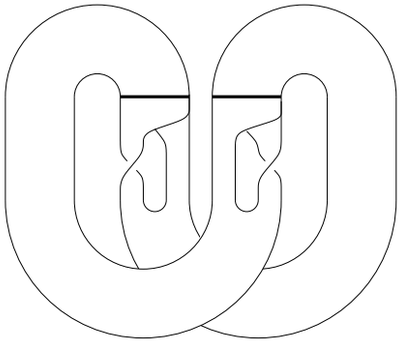

Direct template

Figure 18: Double templates for the Burke and Shaw attractor.

Templex

Let us consider the complex $K(\mathrm{BS})$ shown in Fig. 19(a). Computing the homology groups, one finds a single 0-generator (one connected component), and a single 1-generator (corresponding to the focus-type hole in the attractor).

$$\mathcal{H}_1(K(\mathrm{BS})) = [[\langle 0,4\rangle - \langle 0,17\rangle + \langle 2,3\rangle - \langle 2,9\rangle + \\ +\langle 3,12\rangle + \langle 4,6\rangle + \langle 6,9\rangle + \langle 12,14\rangle + \langle 14,17\rangle]]$$

As expected, no cavities are found.

The generating complex and digraph forming templex $T(\mathrm{BS}) = (K(\mathrm{BS}), G(\mathrm{BS}))$ for this attractor are presented in Fig. 19. The orientation of the generating complex $K(\mathrm{BS})$ is started from the two joining 2-cells: γ_1 and γ_8. The analysis of the templex yields a joining locus with the two components $J_1(\mathrm{BS}) = \langle 1, 0\rangle$ and $J_2(\mathrm{BS}) = \langle 3, 2\rangle$, which correspond to the two components of the Poincaré section in the direct template [Fig. 17(b) or Fig. 18]. There are four stripexes $\mathcal{S}_{1,2,3,4}$, corresponding to the following weak cycles

$$
\begin{aligned}
c_{1_1} &\equiv \underline{1} \to 2 \to 3 \to 5 \to \underline{7} \\
c_{1_2} &\equiv \underline{7} \to 8 \to 9 \to 11 \to \underline{1} \\
c_{2_1} &\equiv \underline{1} \to 2 \to 4 \to 6 \to \underline{7} \\
c_{2_2} &\equiv \underline{7} \to 8 \to 10 \to 12 \to \underline{1}
\end{aligned}
$$

Each pair of weak cycles comes from a degenerated generatex, of order 2. $\mathcal{S}_{1,4}$ have local twists, while $\mathcal{S}_{2,3}$ do not. In the semi-planar diagram, $\gamma_{5,6}$ are on the top of $\gamma_{11,12}$.

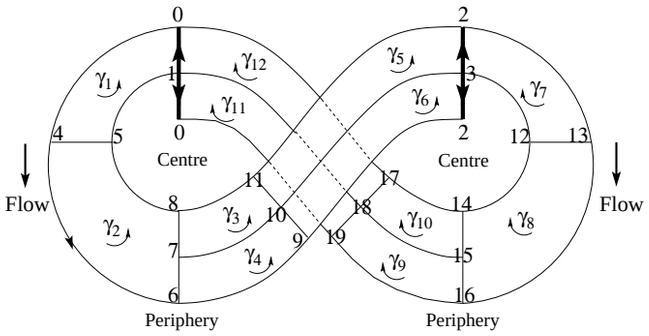

(a) Generating complex

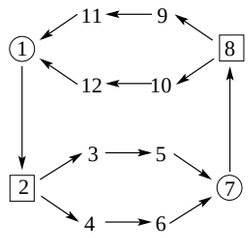

(b) Generating digraph

Figure 19: Templex for the Burke and Shaw attractor: generating complex (a) endowed with a directed graph (b), ingoing and outgoing nodes are squared and circled, respectively. There are two joining 1-cells (thick lines with arrows). They are no splitting 0-cells.

IV. A FOUR-DIMENSIONAL SYSTEM

Let us restart from a four-dimensional system designed by Mindlin and Sciamarella from a three-dimensional system proposed by Deng.[60] The extended system reads[34]

$$
\begin{cases}
\dot{x} = -(z+2)d\,(x - [a + \epsilon_3(2+w)]) + (2-z) \\
\qquad \left[\alpha(x-2) - \beta y - \alpha\,(x-2)\,\dfrac{(x-2)^2 + y^2}{R^2}\right] \\
\dot{y} = -(z+2)\,(y-b) + (2-z) \\
\qquad \left[\beta\,(x-2) + \alpha y - \alpha y \dfrac{(x-2)^2 + y^2}{R^2}\right] \\
\dot{z} = (4 - z^2)\,\dfrac{z + 2 - \mu(x+2)}{\epsilon_1} - cz \\
\dot{w} = (4 - z^2)\,\dfrac{z + 2 - \mu(x+2)}{\epsilon_2} - cz
\end{cases}
\tag{12}
$$

For appropriate parameter values, this system produces a chaotic attractor (Fig. 20). A solution to this system was already investigated with a cell complex (but not with a templex) by Sciamarella and Mindlin.[34] In that work, the purpose was showing that homologies enabled the topological description from short time series, regardless of the nature of the dynamics (periodic, quasi-periodic, chaotic or other). Here, we are focused on chaotic behavior. In fact, the original parameter values (as reported in Fig. 20 but $b = 1.435$) leads to a long limit cycle (its period is at least equal to 100); a chaotic regime was found for a slightly larger value which is now set to 1.45. We used an integration time step of 0.001, initial values for all coordinates equal to 0.2. Four different three-dimensional projections of the resulting chaotic attractor are shown in Fig. 20.

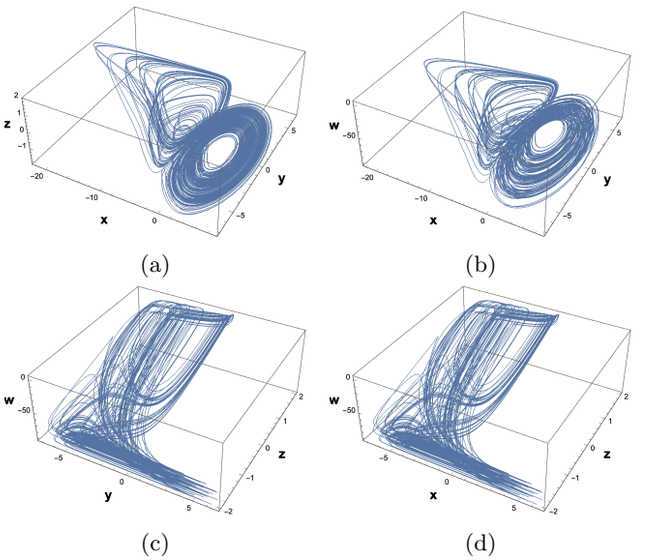

Figure 20: Chaotic attractor produced by the four-dimensional system (12). Parameter values: $a = 7$, $b = 1.45$, $c = 1$, $d = 0.5$, $R = 6$, $\alpha = 0.3$, $\beta = 7$, $\epsilon_1 = 0.165$, $\epsilon_2 = 0.01$, $\epsilon_3 = 2$, and $\mu = 1.543$. Four different three-dimensional projections (x-y-z, x-y-w, y-z-w and x-z-w) are shown.

The BraMAH complex $K(4\mathrm{D})$ is built from a cloud of 24,999 points (once the transient regime is completed).

Applying the methodology described in Appendix A, we obtain a cell complex as shown in Fig. 21. The highest dimensional cells of this complex are the 3-cells γ_i, and the 2-cells σ_i which are not the border of any 3-cell. Its topology is clearly not trivial and no template was proposed for it before.

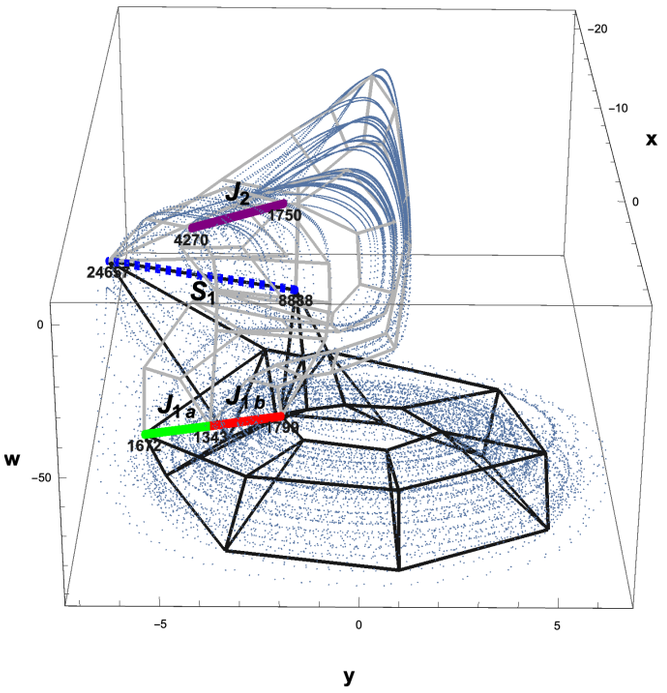

Figure 21: Complex $K(4D)$ in the x-y-w subspace from the cloud of points produced by the four-dimensional system (12). Labeled lines (in color) correspond to the joining loci (solid) or splitting loci (dashed).

The homologies of the $K(4D)$ are: $\mathcal{H}_0 \approx \mathbb{Z}_1$ (there is one connected component), $\mathcal{H}_1 \approx \mathbb{Z}_5$ (there are five non-trivial 1-loops), $\mathcal{H}_2 \approx \varnothing$ (there are no enclosed empty cavities) and $\mathcal{H}_3 \approx \varnothing$.

The joining locus was previously defined for a 2-branched manifold, and therefore for a 2-complex. In this particular case, we will compute it looking for the chain of 1-cells shared by a set of at least three cells which can be either 3-cells (γ_i), or 2-cells (σ_i) that are not the face of any 3-cell. This yields:

1. J_{1a} between the 0-cells 1343 and 1672, and formed by the cells γ_1, γ_8, and σ_{24} ;

2. J_{1b} between the 0-cells 1343 and 1799 made of the cells γ_1, γ_8, σ_9, and σ_{34};

3. J_2 between the 0-cells 1750 and 4270 made of the cells σ_{12}, σ_{13}, and σ_{14};

4. S_1 between the 0-cells 8888 and 24657 made of the cells σ_{36}, σ_{38}, σ_{39}, and γ_{40}.

As shown in Fig. 21, the first two loci form the main joining locus $J_1 = J_{1a} \cup J_{1b}$ in the bottom scroll (Fig. 21) and J_2 is a second joining locus in the upper part of the attractor according to our plot. The third locus is a splitting line between the 3-cell γ_{40} and the three 2-cells σ_{36}, σ_{38} and σ_{39}. The two joining lines are located between the points of the state space as follows.

$$\mathrm{J}_1 \equiv [(3.41, -5.58, -1.93, -61.50), (1.86, -2.01, -1.97, -61.46)]$$

$$\mathrm{J}_2 \equiv [(-1.28, -1.95, 1.98, 1.22), (-0.01, -4.37, 1.49, -2.99)]$$

The splitting locus is found at:

$$\mathrm{S}_1 \equiv [(-2.21, -7.04, 0.70, -48.86), (-5.17, -0.81, -0.87, -66.66)]$$

and is drawn as a dashed line in Fig. 21. As developed in the previous examples, the second step consists in re-orienting the cell complex according to the flow, without propagation through the joining or splitting loci.

The third step consists in equipping $K(4D)$ with the digraph $G(4D)$ plotted in Fig. 22. All the 1-cells of the joining lines J_{1a} and J_{1b} are oriented in the same directions and, consequently, there is no splitting 0-cell. Both are already with a single outgoing cell. No splitting 0-cells are found, and no 0-cells need to be removed. The 2-cells γ_1 and σ_{12} are the outgoing joining 2-cells, and γ_8, σ_9, σ_{13}, σ_{14}, σ_{24}, and σ_{34} are the six ingoing joining 2-cells. The splitting locus has one ingoing 3-cell and three outgoing 2-cells: the fact that the ingoing cell is of dimension 3 allows to preserve the determinism at this splitting locus. This is a feature that we had not observed for three-dimensional systems. The simplest deterministic representation of flow around this splitting locus is to consider that three strips — close to each other as in a foliation within the 3-cell γ_{40} — are sent away from each other. This specificity will require a novel element for drawing a template as explained below. At this stage, the templex can be considered as a generating templex.

From the digraph, we found three order-1 cycles c_1, c_2 and c_3:

$$c_1 \equiv \underline{1} \to 2 \to 3 \to 4 \to 5 \to 6 \to 7 \to 8 \to \underline{1}$$

$$c_2 \equiv \underline{1} \to 2 \to 3 \to 4 \to 5 \to 6 \to 37 \to 40 \to 36 \to 35 \to 25 \to 26 \to 27 \to 28 \to 29 \to 30 \to 31 \to 32 \to 33 \to 34 \to \underline{1}$$

$$c_3 \equiv \underline{1} \to 2 \to 3 \to 4 \to 5 \to 6 \to 37 \to 40 \to 38 \to 20 \to 19 \to 18 \to 17 \to 21 \to 22 \to 23 \to 24 \to \underline{1}$$

and two order-2 cycles c_4 and c_5 which are the union of two weak cycles $c_4 = c_{4_1} \cup c_{4_2}$ and $c_5 = c_{5_1} \cup c_{4_2}$:

$$c_{4_1} \equiv \underline{1} \to 2 \to 3 \to 4 \to 5 \to 6 \to 37 \to 40 \to 38 \to 20 \to 19 \to 18 \to 17 \to 16 \to 15 \to 14 \to \underline{12}$$

$$c_{5_1} \equiv \underline{1} \to 2 \to 3 \to 4 \to 5 \to 6 \to 37 \to 40 \to 39 \to 13 \to \underline{12}$$

$$c_{4_2} \equiv \underline{12} \to 11 \to 10 \to 9 \to \underline{1}$$

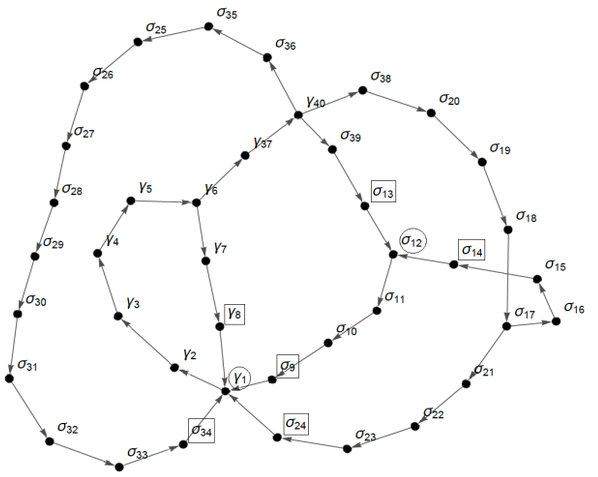

Figure 22: Digraph on the BRAMAH complex constituting the templex for the analysis of the four-dimensional attractor. Ingoing and outgoing nodes are squared and circled, respectively.

To extract the stripexes from the cycles, we only consider J_1 and J_2 (splitting loci are not taken into account for stripex computation). The first three cycles lead to three stripexes:

$$\begin{aligned}
\mathcal{S}_1 &\equiv \gamma_1 ... \gamma_8 \\
\mathcal{S}_2 &\equiv \gamma_1 ... \gamma_6 - \gamma_{37} - \sigma_{40} - \sigma_{36} - \sigma_{35} - \sigma_{25} ... \sigma_{34} \\
\mathcal{S}_3 &\equiv \gamma_1 ... \gamma_6 - \sigma_{37} - \gamma_{40} - \sigma_{38} - \sigma_{20} - \sigma_{19} - \sigma_{18} - \\
&\quad \sigma_{17} - \sigma_{21} ... \sigma_{24}
\end{aligned}$$

The next two cycles lead to:

$$\begin{aligned}
\mathcal{S}_4 &\equiv \gamma_1 ... \gamma_6 - \gamma_{37} - \gamma_{40} - \sigma_{38} - \sigma_{20} - \sigma_{19} - \sigma_{18} - \sigma_{17} - \\
&\quad \sigma_{16} - \sigma_{15} - \sigma_{14} \\
\mathcal{S}_5 &\equiv \gamma_1 ... \gamma_6 - \gamma_{37} - \gamma_{40} - \sigma_{39} - \sigma_{13} \\
\mathcal{S}_6 &\equiv \sigma_{12} - \sigma_{11} - \sigma_{10} - \sigma_9
\end{aligned}$$

The stripex $\mathcal{S}_6$ corresponds to a trivial strip, and the joining line J_2 can be identified with the joining line J_1 under an isotopy. Stripexes $\mathcal{S}_4$ and $\mathcal{S}_5$ thus become:

$$\begin{aligned}
\mathcal{S}'_4 &\equiv \gamma_1 ... \gamma_6 - \gamma_{37} - \gamma_{40} - \sigma_{38} - \sigma_{20} - \sigma_{19} - \sigma_{18} - \sigma_{17} - \\
&\quad \sigma_{16} - \sigma_{15} - \sigma_{14} - \sigma_{12} - \sigma_{11} - \sigma_{10} - \sigma_9 \\
\mathcal{S}'_5 &\equiv \gamma_1 ... \gamma_6 - \gamma_{37} - \gamma_{40} - \sigma_{39} - \sigma_{13} - \sigma_{12} - \sigma_{11} - \sigma_{10} - \sigma_9
\end{aligned}$$

Local twists are found in $\mathcal{S}_3$ and $\mathcal{S}'_5$.

Thus, the four-dimensional attractor can be described with five stripexes, that is, with a five symbol dynamics. In order to build the template that would correspond to the templex, we will resort to our know-how in the topological characterization of chaotic attractors. To be honest, and in order to construct a template that unveils the complex structure of the attractor produced by the four-dimensional system (12), we constructed a paper model similar to the *xyz* projection of the system, as shown in Fig. 23. In order to reproduce the model shown in the picture, supplementary material is provided with simple shapes to cut out. The volume formed by the ten 3-cells of $K(4D)$, namely γ_1, γ_2, γ_3, γ_4, γ_5, γ_6, γ_7, γ_8, γ_{37} and γ_{40}, is topologically equivalent to a solid (filled) torus. Notice that the homologies of the solid torus ($\mathcal{H}_0 \approx \mathbb{Z}_1$, $\mathcal{H}_1 \approx \mathbb{Z}_1$, $\mathcal{H}_2 \approx \varnothing$, $\mathcal{H}_3 \approx \varnothing$) are equivalent to those of the cylinder or normal band. Because of this, the paper model is homologically equivalent to $K(4D)$. This paper model revealed some features we were never able to exhibit during our long history in characterizing chaotic attractors.

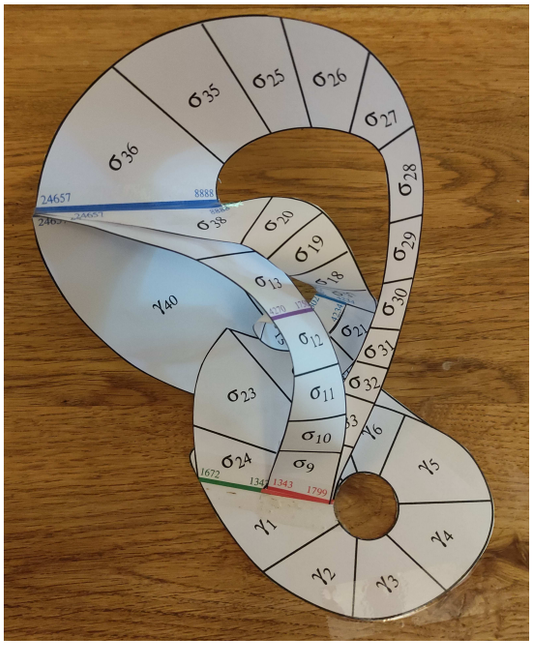

Figure 23: Paper model of a 2-complex where the 3-cells of $K(4D)$ have been contracted to equivalent 2-cells. It is used as a guide to construct the template of the attractor produced by the four-dimensional system (12). The flow is counterclockwise in this paper model. The main joining locus where four strips are merged is located at the bottom left of the construction (green and red); the splitting locus (blue) is located slightly above the left middle of the paper model. Between these two loci, there is the second joining locus (purple).

The strips visiting the 3-cell γ_{40} required to sketch them as one foliated strip, leading to a new splitting chart drawn in Fig. 24. The strip associated with the 3-cell γ_{40} is drawn as a three-foliated strip which is then split into three distinct strips corresponding to the 2-cells σ_{36}, σ_{38} and σ_{39}, respectively. The determinism is not broken since the 3-cell is in fact a volume. The three-foliated strip is distinguished in tripling one of its boundary. In doing this, we lose the non-ambiguous description of the relative position between periodic orbits. This would have been crucial for three-dimensional links and the computation of their linking numbers, for instance,

but in a four-dimensional space, all knots are trivial and unknotted and this is no longer relevant. What persists with this description is the possibility to have a 'knot-holder' associated with a generating symbolic dynamics, that is, with a symbolic dynamics with a minimum number of symbols allowing a non-ambiguous description of all the periodic orbits.

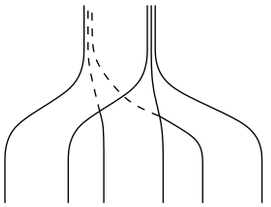

Figure 24: Convention for drawing a splitting chart between a foliated ingoing strip and a few — here three — outgoing non-foliated strips. Here, the hidden boundaries are drawn with dashed lines; they are omitted in template for the sake of readability of the final picture.

Once this key point overcome, it was rather easy to construct a representation in the fashion of the template commonly used in the topological characterization of chaotic attractors, leading to the direct template drawn in Fig. 25. Among its specificities, we have the previously described splitting chart, and the joining line J_2. Typically, this is a template bounded by a genus-one torus. Here the template with the common convention according which all possible transitions between the strips is made possible (this is discussed, for instance, by Mindlin and Gilmore[13]). From this direct template, it can be easily understood why the joining line J_2 can be identified with the joining line J_1 under an isotopy.

In spite of the foliated representation, the structure of the strips between the splitting and the joining charts can still be synthetized with the help of the linking matrix

$$\begin{bmatrix} 0 & -1 & -1 & -1 & -1 \\ -1 & -2 & -3 & -2 & -3 \\ -1 & -3 & -2 & -2 & -3 \\ -1 & -2 & -2 & -1 & -3 \\ -1 & -3 & -3 & -3 & -1 \end{bmatrix}. \tag{13}$$

It was built by counting the local torsion in each strip and the permutations between pairs of them. From this linking matrix, it was possible to draw a reduced template (Fig. 26) from which the unusual nature of the attractor here investigated is better exhibited in its upper part with the foliated splitting chart. Another particularity lies in the bottom part of the permutation between strips 5 and 7. From this representation, the strips can be univocally labelled according to the parity of the local torsion of each strip, and increasing integers, from the centre of the attractor to its periphery as required.[43] Note that the linking matrix (13) should not be used to compute linking numbers.

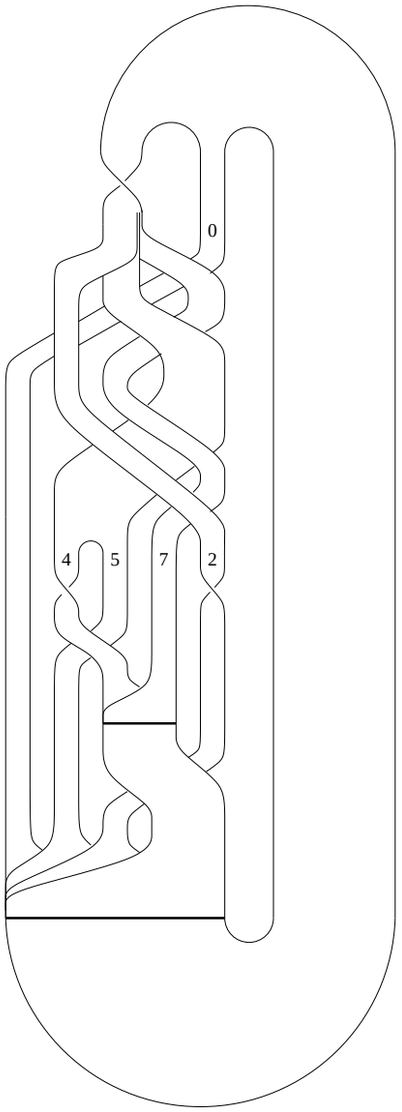

Figure 25: Direct template for the attractor produced by the four-dimensional system (12).

Although characterized by a genus-1 torus, to unfold the foliated structure for computing a readable first-return map, the Poincaré section should have four components, one corresponding to the joining locus J_1, one in each of the strips 2 and 7, and one before the splitting of the two strips 4 and 5.

Notice that such a labelling is obvious neither from the direct template nor from the cell complex. The fourth dimension, even for an attractor that is well-described by a two-dimensional manifold, offers more possibilities to intricate the different strips, a complexity which would have not been able to extract without our Bramah complex and our analysis in terms of homologies. The topological characterization of the attractor plotted in Fig 20 is now completed.

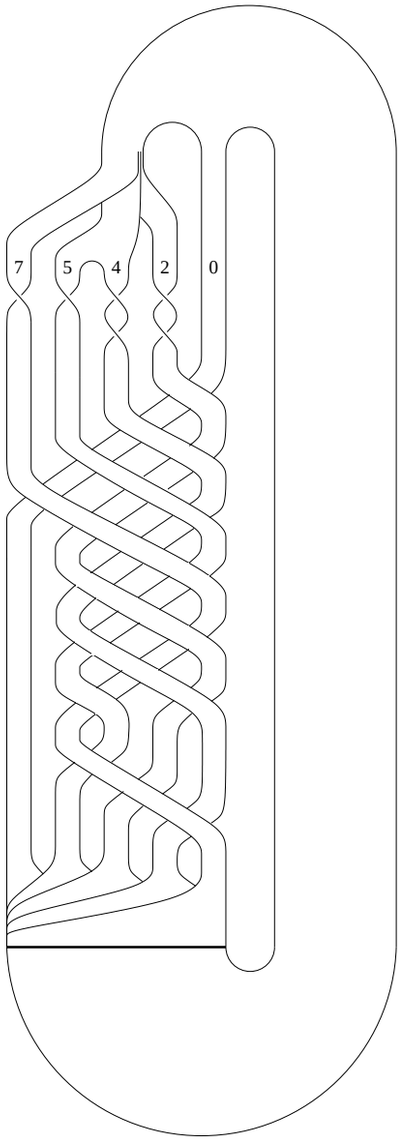

Figure 26: Reduced template for the attractor produced by the four-dimensional system (12).

V. CONCLUSION

A new concept, named templex, is here introduced with the scope of extending the description of chaotic attractors in terms of cell complexes and homology groups. The new elements that we added to the BraMAH complex are (i) the joining/splitting loci (thus allowing for an appropriate description of branched manifolds), (ii) the direction of the flow for the orientation of the cells, and (iii) the non-equivalent cycles from a digraph now associated with the complex. Indeed, the underlying flow implies that there are only some transitions between cells which are possible. This information is encoded with a directed graph whose nodes are the highest dimensional cells of the complex. The digraph is the key companion of the cell complex, both forming a templex. The templex contains all the information that is necessary to decompose the original complex into an invariant number of smaller units, the analogs of the strips in a template.

Studying the topological structure of a system through a templex involves a few steps as follows.

- Constructing a BraMAH complex from the cloud of points;
- Locating the joining/splitting loci;
- Re-orienting the cells according to the flow;
- Endowing the complex with a digraph describing how the cells are visited by the flow;
- Extracting the characteristics of the templex (generatex, stripex, twists) from the cell complex and the digraph.
- Drawing a direct template, writing the linking matrix and drawing the reduced template.

The first step was already used in previous works and outlined in Appendix A. All the next steps correspond to the main contribution of this work. The complex is handled algorithmically in terms of its cells and its border matrices. The procedure was successfully applied to four inequivalent chaotic attractors, namely the Lorenz attractor, the Rössler attractor, the three-strip Rössler attractor, the Burke-and-Shaw attractor and a four-dimensional system. Not compulsory but helpful for complex attractors, we constructed paper models to help draw the template. The attractor produced by the four-dimensional system here investigated can still be described with a template from the generating templex. Even if there is no intrinsic limitation to branched manifolds in the construction of a templex, its transcription into a template will have to be extended for more complex attractors, in the spirit of what was done for the four-dimensional attractor here characterized. The gate to a topological characterization of chaotic attractors produced by dynamical systems whose dimension is greater than three is therefore opened: other cases are currently under consideration and will be reported in forthcoming papers.

ACKNOWLEDGMENTS

Some of the ideas that led to the consideration of the templex came from stimulating discussions with Ivan Sadofschi Costa. We also thank Sylvain Mangiarotti for enriching discussions. This work is supported by the French National program LEFE (Les Enveloppes Fluides et l'Environnement) and by the CLIMAT-AMSUD 21-CLIMAT-05 project (D.S.). G.D.C. gratefully acknowledges her postdoctoral scholarship from CONICET.

SUPPLEMENTARY MATERIAL

See supplementary material for instructions to reproduce the paper model in Fig. 23.

DATA AVAILABILITY

The data that support the findings of this study are available within the article and its supplementary material, as well as from the corresponding author upon request.

Appendix A: Construction of a BraMAH complex

There are many ways of building a cell complex from a cloud of points $\mathcal{P}$ in $\mathbb{R}^N$. In this work, N is the dimension of the phase space. A BraMAH complex $K(\mathcal{P})$ is constructed in such a way that the 0-cells are a sparse subset of $\mathcal{P}$ and that each d-cell ($d \geq 2$) represents a subset of points which are locally approximating a d-ball (or a half d-ball) in $\mathbb{R}^N$. The first implementation of this scheme dates back to 1999.[33]

A brief account of the procedure is as follows. A first point $\boldsymbol{x}_0 = (x_{0,1}, x_{0,2}, \cdots, x_{0,N})$ is chosen arbitrarily. The set of neighboring points $\{\boldsymbol{x}_i = (x_{i,1}, x_{i,2}, \cdots, x_{i,N}), i = 1, \cdots, m_0\}$ with m_0 the number of neighbors of $\boldsymbol{x}_0$, is called a *patch*. To determine the value of m_0, the neighbourhood matrix $X \in \mathbb{R}^{m_0 \times N}$ around $\boldsymbol{x}_0$

$$X^0_{i,j} = \frac{1}{\sqrt{m_0}}(x_{i,j} - x_{0,j})$$

is built. A local coordinate system centered at $\boldsymbol{x}_0$ is provided by the singular vectors of X, with the singular values describing the distribution of the points inside the ball centered at $\boldsymbol{x}_0$. For a patch that is approximately lying on a d-ball in $\mathbb{R}^N$, the local singular spectrum of X has d singular values that scale linearly with the number of points m_0 in the patch as the radius r of the d-ball is increased. This property holds as long as the effects of curvature in the manifold become apparent.[32,61] The remaining $(N-d)$ singular values, which measure the deviation from the tangent space, scale as r^l with $l \geq 2$. Using this rule, the d singular values and the vectors that span the tangent space approximating the patch with axis $\boldsymbol{x}_0$ can be identified. The largest possible size m_0 of the patch is obtained when the d singular values as functions of m_0 with $m_{\min} < m_0 < m_{\max}$ present the best linear regression coefficient. Successive axes $\boldsymbol{x}_p$ with $p \geq 1$ are taken so that they are least separated from the previously chosen axis $\boldsymbol{x}_{p-1}$, until every point in $\mathcal{P}$ is in at least one patch. The regression is carried out to determine m_p for every patch p. Convex hulls are used to transform each patch of points into a κ-cell with $d = \kappa$. Due to the fact that the value of d is computed for every patch (and not imposed), $d = d(p)$ and the procedure allows for the existence of hybrid-dimensional complexes, that is, of complexes that are the union of subcomplexes of different dimensions, as in the four-dimensional system ($N = 4$) discussed in this work.

Notice that the k-cells ($0 \leq k \leq \kappa$) obtained with this procedure are not necessarily simplices, i.e. cells for which the number of vertices depends simply on k. A BraMAH complex is not simplicial by construction, but can – if necessary – be triangulated to become one, and to compute homology groups with a simplicial algorithm. Here, we use a non-simplicial algebraic code to compute homologies, as in most of our works.[33–36,62] As all complexes formed from clouds of points, a BraMAH complex will depend on the number of points in $\mathcal{P}$, that is, in this work, on the integration time window and time step. Tailored so that the nature of its highest dimensional cells is tied to the local dimension and curvature of the underlying branched manifold, a BraMAH complex is topologically faithful to the latter.

Appendix B: Computing the homology groups of the torus

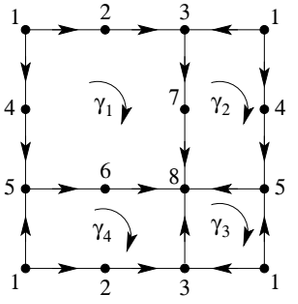

Figure 27: Complex $K(T^2)$ for the torus. The 0-cells are arbitrarily numbered. The 1-cells are oriented according to this numbering (see the arrows) and the four 2-cells are clockwise.

Let $K(T^2)$ denote a complex whose underlying space is the torus T^2 (Fig. 27). Let all the 2-cells γ_i ($i = 1, 2, 3, 4$) be clockwise oriented. Every 0-cell is a 0-cycle since, by definition, $\partial_0(C_0) = 0$. All the 0-cells are homologous because one can reach all of them travelling through the 1-cells of the complex, and there is a single 0-generator. The four 2-cells are bounded by the 1-chains

$$\begin{cases} \partial_2(\gamma_1) = C_1^1 = \langle 1,2\rangle + \langle 2,3\rangle + \langle 3,7\rangle + \langle 7,8\rangle - \langle 6,8\rangle - \langle 5,6\rangle \\ \quad -\langle 4,5\rangle - \langle 1,4\rangle \\ \partial_2(\gamma_2) = C_1^2 = -\langle 1,3\rangle + \langle 1,4\rangle + \langle 4,5\rangle + \langle 5,8\rangle - \langle 7,8\rangle - \langle 3,7\rangle \\ \partial_2(\gamma_3) = C_1^3 = -\langle 5,8\rangle - \langle 1,5\rangle + \langle 1,3\rangle + \langle 3,8\rangle \\ \partial_2(\gamma_4) = C_1^4 = \langle 5,6\rangle + \langle 6,8\rangle - \langle 3,8\rangle - \langle 2,3\rangle - \langle 1,2\rangle + \langle 1,5\rangle, \end{cases}$$

respectively. By definition, these boundaries $[\partial_1(C_1^i) = 0]$ are 1-cycles and form the set $\mathcal{B}_1(K(T^2)) = \mathrm{im}(\partial_2)$. In order to compute the set of 1-generators, let us first

compute $\mathcal{Z}_1$, i.e. the kernel of the transpose of M_1, in which only non-zero elements are reported:

$$M_1^T = \begin{array}{c|cccccccc} \partial_1 & \langle 1\rangle & \langle 2\rangle & \langle 3\rangle & \langle 4\rangle & \langle 5\rangle & \langle 6\rangle & \langle 7\rangle & \langle 8\rangle \\ \hline \langle 1,2\rangle & -1 & 1 & & & & & & \\ \langle 1,3\rangle & -1 & & 1 & & & & & \\ \langle 1,4\rangle & -1 & & & 1 & & & & \\ \langle 1,5\rangle & -1 & & & & 1 & & & \\ \langle 2,3\rangle & & -1 & 1 & & & & & \\ \langle 3,7\rangle & & & -1 & & & & 1 & \\ \langle 3,8\rangle & & & -1 & & & & & 1 \\ \langle 4,5\rangle & & & & -1 & 1 & & & \\ \langle 5,6\rangle & & & & & -1 & 1 & & \\ \langle 5,8\rangle & & & & & -1 & & & 1 \\ \langle 6,8\rangle & & & & & & -1 & & 1 \\ \langle 7,8\rangle & & & & & & & -1 & 1 \end{array} \tag{B1}$$

$$\begin{cases} C_1^5 = \langle 1,2\rangle + \langle 2,3\rangle - \langle 1,3\rangle \\ C_1^6 = -\langle 1,3\rangle + \langle 1,5\rangle - \langle 3,8\rangle + \langle 5,8\rangle \\ C_1^7 = \langle 1,4\rangle + \langle 4,5\rangle - \langle 1,5\rangle \\ C_1^8 = \langle 3,7\rangle + \langle 7,8\rangle - \langle 3,8\rangle \\ C_1^9 = -\langle 1,3\rangle + \langle 1,5\rangle - \langle 3,8\rangle + \langle 5,6\rangle + \langle 6,8\rangle. \end{cases} \tag{B2}$$

Let us show that $C_1^5 \sim C_1^9 - C_1^6$. They are homologous if there is a 2-chain C_2 such that $\partial_2(C_2) = C_1^5 - (C_1^9 - C_1^6)$. The action of the boundary operator ∂_2 can be written in the matrix form M_2. This matrix is used to compute $\mathcal{B}_1(K(T^2))$, and therefore $C_1^6 \in \mathcal{B}_1(K(T^2))$.

$$M_2 = \begin{array}{c|cccc} \partial_2 & \gamma_1 & \gamma_2 & \gamma_3 & \gamma_4 \\ \hline \langle 1,2\rangle & 1 & & & -1 \\ \langle 1,3\rangle & & -1 & 1 & \\ \langle 1,4\rangle & -1 & 1 & & \\ \langle 1,5\rangle & & & -1 & 1 \\ \langle 2,3\rangle & 1 & & & -1 \\ \langle 3,7\rangle & 1 & -1 & & \\ \langle 3,8\rangle & & & 1 & -1 \\ \langle 4,5\rangle & -1 & 1 & & \\ \langle 5,6\rangle & -1 & & & 1 \\ \langle 5,8\rangle & & 1 & -1 & \\ \langle 6,8\rangle & -1 & & & 1 \\ \langle 7,8\rangle & 1 & -1 & & \end{array} \tag{B3}$$

in which only non-zero elements are reported. Using the 2-chain $\gamma_1 + \gamma_2$, we get

$$\begin{aligned} \partial_2(\gamma_1+\gamma_2) &= \langle 1,2\rangle + \langle 2,3\rangle - \langle 1,3\rangle + \langle 1,4\rangle + \langle 4,5\rangle \\ &\quad + \langle 5,8\rangle - \langle 6,8\rangle - \langle 5,6\rangle - \langle 4,5\rangle - \langle 1,4\rangle \\ &= \langle 1,2\rangle + \langle 2,3\rangle - \langle 1,3\rangle - (\langle 5,6\rangle + \langle 6,8\rangle - \langle 5,8\rangle) \\ &= C_1^5 - (C_1^9 - C_1^6) \end{aligned}$$

Similarly, one can prove that $\partial_2(\gamma_1 + \gamma_4) = C_1^8 - C_1^7$. It is thus possible to show that the torus T^2 is associated with $\mathcal{H}_1 = \{C_1^5, C_1^7\}$, that is, it has two 1-generators.

Since there are no 3-cells in a complex of dimension 2, $\mathcal{B}_2(K(T^2)) = \varnothing$. Using that $C_1^5 \sim C_1^9 - C_1^6$, one can show that $\partial_2(\gamma_1 + \gamma_2 + \gamma_3 + \gamma_4) = 0$: this 2-chain is therefore a 2-cycle. It can be shown that all the 2-cycles are homologous to $\gamma_1 + \gamma_2 + \gamma_3 + \gamma_4$. Consequently, $\mathcal{H}_2(K(T^2)) = \{\gamma_1 + \gamma_2 + \gamma_3 + \gamma_4\}$: it is made of a single 2-cycle. The Betti numbers for a torus are thus $\beta_0 = 1$, $\beta_1 = 2$, and $\beta_2 = 1$, meaning that a torus T^2 is a single connected set, with two 1-generators, and one cavity.

To sum up:

$$\begin{aligned} \mathcal{H}_0 &= [[\langle 1\rangle]] \\ \mathcal{H}_1 &= [[\langle 1,4\rangle - \langle 1,5\rangle + \langle 4,5\rangle, \langle 1,2\rangle - \langle 1,3\rangle + \langle 2,3\rangle]] \\ \mathcal{H}_2 &= [[\gamma_1 + \gamma_2 + \gamma_3 + \gamma_4]] \end{aligned}$$

Since $K(T^2)$ is uniformly oriented, additional properties can be extracted. Here:

$$\partial(\Gamma) = \partial\left(\sum_i \gamma_i\right) = 0$$

since when the boundary operator is applied to the sum of all the 2-cells, the totality of the 1-cells cancel each other. This means that the torus has no boundaries: in other words, all the 1-cells in the contour of the complex in its planar representation are matched, without torsions. On the other hand, as $\partial\Gamma$ is null, there are no torsion elements.

Appendix C: From the direct template to the reduced one

The direct template drawn in Fig. 17(a) can be described by the linking matrices

$$L_{ij} = \left[\begin{array}{cc|cc} +1 & +1 & +1 & 0 \\ +1 & +1 & 0 & 0 \end{array}\right] \otimes \left[\begin{array}{cc|cc} +1 & +1 & +1 & 0 \\ +1 & +1 & 0 & 0 \end{array}\right] \tag{C1}$$

Combining each global torsion with the next mixer, we get

$$L_{ij} = \left[\begin{array}{cc} +1 & +1 \\ +1 & +2 \end{array}\right] \otimes \left[\begin{array}{cc} +1 & +1 \\ +1 & +2 \end{array}\right] \tag{C2}$$

To transform a multiplication into an addition between linking matrices, it is necessary to extend each matrix into a 4×4 matrix with some rules as follows.[63] The first matrix is simply expanded by replacing each of its element L_{ij} into a 2×2 submatrix whose elements are copies of the initial element L_{ij}. The second matrix is obtained by replacing each of its elements L_{ij} with a block B corresponding to the initial 2×2 second linking matrix transformed as[63]

$$L_{ij}^{\mathrm{E}} = \begin{cases} B & L_{ii} \text{ and } L_{jj} \text{ are both even;} \\ B^{\text{-}} & L_{ii} \text{ is odd and } L_{jj} \text{ is even;} \\ B^{|} & L_{ii} \text{ is even and } L_{jj} \text{ is odd;} \\ B^{p} & L_{ii} \text{ and } L_{jj} \text{ are both odd.} \end{cases} \tag{C3}$$

where

- $B^{\text{-}\_}$ is matrix B whose row order is reversed;
- $B^{|}$ is matrix B whose column order is reversed;
- B^{p} is matrix B which was permuted.

In the present case, the linking matrix L_{ij}^{E} is thus expanded as

$$L_{ij}^{\mathrm{E}} = \begin{bmatrix} B^{\mathrm{p}} & B^{\text{--}} \\ B^{|} & B \end{bmatrix} = \begin{bmatrix} 2 & 1 & 1 & 2 \\ 1 & 1 & 1 & 1 \\ 1 & 1 & 1 & 1 \\ 2 & 1 & 1 & 2 \end{bmatrix} \tag{C4}$$

$$\begin{aligned} L_{ij}^{\mathrm{E}} &= \begin{vmatrix} 1 & 1 & 1 & 1 \\ 1 & 1 & 1 & 1 \\ 1 & 1 & 2 & 2 \\ 1 & 1 & 2 & 2 \end{vmatrix} + \begin{vmatrix} 0 & 0 & 0 & 0 \\ 0 & 0 & 0 & 1 \\ 0 & 0 & 0 & 0 \\ 0 & 1 & 0 & 0 \end{vmatrix} + \begin{bmatrix} 2 & 1 & 1 & 2 \\ 1 & 1 & 1 & 1 \\ 1 & 1 & 1 & 1 \\ 2 & 1 & 1 & 2 \end{bmatrix} \\ &= \begin{Vmatrix} 3 & 2 & 2 & 3 \\ 2 & 2 & 2 & 3 \\ 2 & 2 & 3 & 3 \\ 3 & 3 & 3 & 4 \end{Vmatrix} \end{aligned} \tag{C5}$$

where the second matrix is a permutation matrix added to restore the correct branching between the different strips (see Rosalie and Letellier,[63] for details). This linking matrix is in agreement with the matrix proposed for this Burke and Shaw attractor.[58]

REFERENCES

[1] J. Barrow-Green, *Poincaré and the three body problem*, History of Mathematics, Vol. 11 (American Mathematical Society, 1997).
[2] H. Poincaré, "Sur le problème des trois corps et les équations de la dynamique," Acta mathematica **13**, 1–270 (1890).
[3] H. Poincaré, "Analysis situs," Journal de l'École Polytechnique **1**, 1–121 (1895).
[4] P. G. Tait, "On knots I," Transactions of the Royal Society of Edinburgh **28**, 145–190 (1877).
[5] P. G. Tait, "On knots II," Transactions of the Royal Society of Edinburgh **32**, 327–342 (1884).
[6] J. W. Alexander, "A proof of the invariance of certain constants of analysis situs," Transactions of the American Mathematical Society **16**, 148–154 (1915).
[7] J. W. Alexander and G. B. Briggs, "On types of knotted curves," Annals of Mathematics II **28**, 562–586 (1926).
[8] K. Reidemeister, "Knoten und Gruppen," Abhandlungen aus dem Mathematischen Seminar der Universität Hamburg **5**, 7–23 (1927).
[9] V. K. Mel'nikov, "On the stability of a center for time-periodic perturbations," Trudy Moskovskogo Matematicheskogo Obshchestva **12**, 3–52 (1963), in Russian.
[10] E. N. Lorenz, "Deterministic nonperiodic flow," Journal of the Atmospheric Sciences **20**, 130–141 (1963).
[11] R. F. Williams, "Expanding attractors," Publications Mathématiques de l'Institut des Hautes Études Scientifiques **43**, 169–203 (1974).
[12] J. Birman and R. F. Williams, "Knotted periodic orbits in dynamical systems I. Lorenz's equations," Topology **22**, 47–82 (1983).
[13] G. B. Mindlin and R. Gilmore, "Topological analysis and synthesis of chaotic time series," Physica D **58**, 229–242 (1992).
[14] R. W. Ghrist, P. J. Holmes, and M. C. Sullivan, "Knots and links in three-dimensional flows," in *Lecture Notes in Mathematics*, Vol. 1654 (Springer, Berlin, Heidelberg, 1997).
[15] R. Gilmore, "Topological analysis of chaotic dynamical systems," Reviews of Modern Physics **70**, 1455–1529 (1998).
[16] N. B. Tufillaro, T. Abbott, and J. Reilly, *An experimental approach to nonlinear dynamics and chaos* (Addison-Wesley, Redwood City, CA, 1992).
[17] D. Ruelle and F. Takens, "On the nature of turbulence," Communications in Mathematical Physics **20**, 167–192 (1971).
[18] R. Gilmore and M. Lefranc, *The topology of chaos* (Wiley, 2003).
[19] C. Letellier, E. Roulin, and O. E. Rössler, "Inequivalent topologies of chaos in simple equations," Chaos, Solitons & Fractals **28**, 337–360 (2006).
[20] C. Letellier, "Branched manifolds for the three types of unimodal maps," Communications in Nonlinear Science and Numerical Simulation **101**, 105869 (2021).
[21] E. Betti, "Sopra gli spazi di un numero qualunque di dimensioni," Annali di Matematica Pura ed Applicata **2**, 140–158 (1871).
[22] H. Poincaré, "Second complément à l'analysis situs," Proceedings of the London Mathematical Society **32**, 277–308 (1900).
[23] L. Vietoris, "über den höheren Zusammenhang kompakter Räume und eine Klasse von zusammenhangstreuen Abbildungen," Mathematische Annalen **97**, 454–472 (1927).
[24] H. Hopf, "verbessert in eine Verallgemeinerung der Euler-Poincaréschen Formel," Nachrichten der Göttinger Akademie der Wissenschaften , 127–136 (1928).
[25] H. Hopf, "A new proof of the Lefschetz formula for invariant points," Proceedings of the National Academy of Sciences **14**, 149–153 (1928).
[26] W. Mayer, "Über abstrakte Topologie," Monatschefte für Mathematik und Physik **36**, 1–42 and 219–258 (1929).
[27] J. Dieudonné, *A history of algebraic and differential topology 1900-1960* (Birkhäuser, Boston, MA, 1989).
[28] C. A. Weibel, "History of homological algebra," in *History of Topology*, edited by I. James (North-Holland, Amsterdam, 1999) pp. 797–836.
[29] E. Noether, "Ableitung der Elementarteilertheorie aus der Gruppentheorie," Jahresbericht der Deutschen Mathematiker-Vereinigung **34** (1926).
[30] L. C. Kinsey, *Topology of surfaces* (Springer-Verlag, New York, 1993).
[31] J. R. Munkres, *Elements of algebraic topology* (CRC press, 2018).
[32] M. R. Muldoon, R. S. MacKay, J. P. Huke, and D. S. Broomhead, "Topology from time series," Physica D **65**, 1–16 (1993).
[33] D. Sciamarella and G. B. Mindlin, "Topological structure of chaotic flows from human speech data," Physical Review Letters **64**, 1450–1453 (2001).
[34] D. Sciamarella and G. B. Mindlin, "Unveiling the topological structure of chaotic flows from data," Physical Review E **64**, 036209 (2001).
[35] G. D. Charó, G. Artana, and D. Sciamarella, "Topology of dynamical reconstructions from Lagrangian data," Physica D **405**, 132371 (2020).
[36] G. D. Charó, G. Artana, and D. Sciamarella, "Topological colouring of fluid particles unravels finite-time coherent sets," Journal of Fluid Mechanics **923**, A17 (2021).
[37] K. Mischaikow, M. Mrozek, J. Reiss, and A. Szymczak, "Construction of symbolic dynamics from experimental time series," Physical Review Letters **82**, 1144–1147 (1999).
[38] M. Lefranc, "Alternative determinism principle for topological analysis of chaos," Physical Review E **74**, 035202 (2006).
[39] M. Lefranc, "Reflections from the fourth dimension," in *Topology and Dynamics of Chaos*, edited by C. Letellier and R. Gilmore (World Scientific Publishing, 2013) pp. 205–226.
[40] S. Neukirch and H. Giacomini, "Shape of attractors for three-dimensional dissipative dynamical systems," Physical Review E **61**, 5098–5107 (2000).

[41]T. D. Tsankov and R. Gilmore, "Strange attractors are classified by bounding tori," Physical Review Letters **91**, 134104 (2003).
[42]T. D. Tsankov and R. Gilmore, "Topological aspects of the structure of chaotic attractors in $\mathbb{R}^3$," Physical Review E **69**, 056206 (2004).
[43]M. Rosalie and C. Letellier, "Systematic template extraction from chaotic attractors: I. Genus-one attractors with an inversion symmetry," Journal of Physics A **46**, 375101 (2013).
[44]C. Letellier, P. Dutertre, and B. Maheu, "Unstable periodic orbits and templates of the Rössler system: Toward a systematic topological characterization," Chaos **5**, 271–282 (1995).
[45]R. Miranda and E. Stone, "The proto-Lorenz system," Physics Letters A **178**, 105–113 (1993).
[46]C. Letellier and G. Gouesbet, "Topological characterization of a system with high-order symmetries: the proto-Lorenz system," Physical Review E **52**, 4754–4761 (1995).
[47]J. Birman and R. F. Williams, "Knotted periodic orbits in dynamical systems II. Knot holders for fibred knots," Contemporary Mathematics **20**, 1–60 (1983).
[48]D. Rolfsen, *Knots and Links* (AMS Chelsea Publishing, 1976).
[49]R. Ghrist, *Elementary Applied Topology*, 1st ed. (Createspace, 2014).
[50]G. D. Charó, M. D. Chekroun, D. Sciamarella, and M. Ghil, "Noise-driven topological changes in chaotic dynamics," Chaos **31**, 103115 (2021).
[51]D. D. Nolte, "The tangled tale of phase space," Physics today **63**, 33–38 (2010).
[52]C. Letellier, L. A. Aguirre, and J. Maquet, "Relation between observability and differential embeddings for nonlinear dynamics," Physical Review E **71**, 066213 (2005).
[53]C. Letellier and R. Gilmore, "Covering dynamical systems: Two-fold covers," Physical Review E **63**, 016206 (2001).
[54]O. E. Rössler, "An equation for continuous chaos," Physics Letters A **57**, 397–398 (1976).
[55]C. Letellier, N. Stankevich, and O. E. Rössler, "Dynamical taxonomy : some taxonomic ranks to systematically classify every chaotic attractor," International Journal of Bifurcation & Chaos , To appear (2022).
[56]O. E. Rössler, "Chaotic behavior in simple reaction system," Zeitschrift für Naturforschung A **31**, 259–264 (1976).
[57]R. Shaw, "Strange attractor, chaotic behavior and information flow," Zeitschrift für Naturforschung A **36**, 80–112 (1981).
[58]C. Letellier, P. Dutertre, J. Reizner, and G. Gouesbet, "Evolution of multimodal map induced by an equivariant vector field," Journal of Physics A **29**, 5359–5373 (1996).
[59]C. Letellier, T. D. Tsankov, G. Byrne, and R. Gilmore, "Large-scale structural reorganization of strange attractors," Physical Review E **72**, 026212 (2005).
[60]B. Deng, "Constructing homoclinic orbits and chaotic attractors," International Journal of Bifurcation & Chaos **4**, 823–841 (1994).
[61]D. S. Broomhead, R. Jones, and G. P. King, "Topological dimension and local coordinates from time series data," Journal of Physics A **20**, L563–L569 (1987).
[62]G. D. Charó, D. Sciamarella, S. Mangiarotti, G. Artana, and C. Letellier, "Equivalence between the unsteady double-gyre system and a 4D autonomous conservative chaotic system," Chaos **29**, 123126 (2019).
[63]M. Rosalie and C. Letellier, "Systematic template extraction from chaotic attractors: II. Genus-one attractors with multiple unimodal folding mechanisms," Journal of Physics A **48**, 235101 (2015).

PLEASE CITE THIS ARTICLE AS DOI: 10.1063/5.0092933

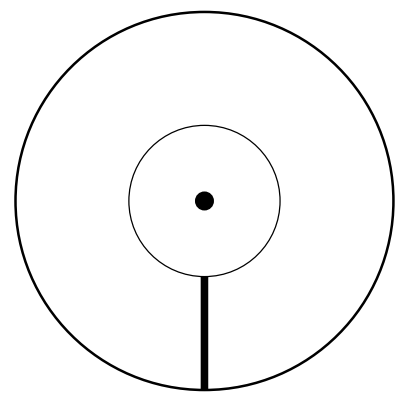

PLEASE CITE THIS ARTICLE AS DOI: 10.1063/5.0092933

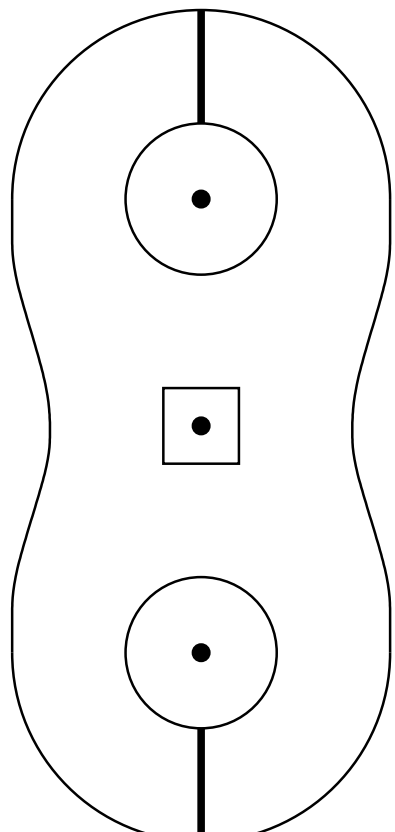

PLEASE CITE THIS ARTICLE AS DOI: 10.1063/5.0092933

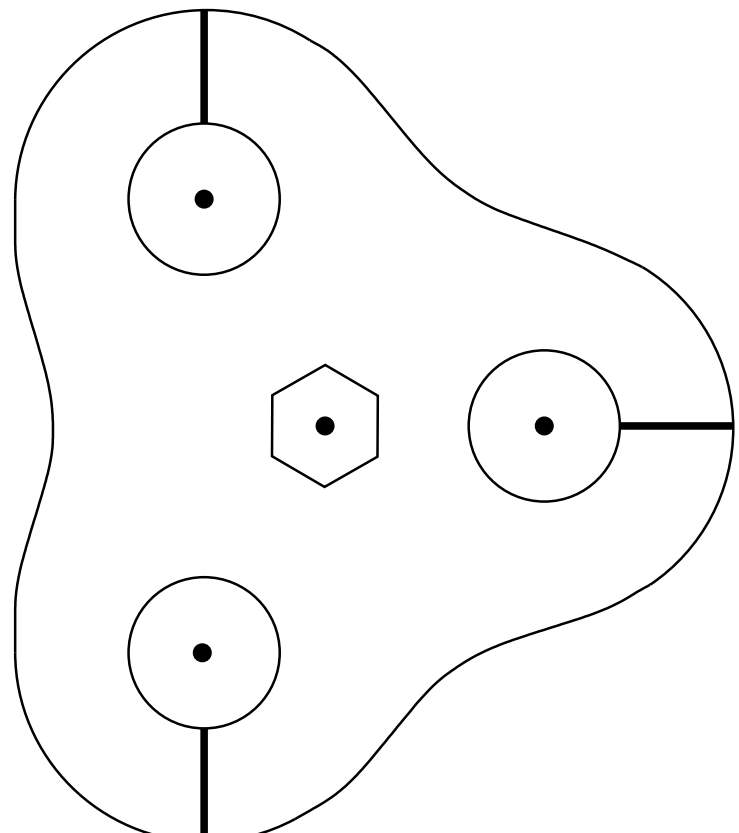

PLEASE CITE THIS ARTICLE AS DOI: 10.1063/5.0092933

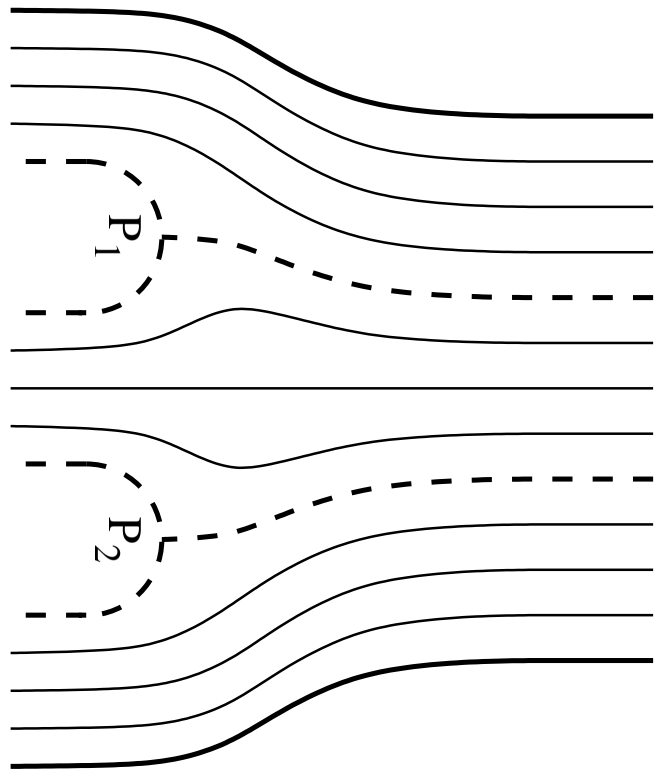

PLEASE CITE THIS ARTICLE AS DOI: 10.1063/5.0092933

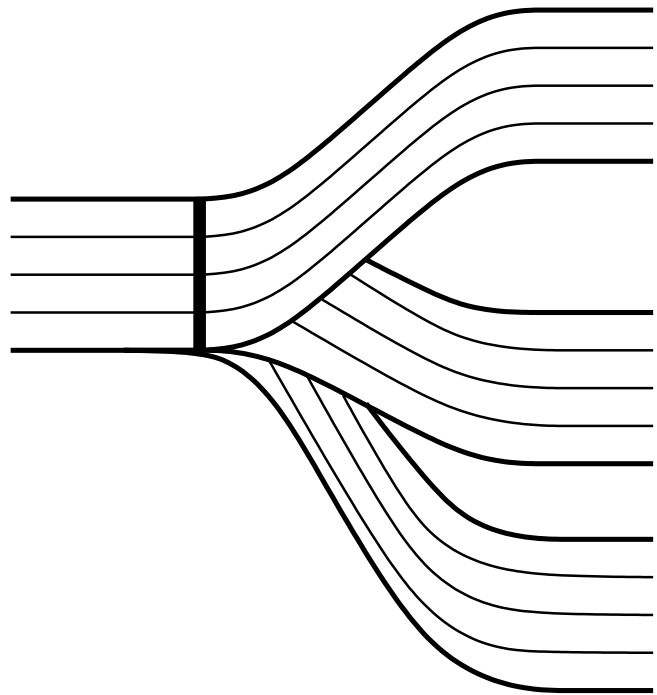

Chaos

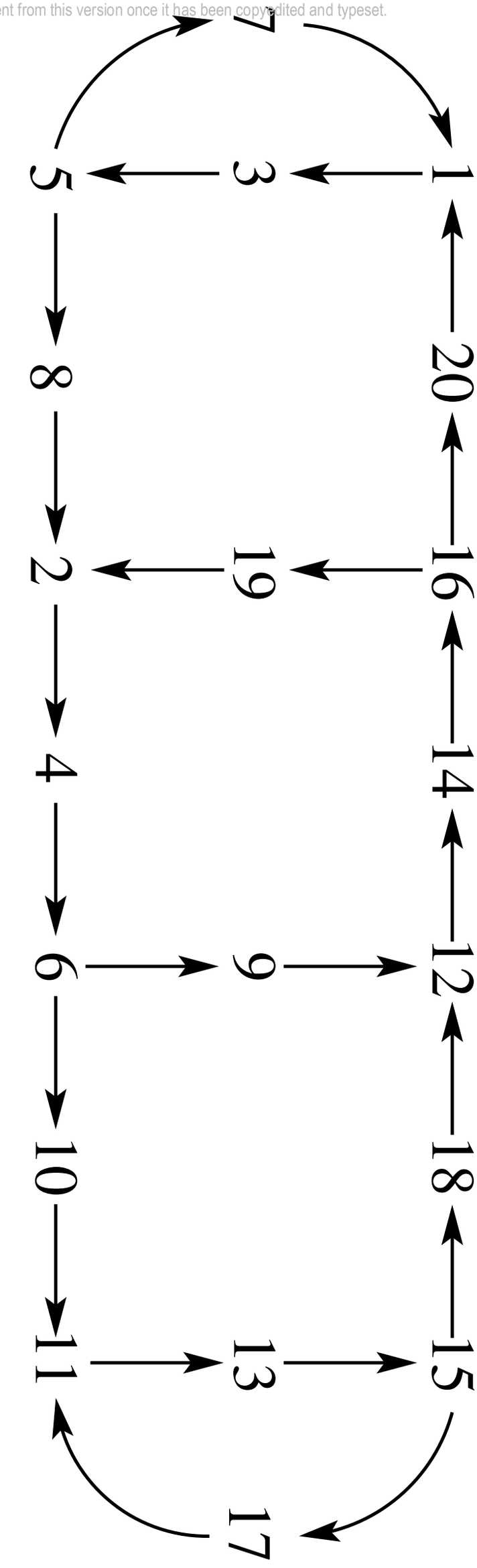

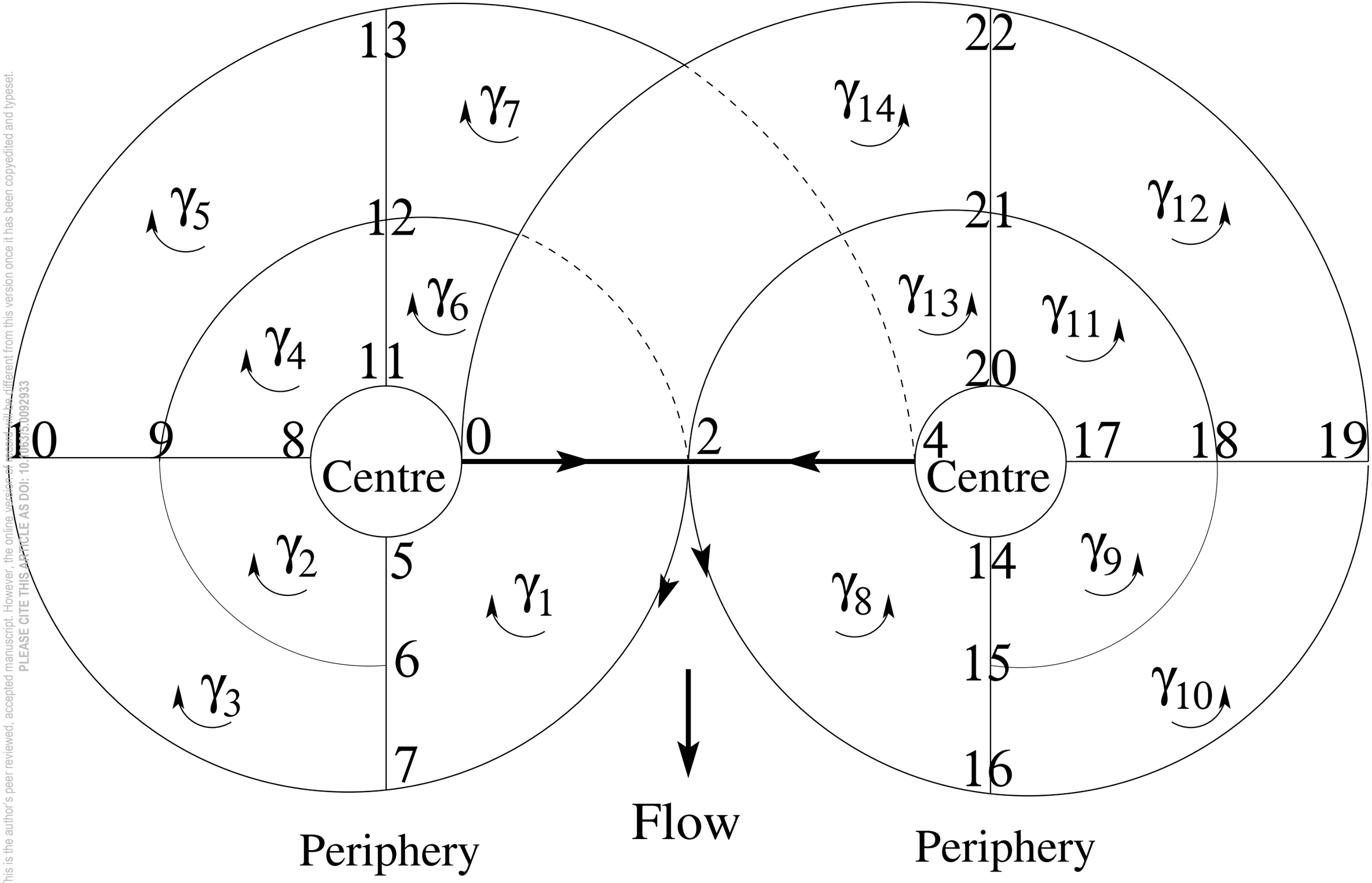

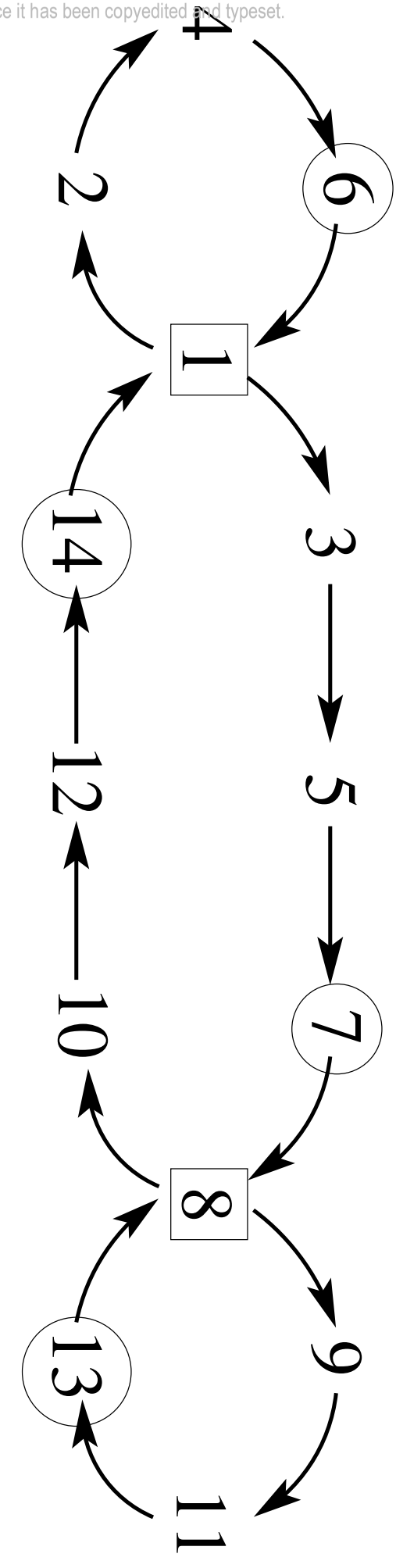

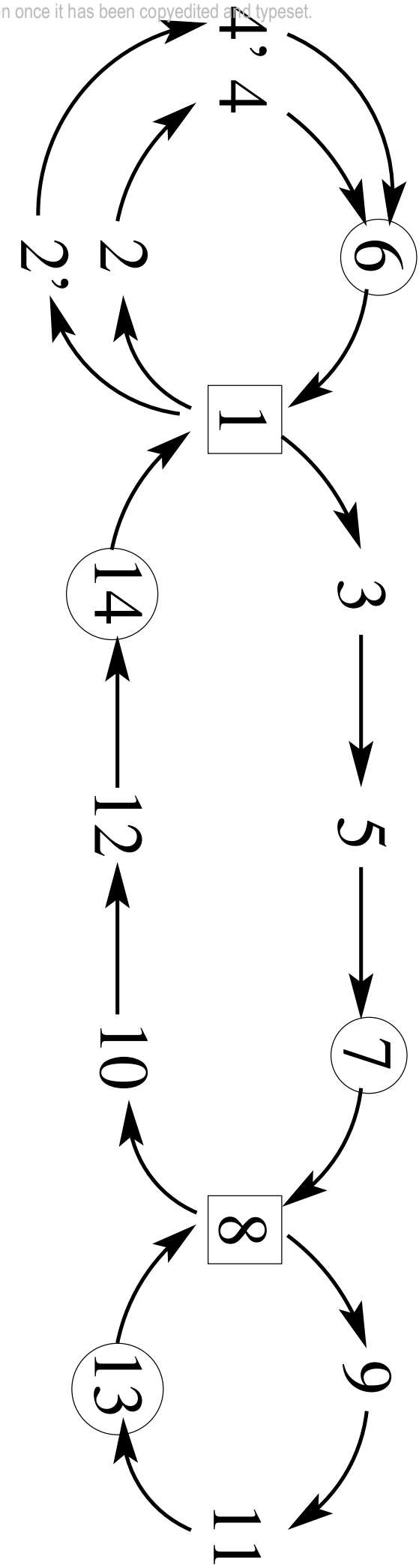

Chaos

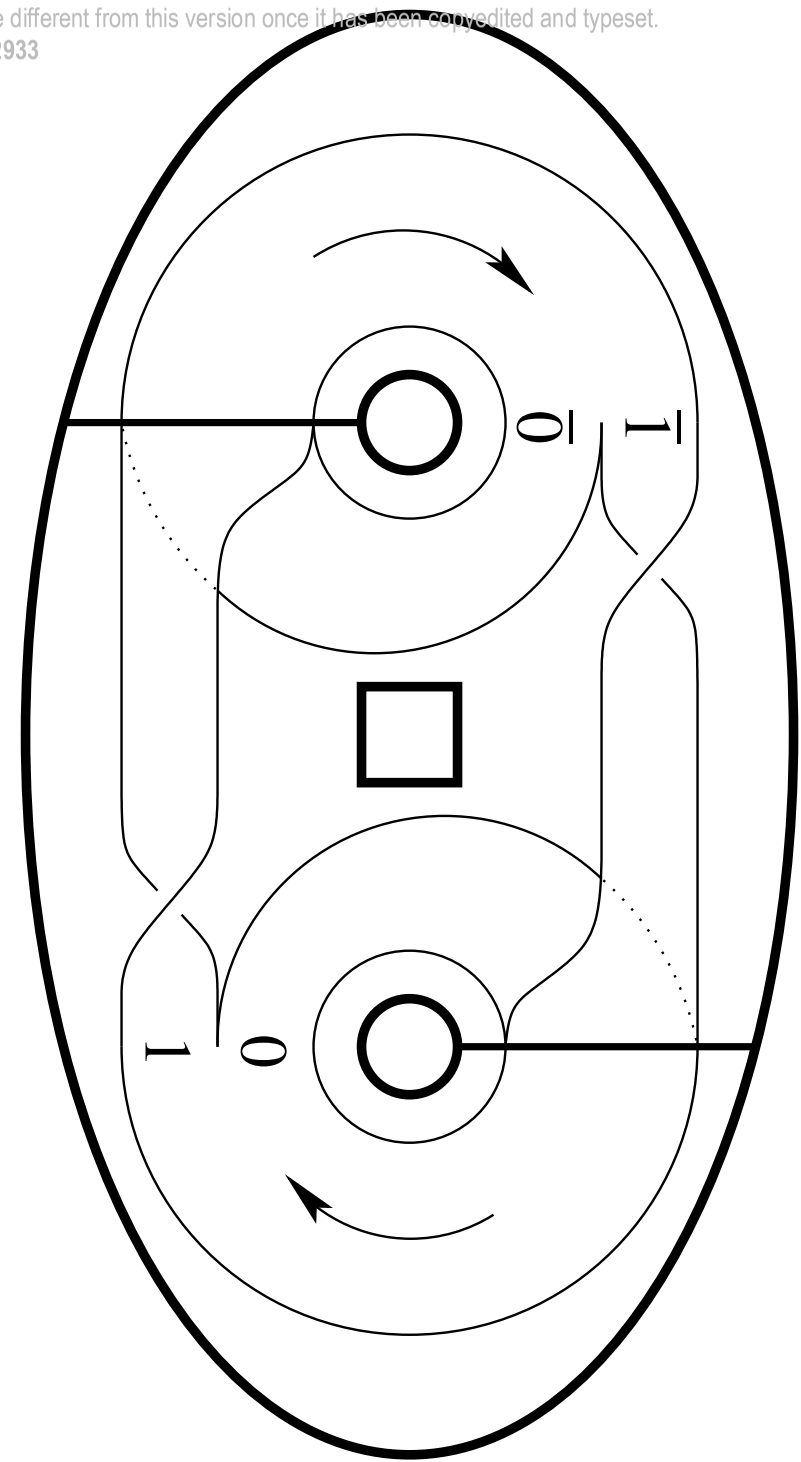

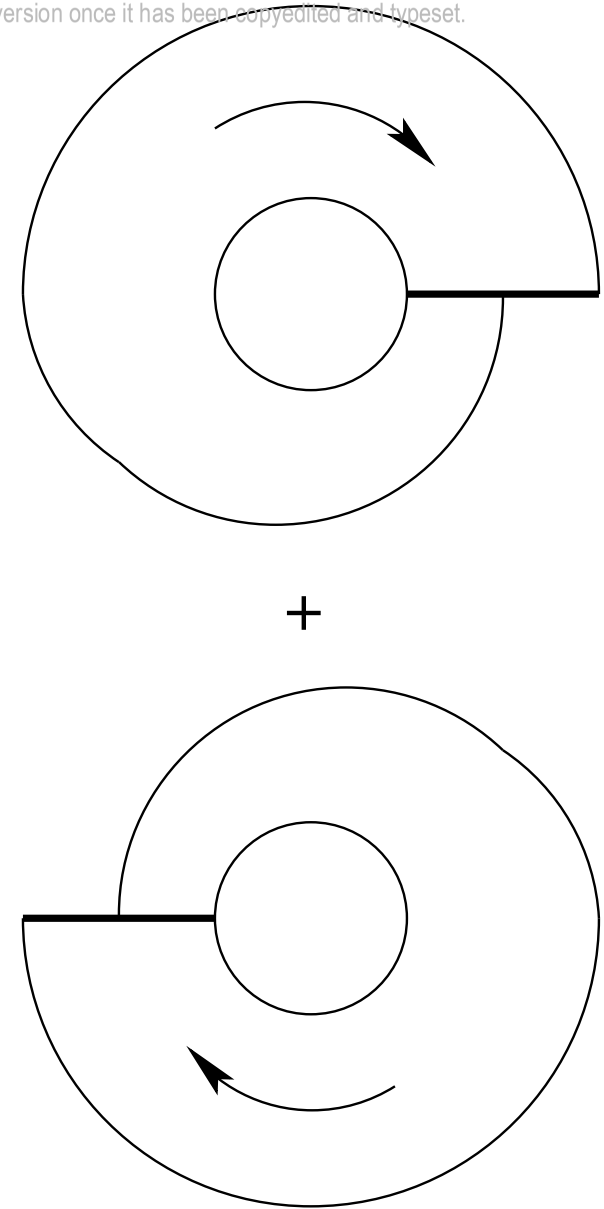

PLEASE CITE THIS ARTICLE AS DOI: 10.1063/5.0092933

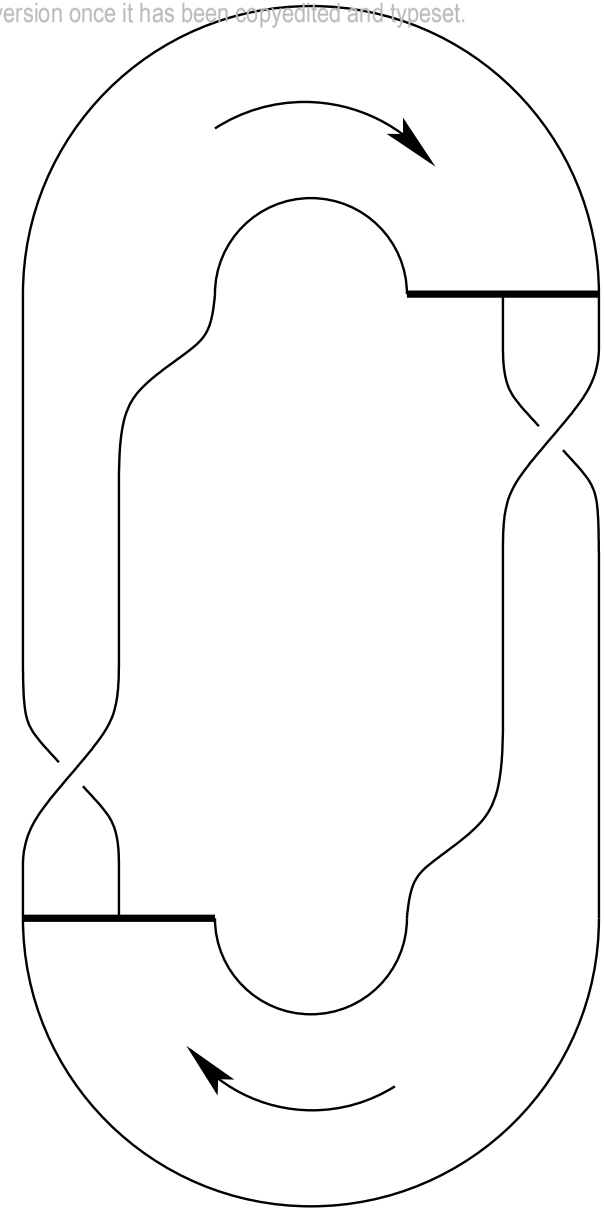

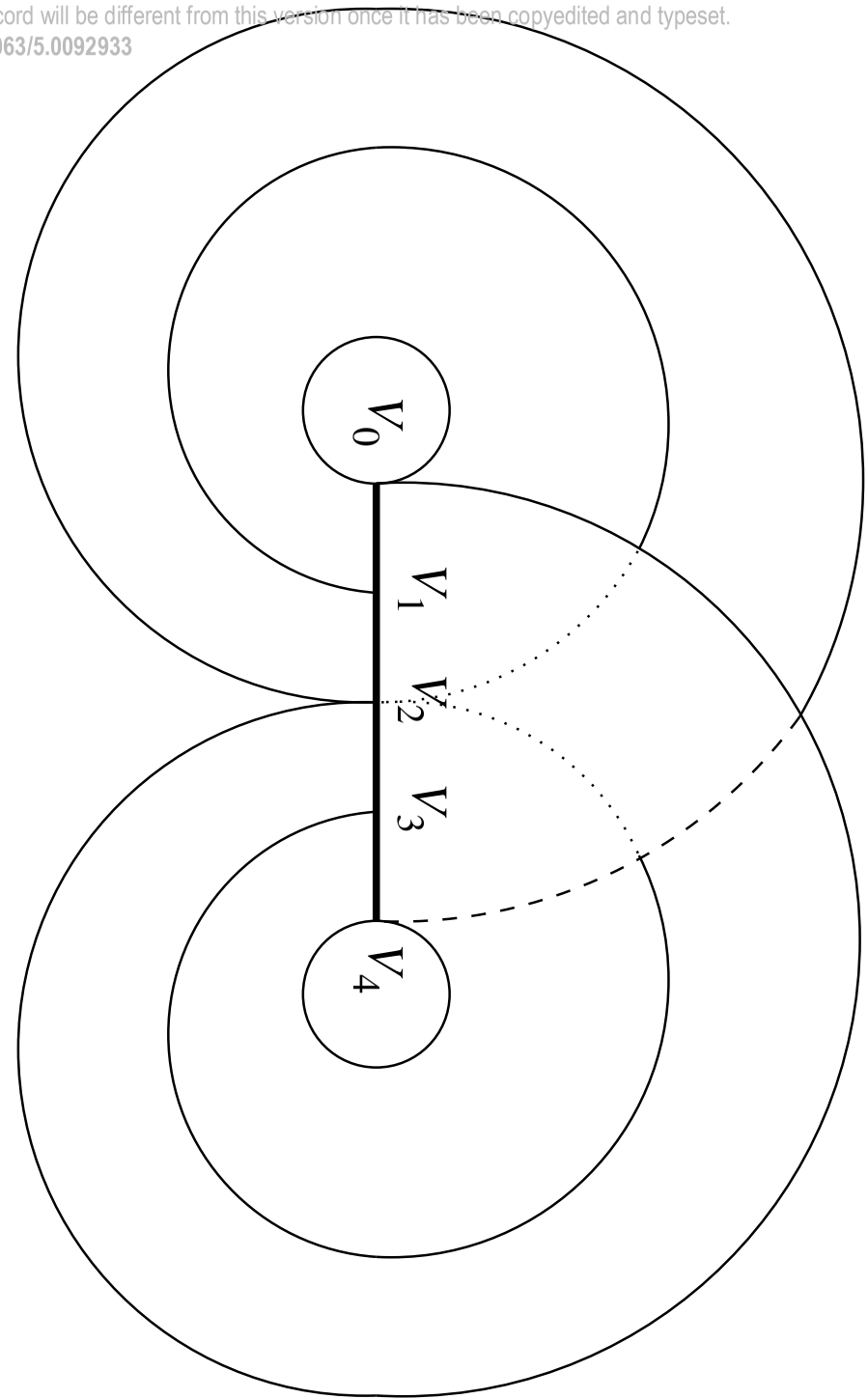

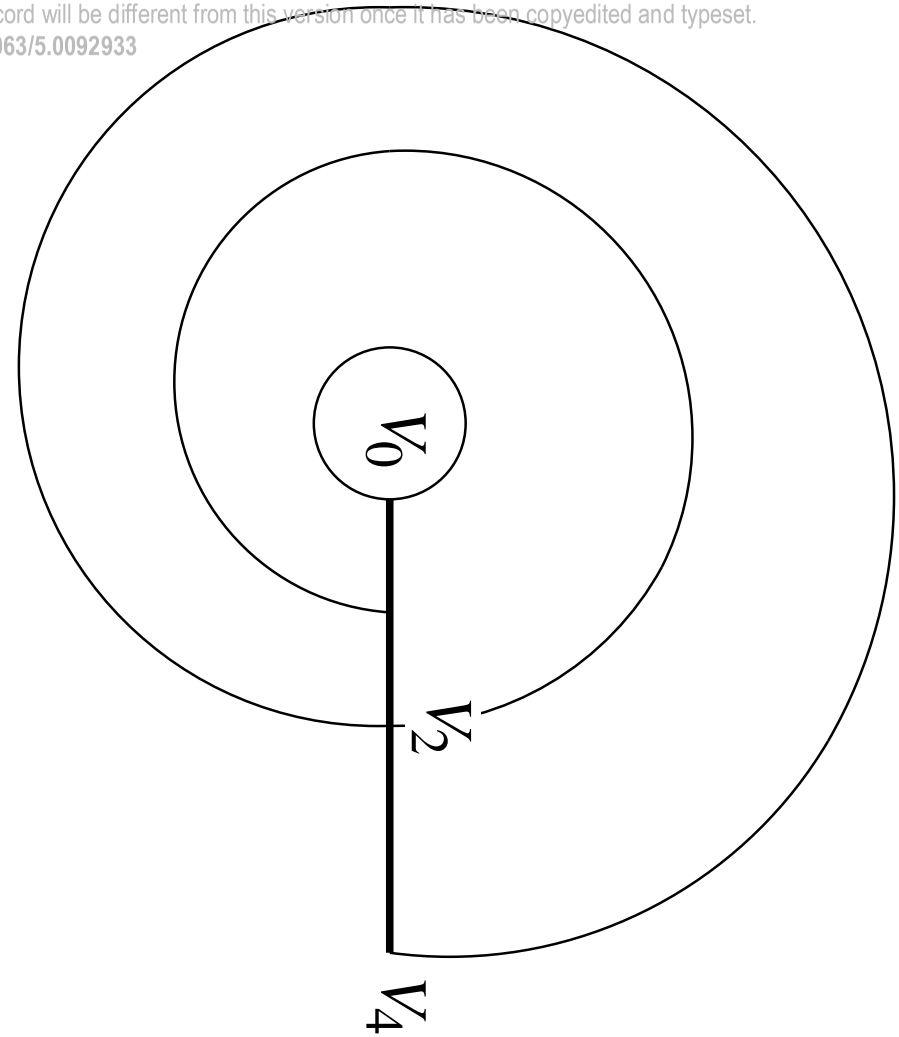

PLEASE CITE THIS ARTICLE AS DOI: 10.1063/5.0092933

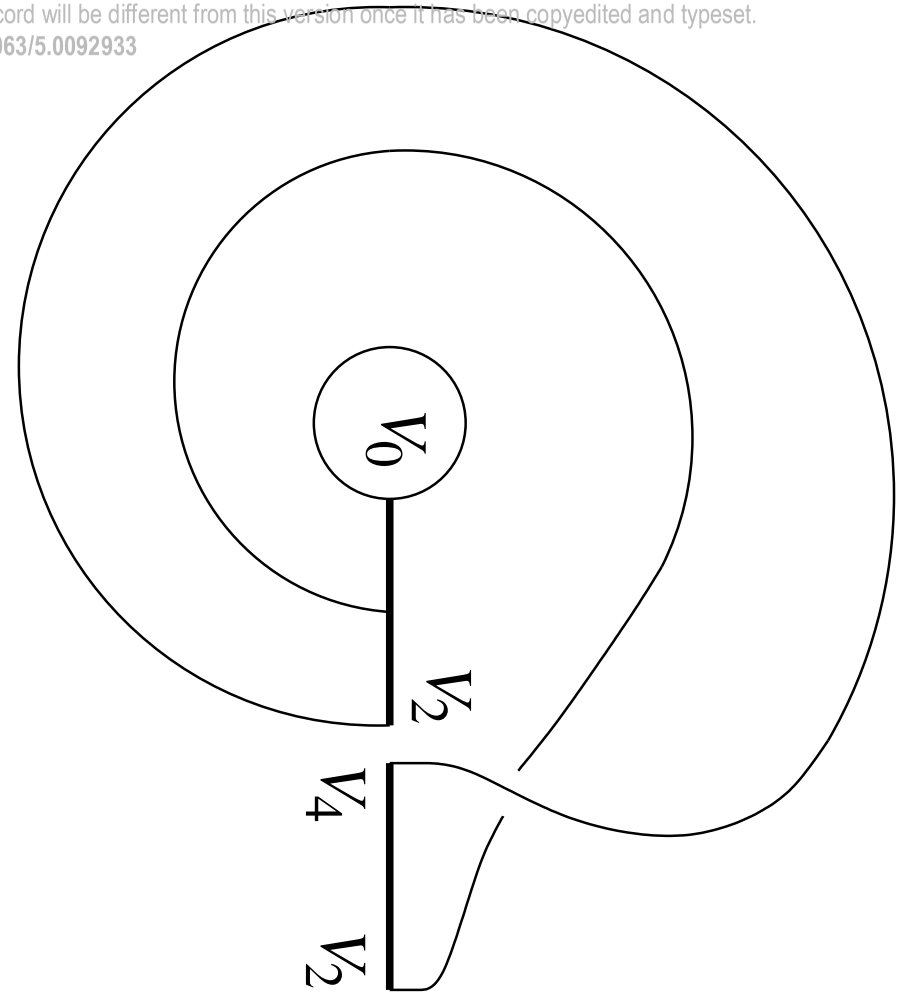

PLEASE CITE THIS ARTICLE AS DOI: 10.1063/5.0092933

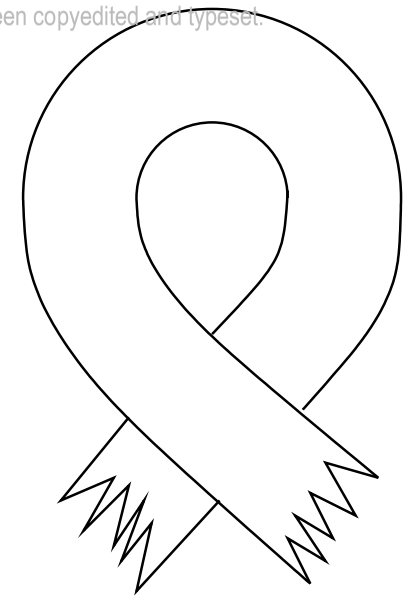

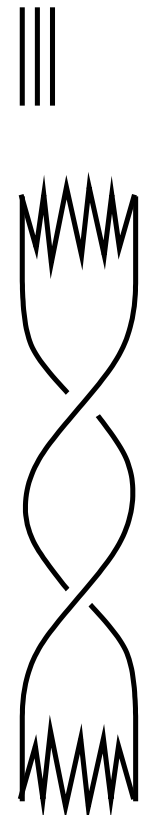

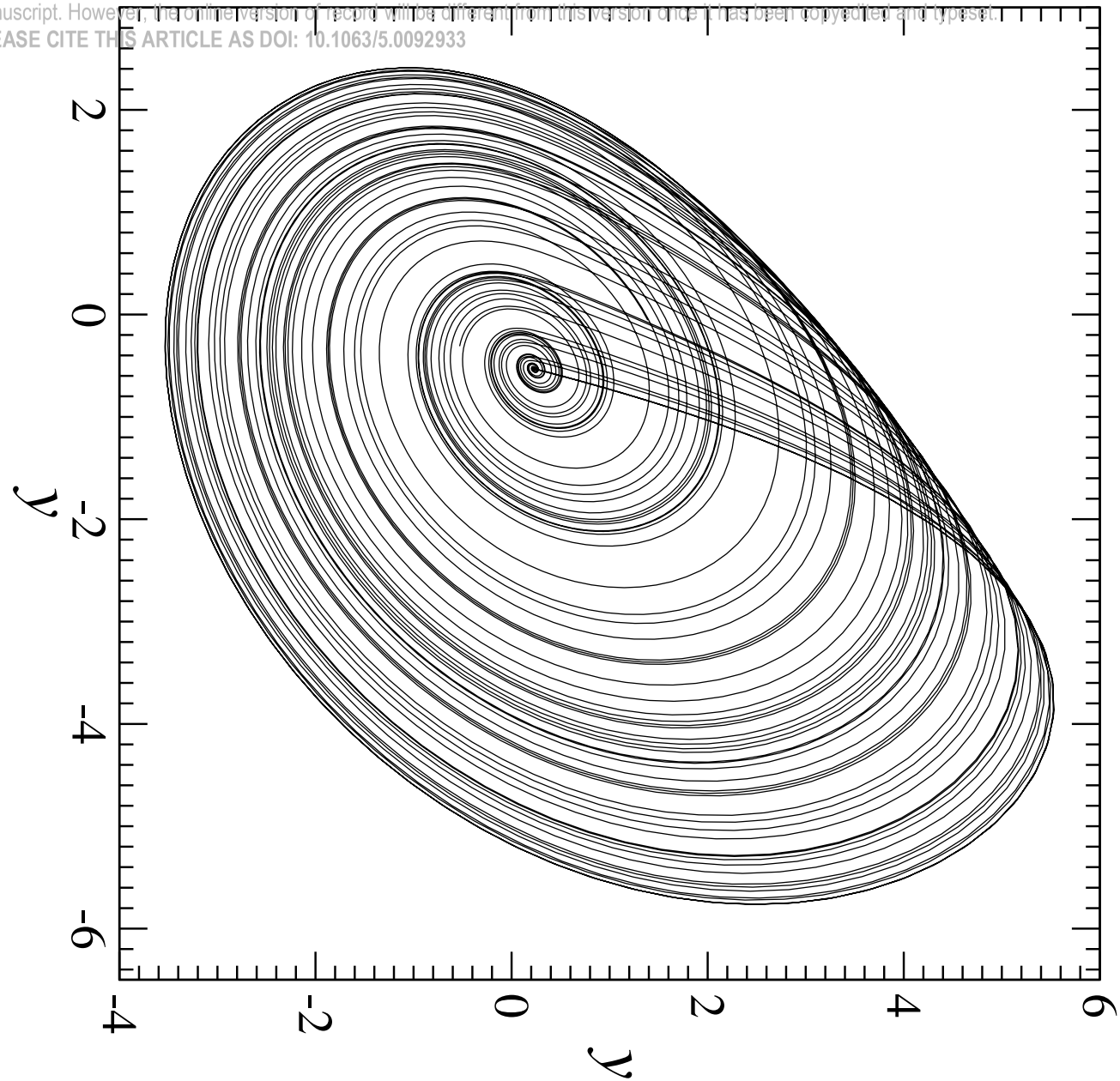

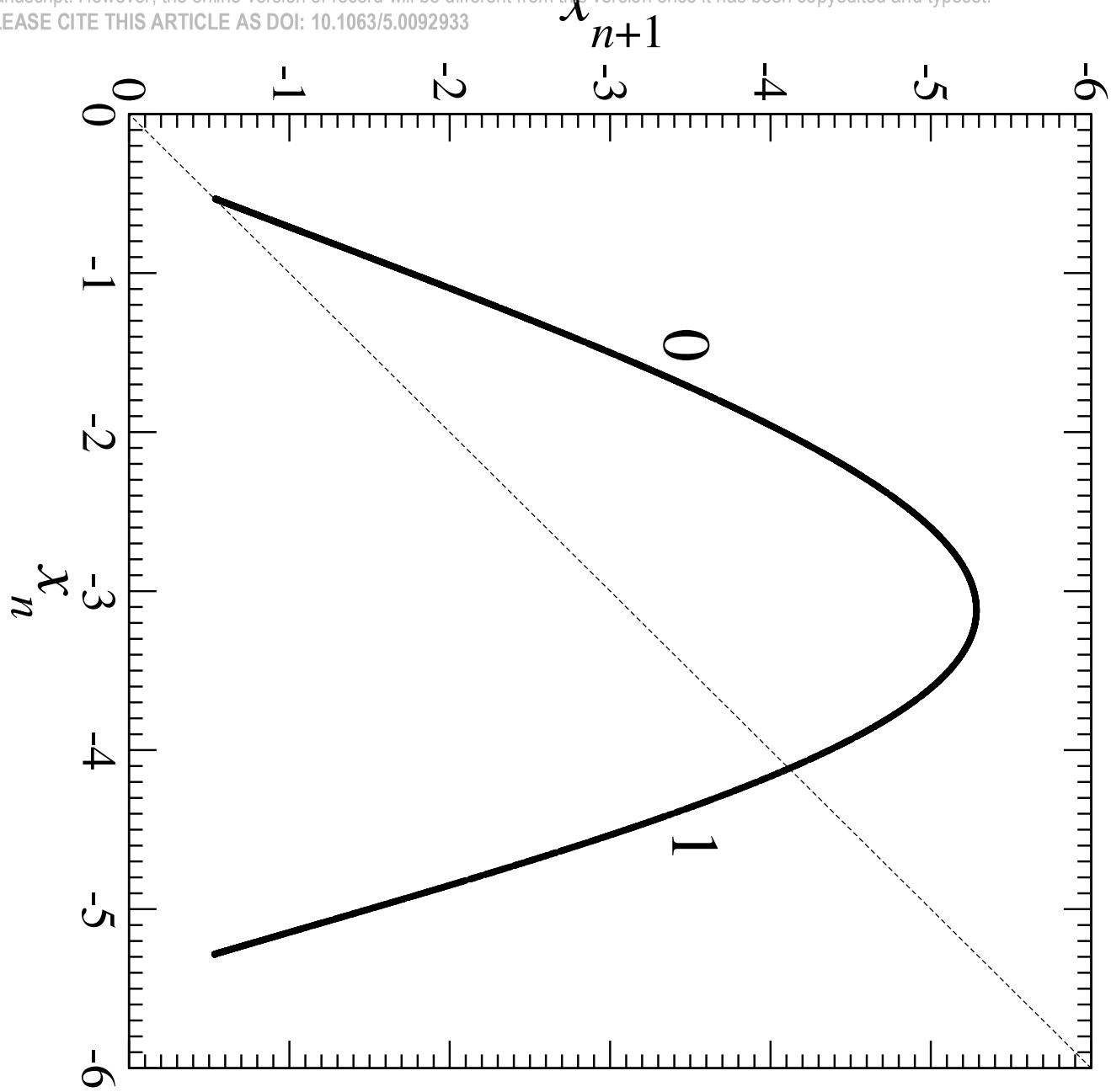

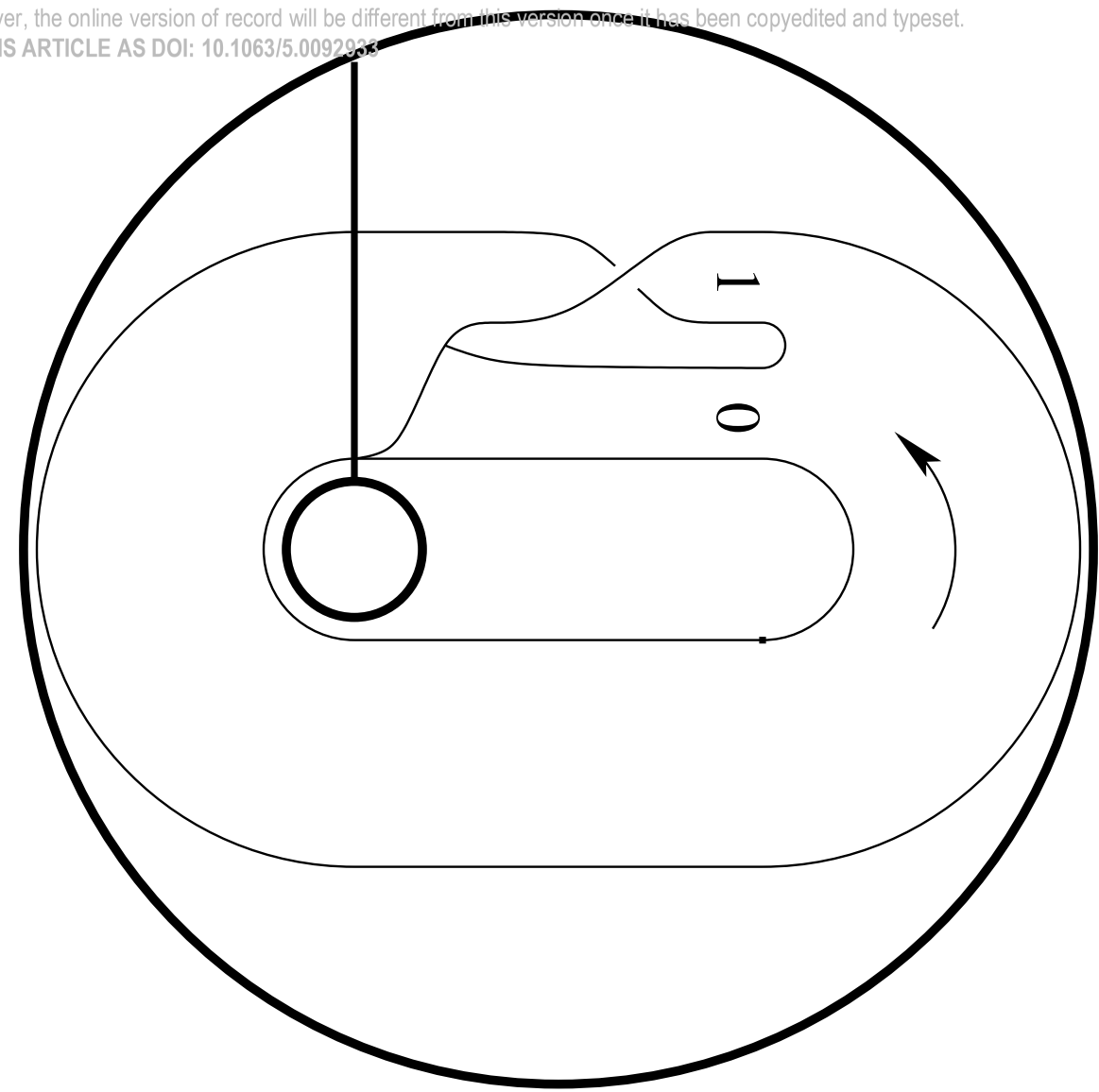

PLEASE CITE THIS ARTICLE AS DOI: 10.1063/5.0092933

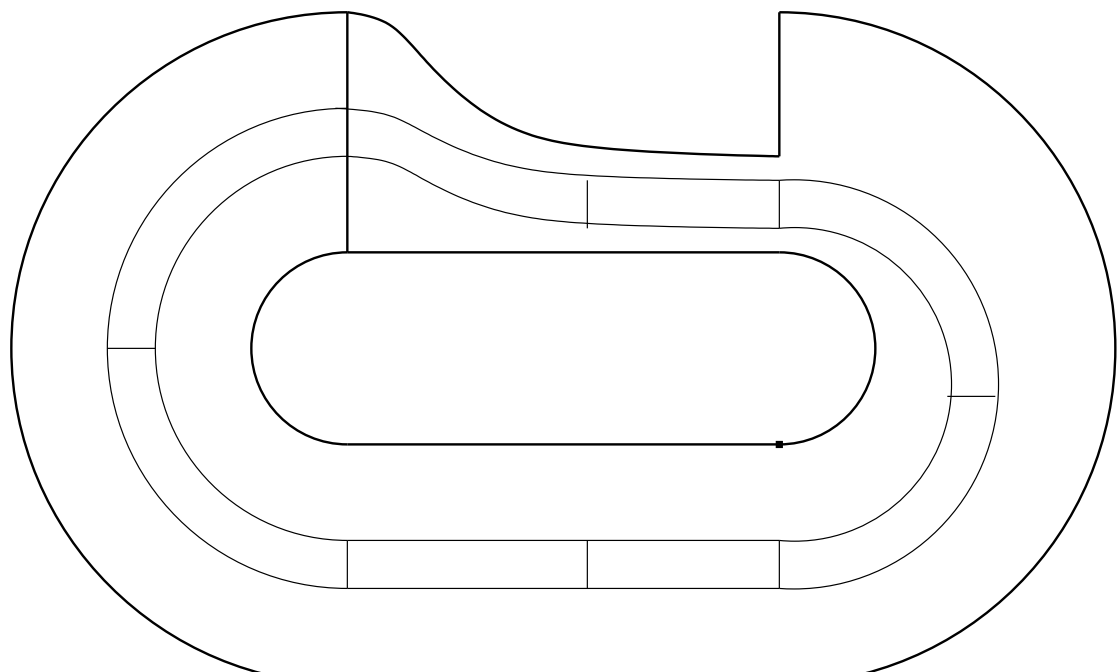

PLEASE CITE THIS ARTICLE AS DOI: 10.1063/5.0092933

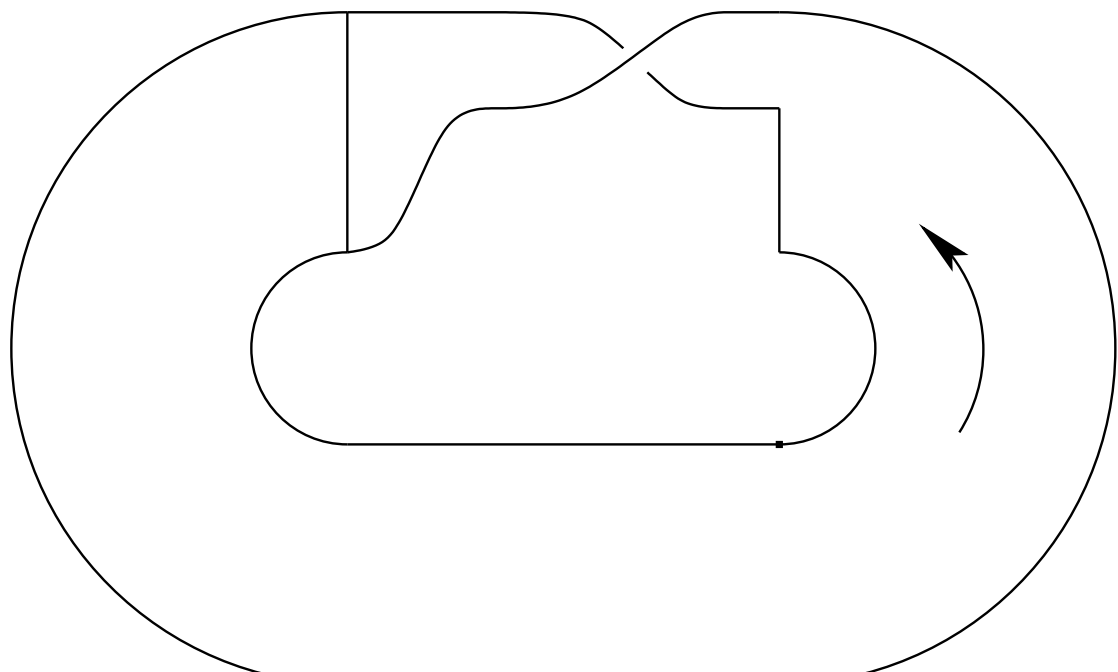

Chaos

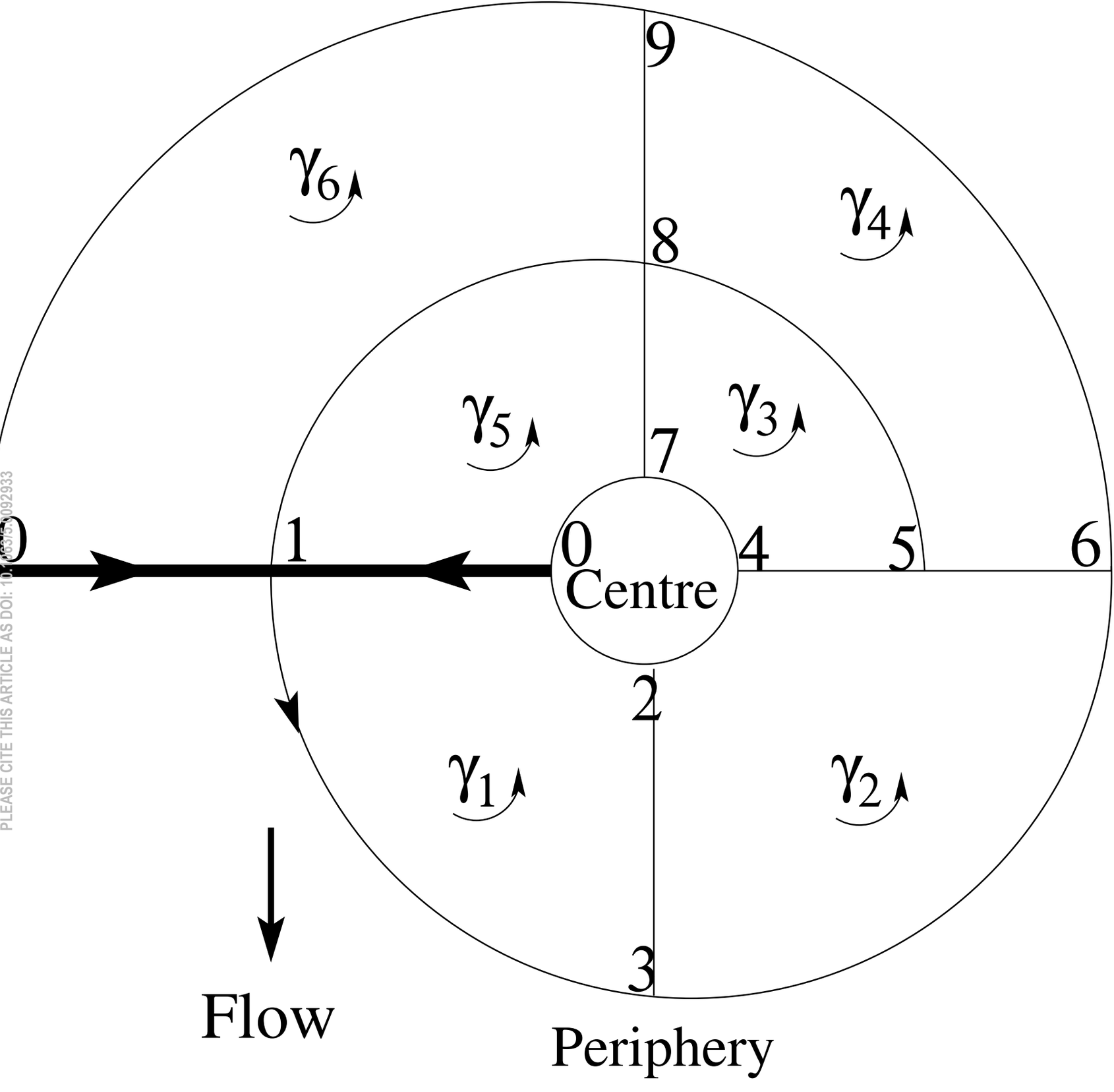

PLEASE CITE THIS ARTICLE AS DOI: 10.1063/5.0092933

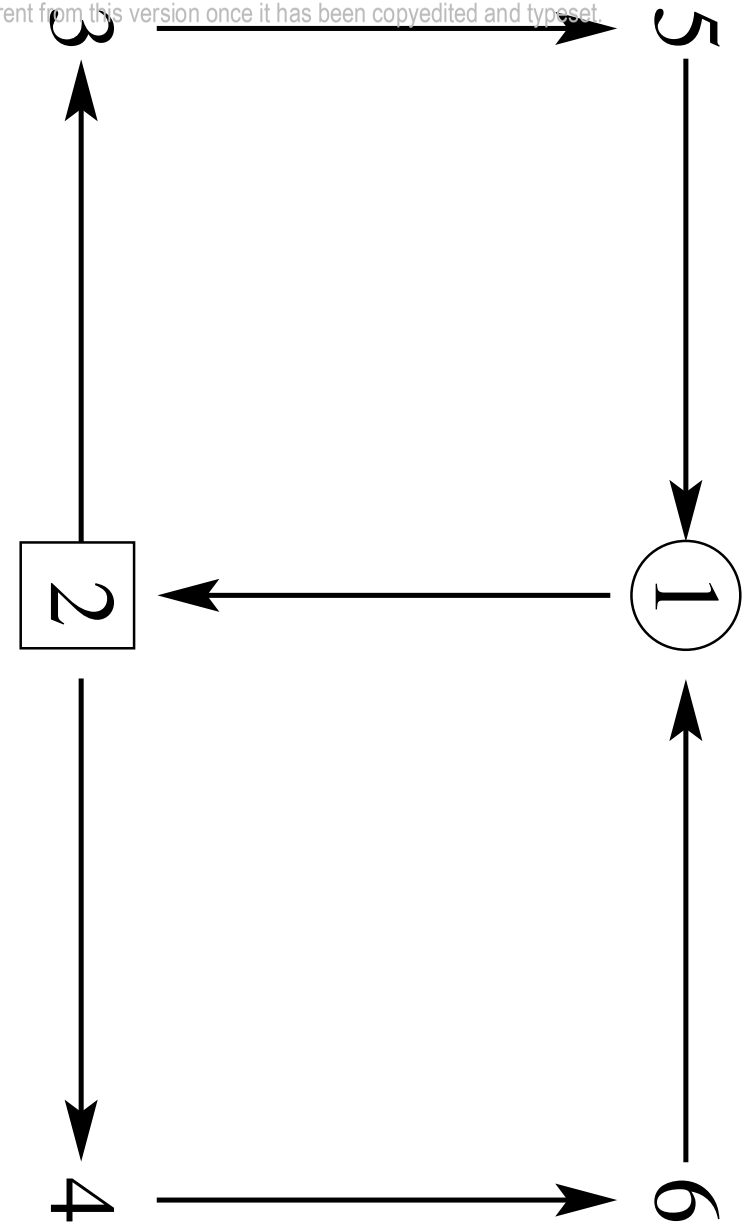

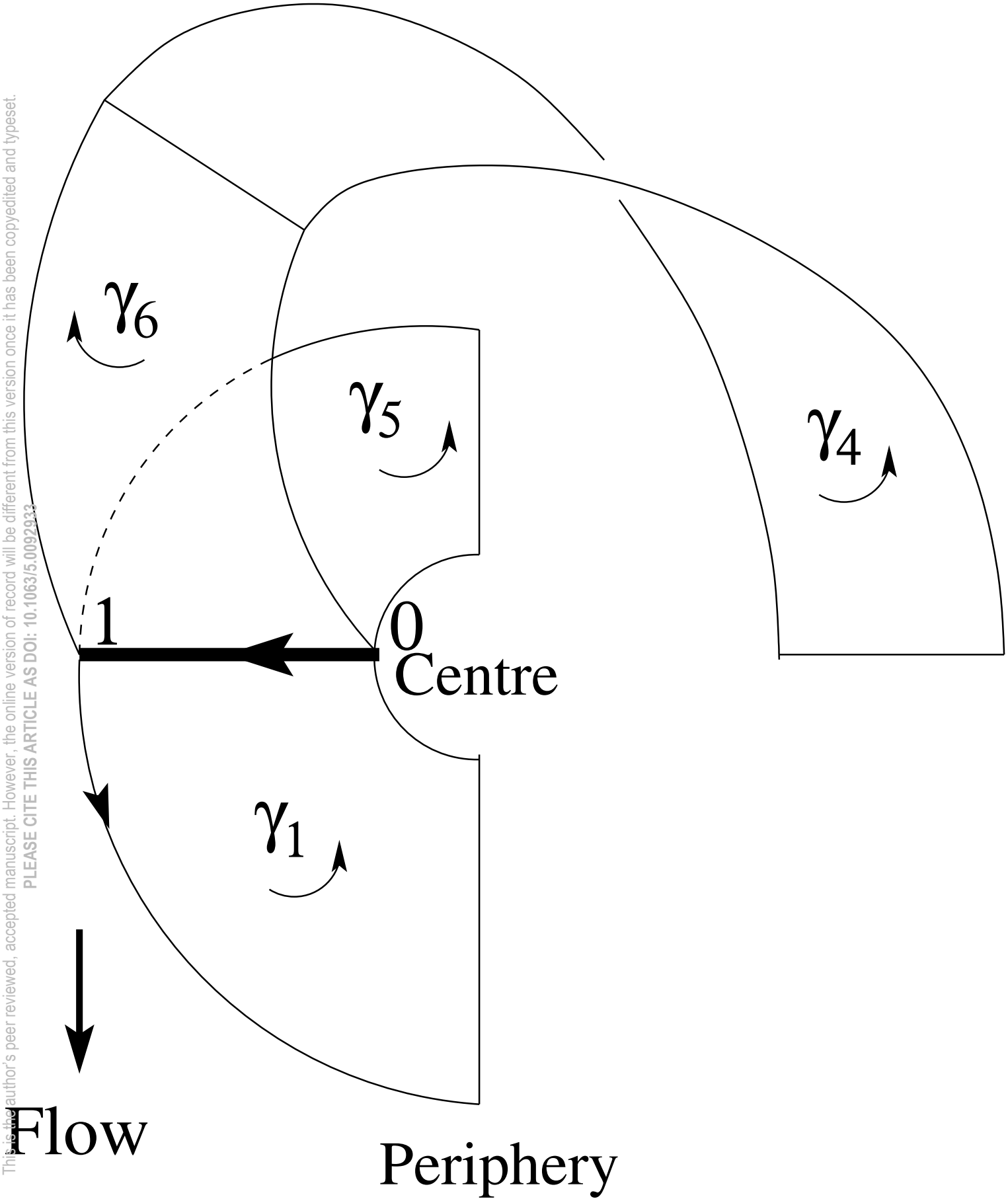

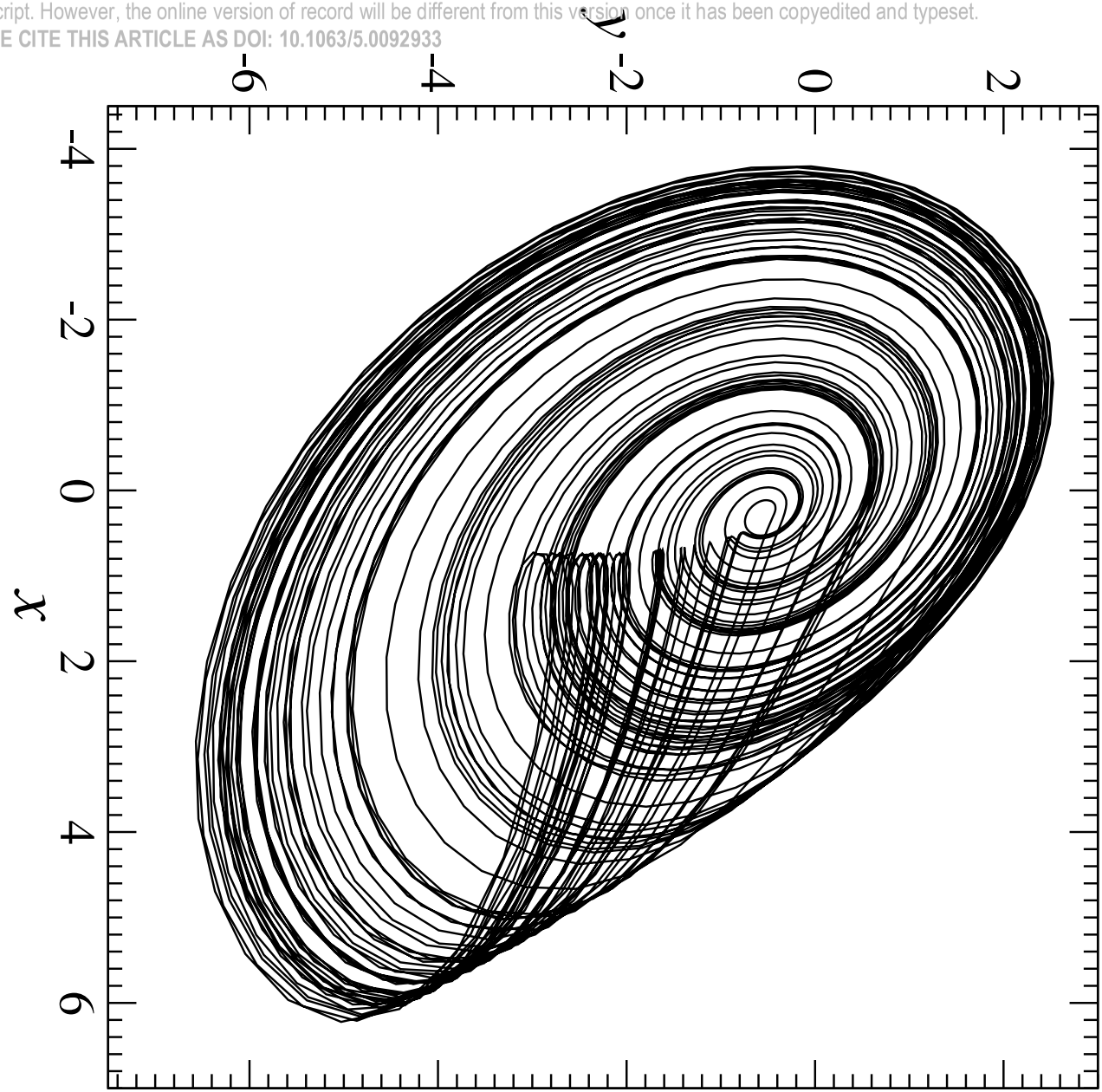

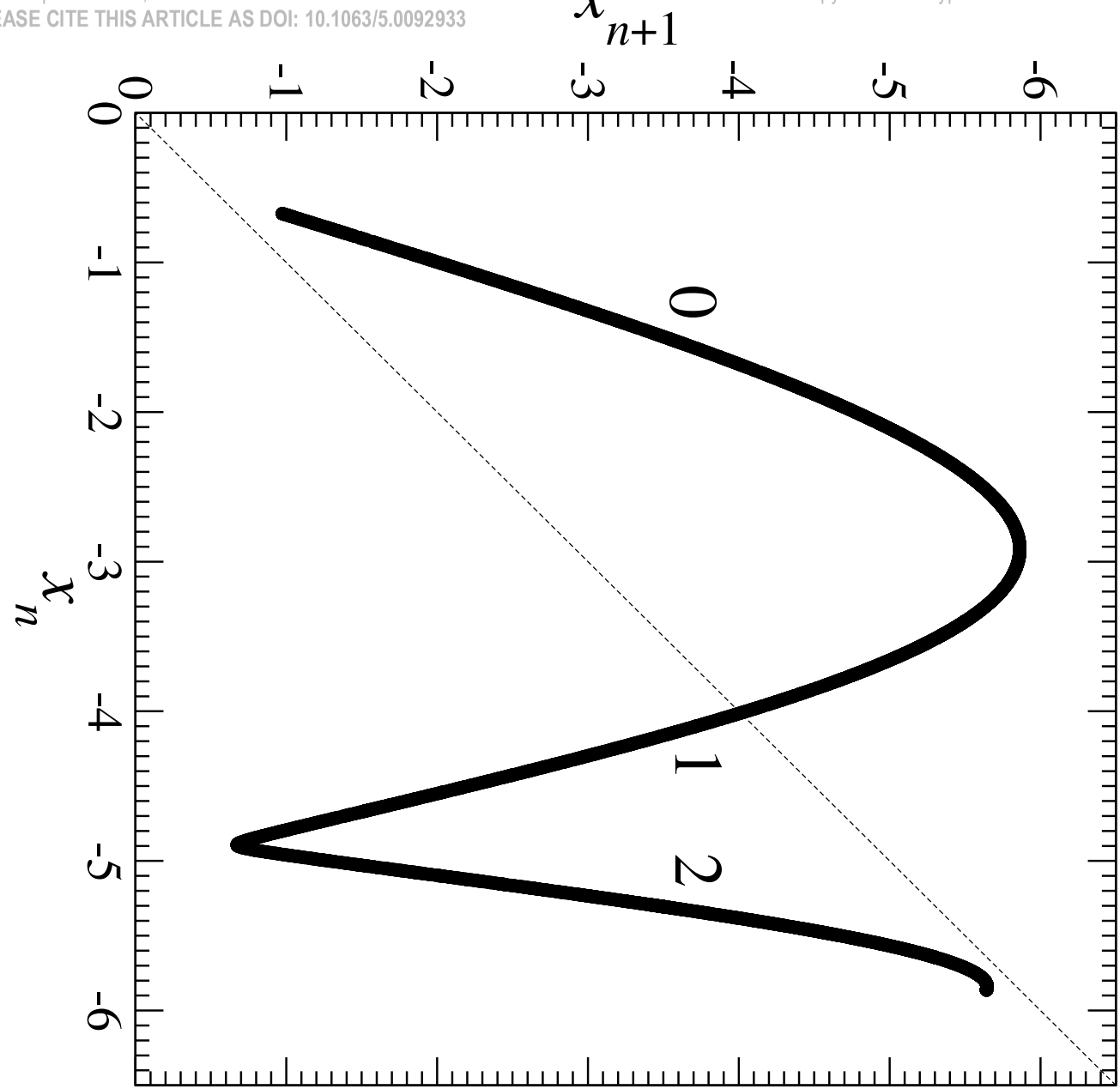

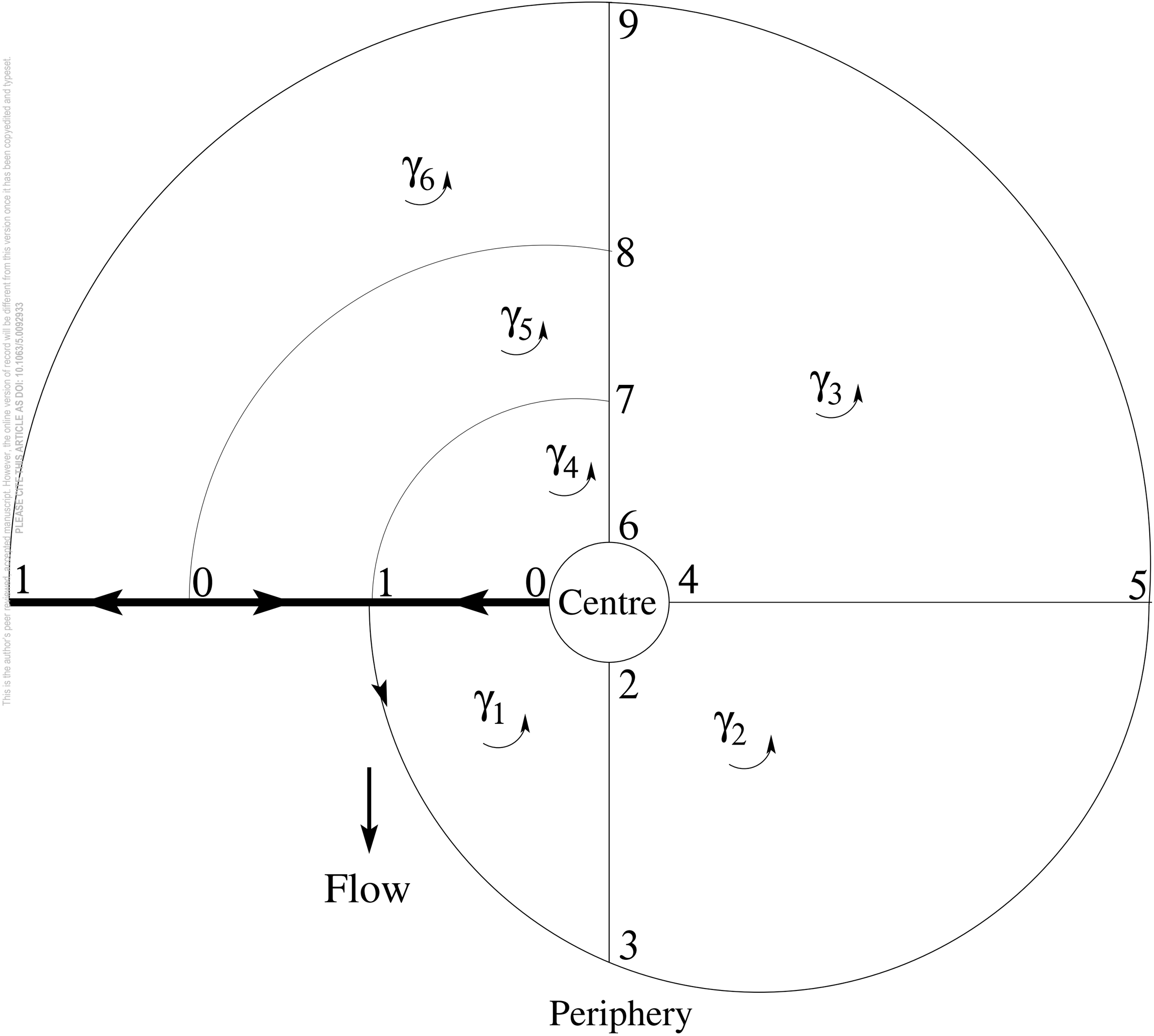

PLEASE CITE THIS ARTICLE AS DOI: 10.1063/5.0092933

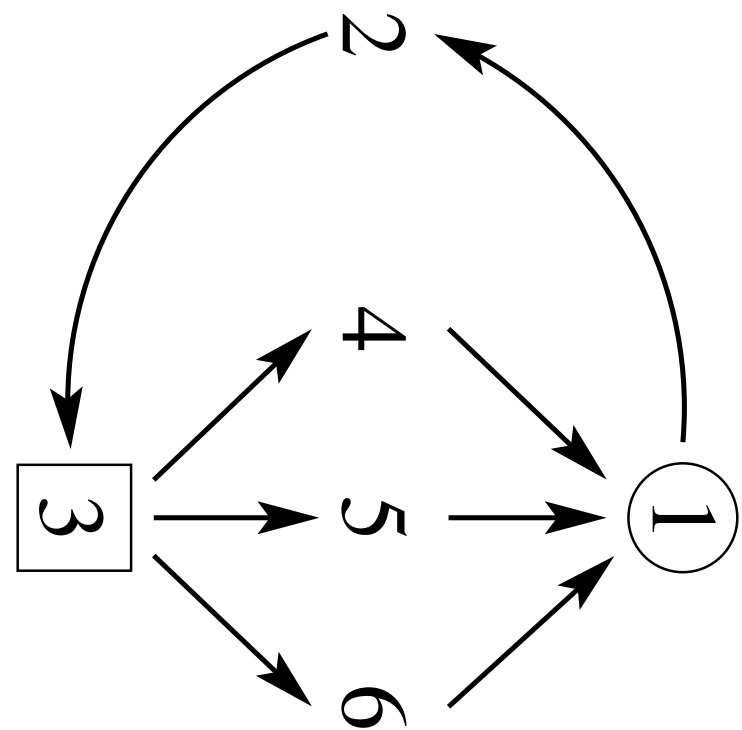

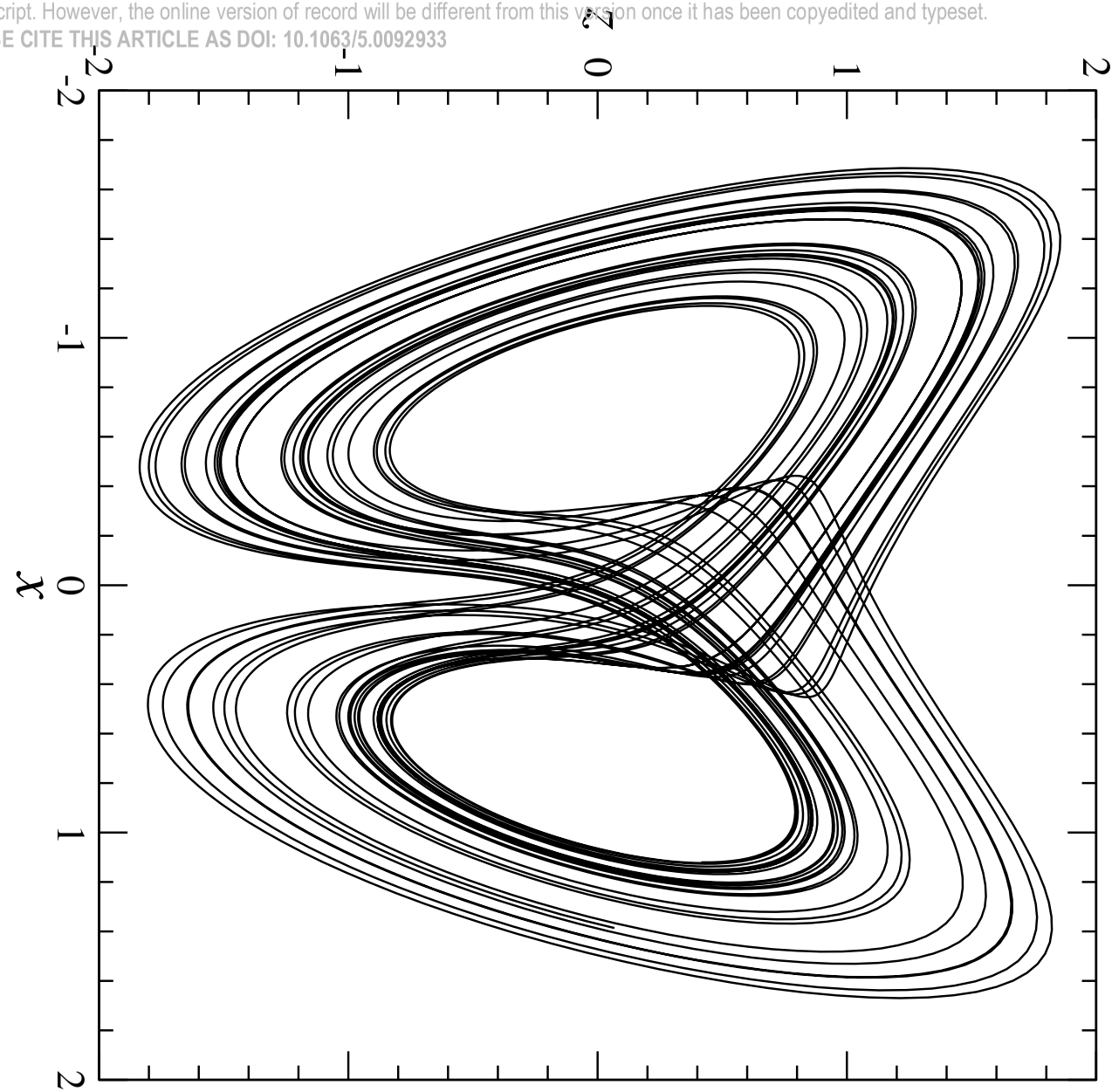

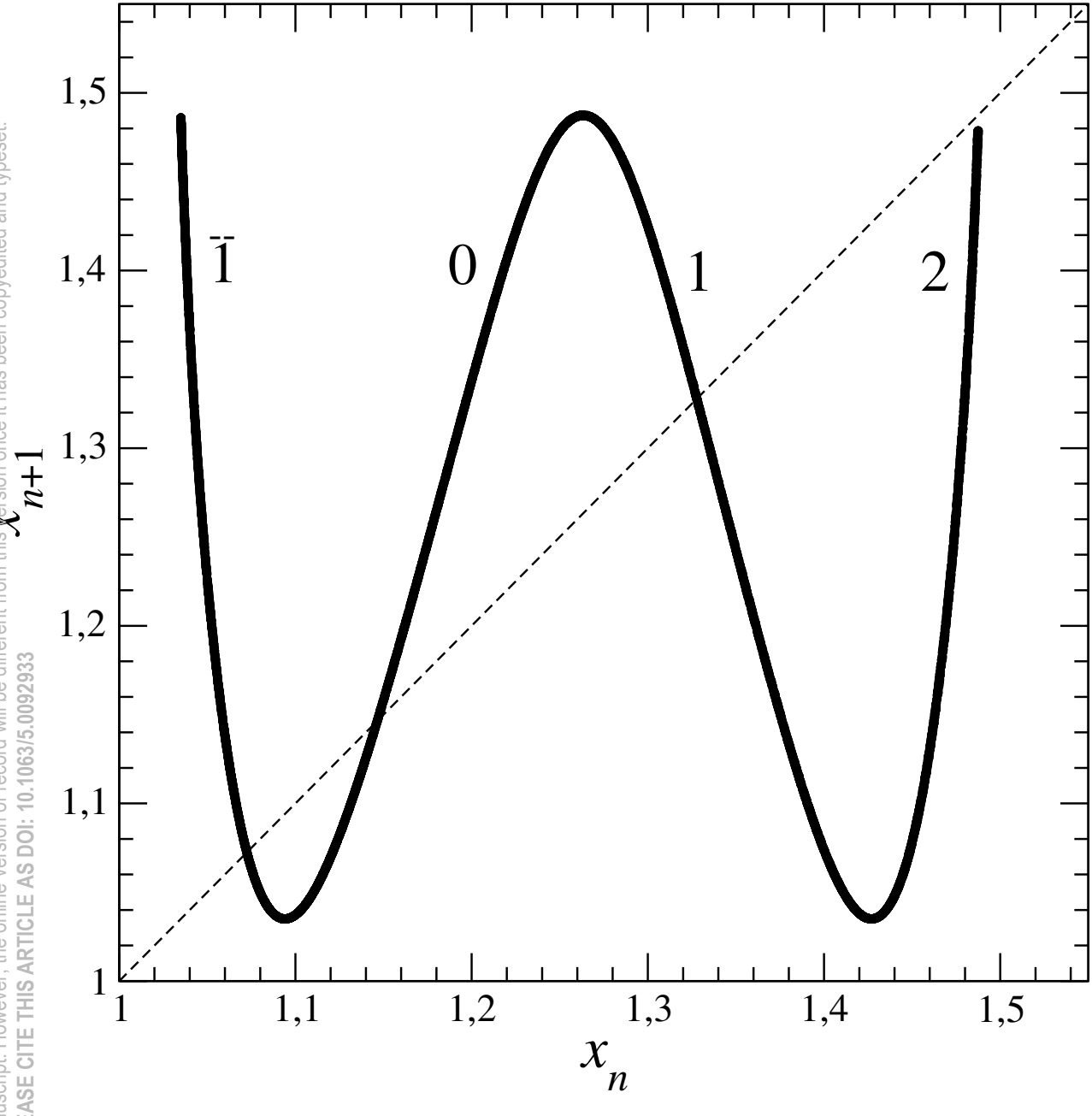

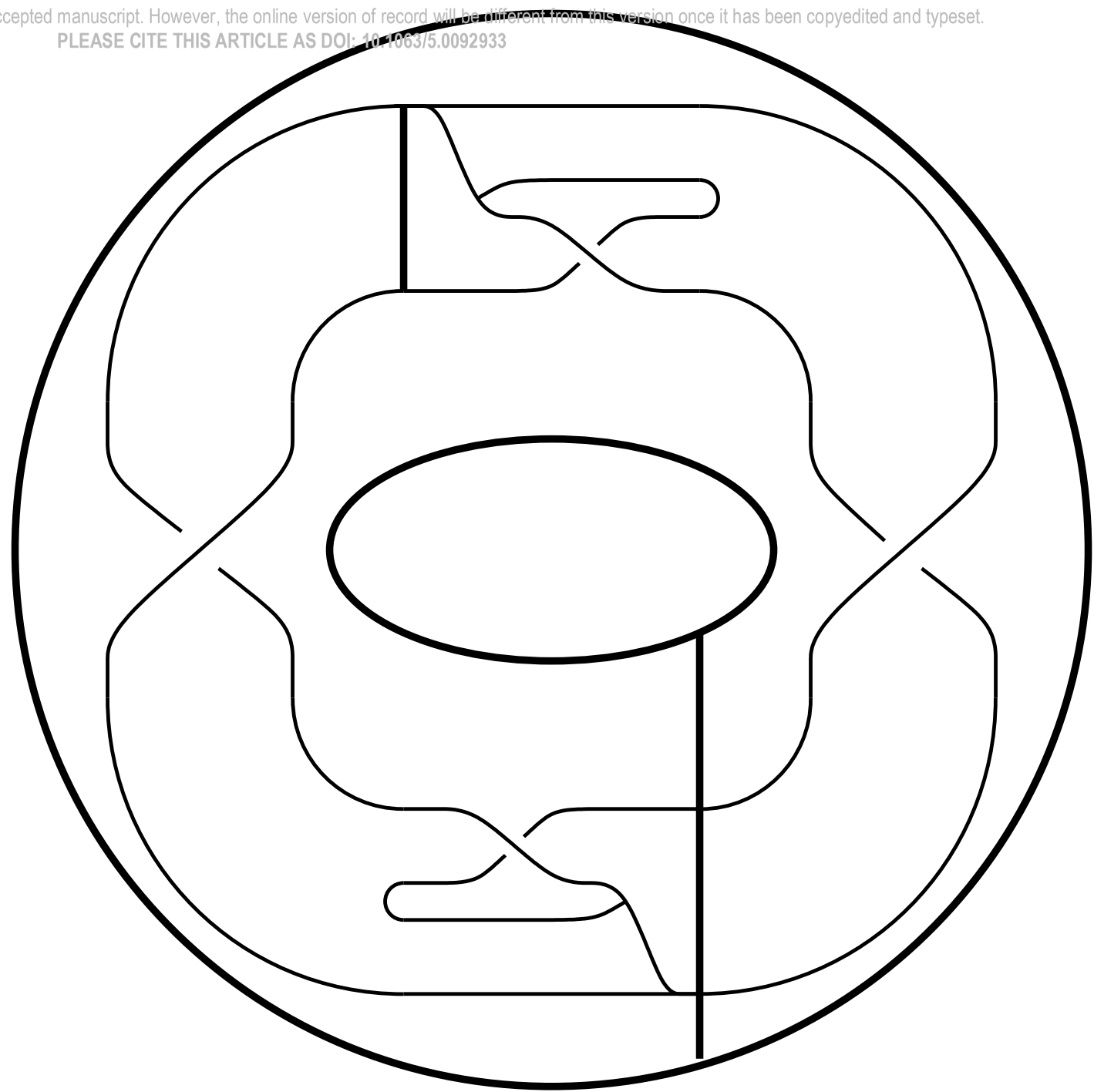

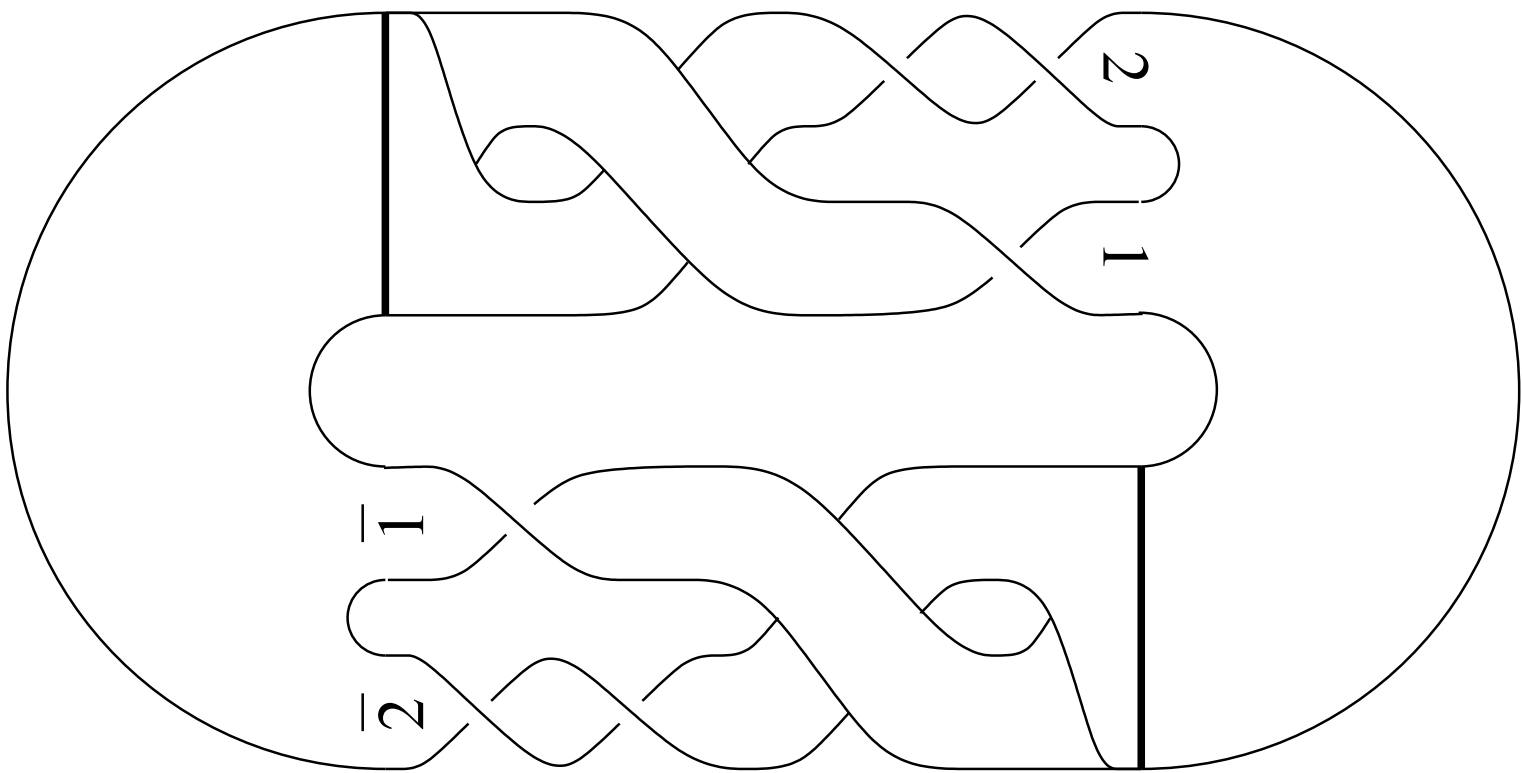

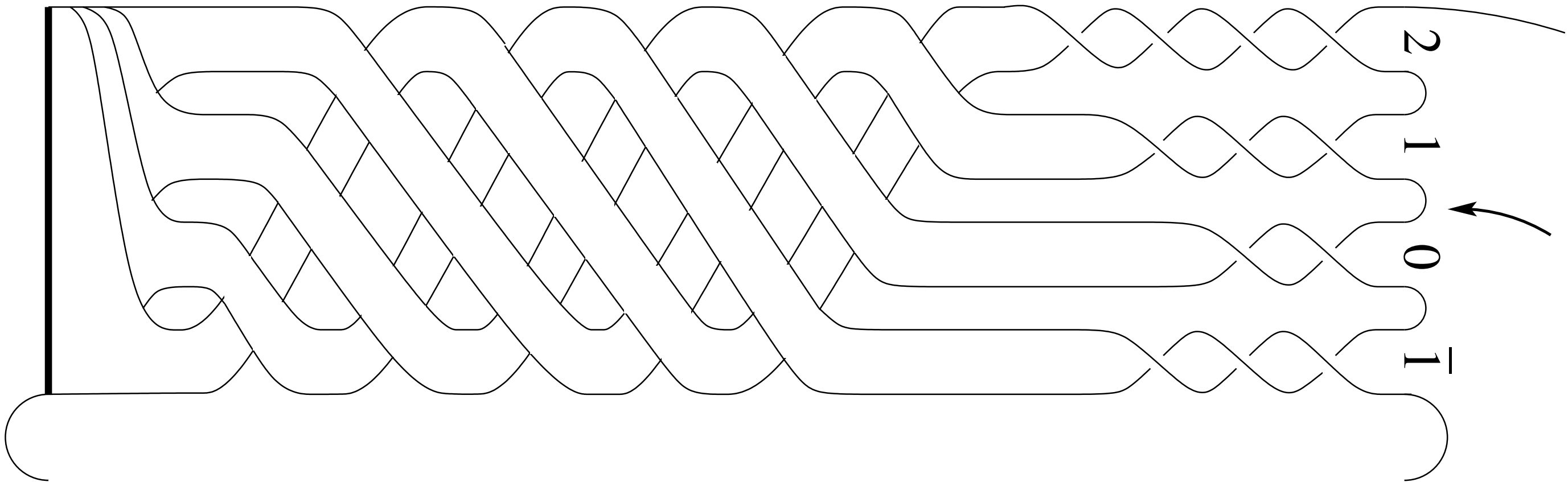

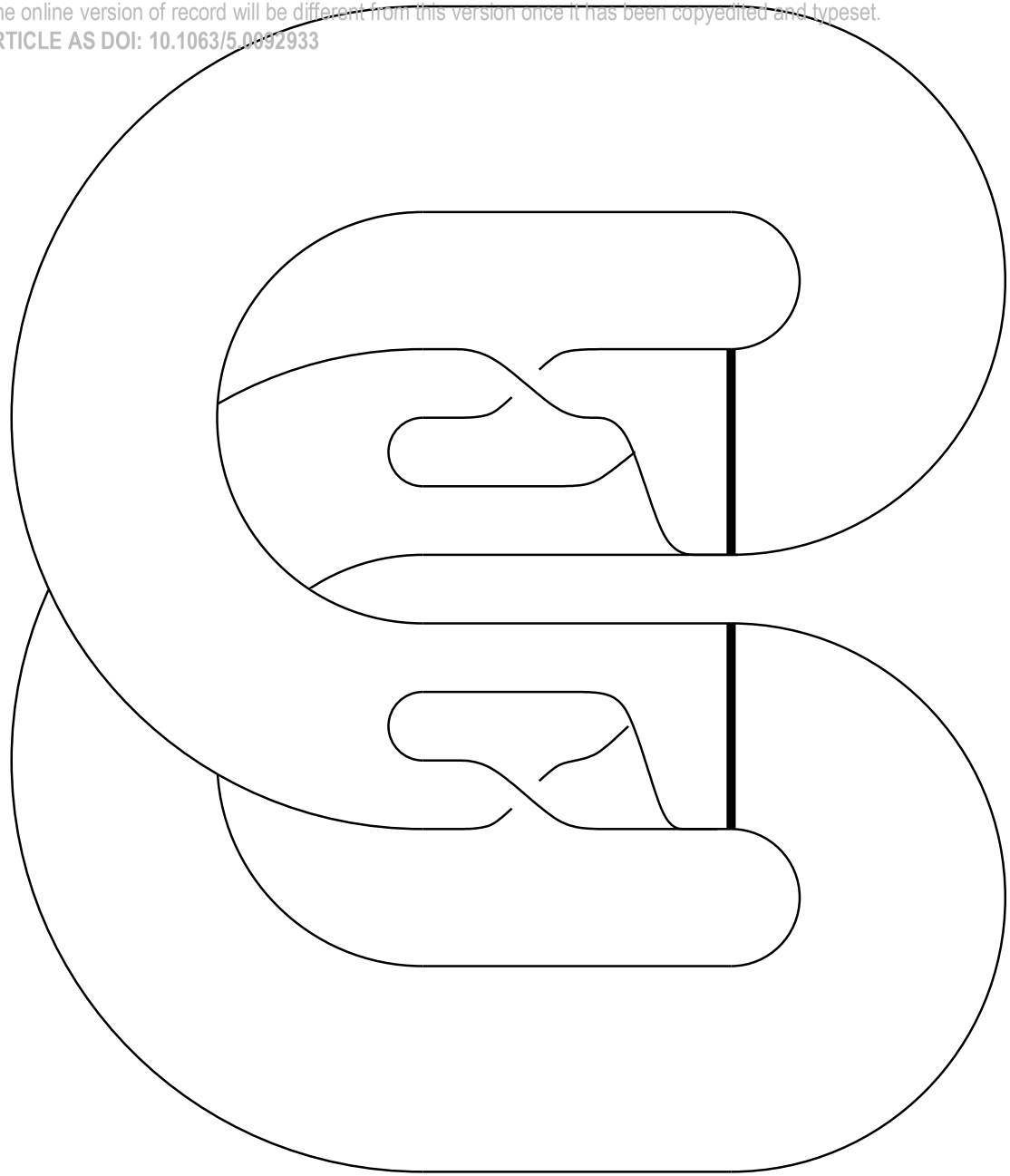

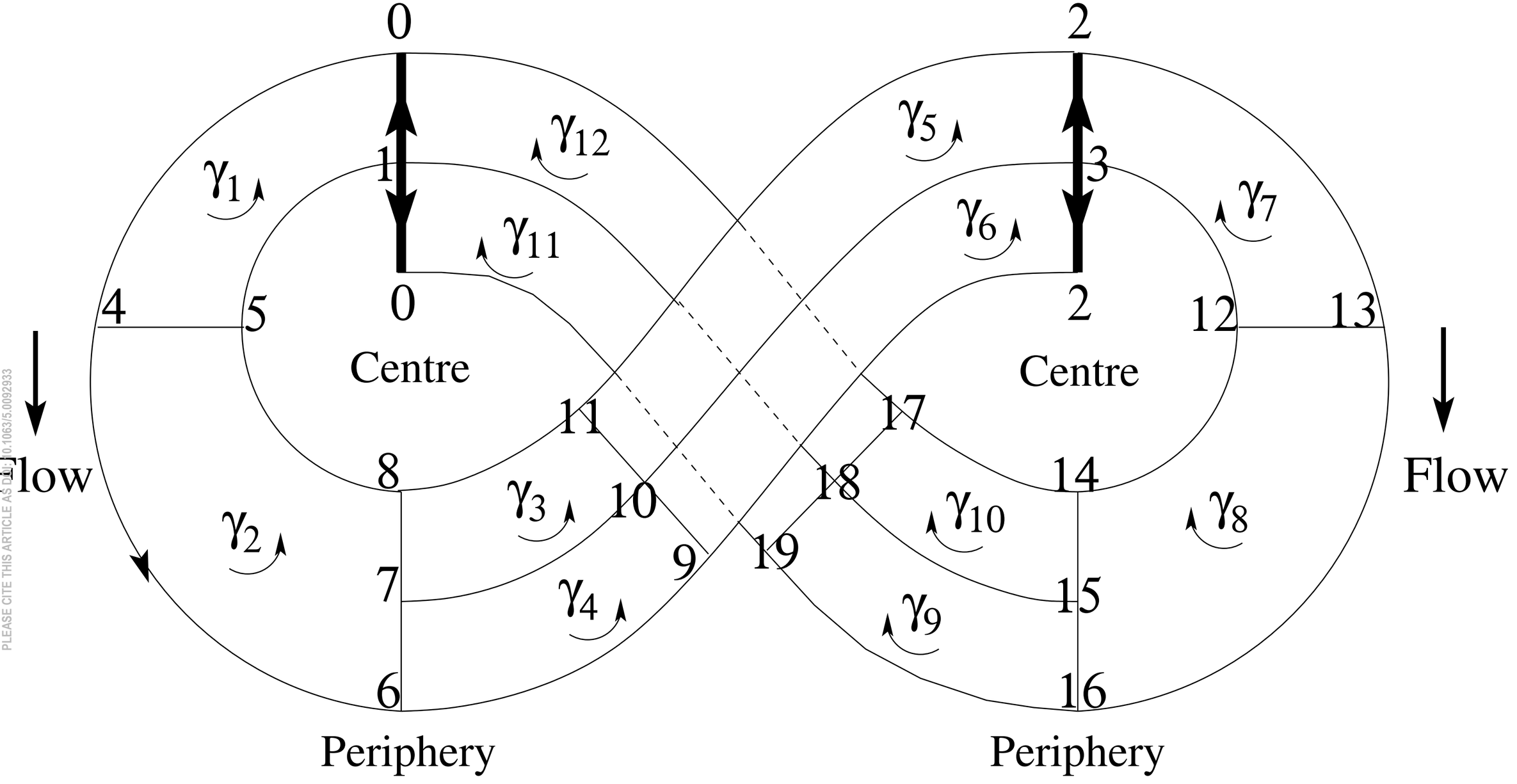

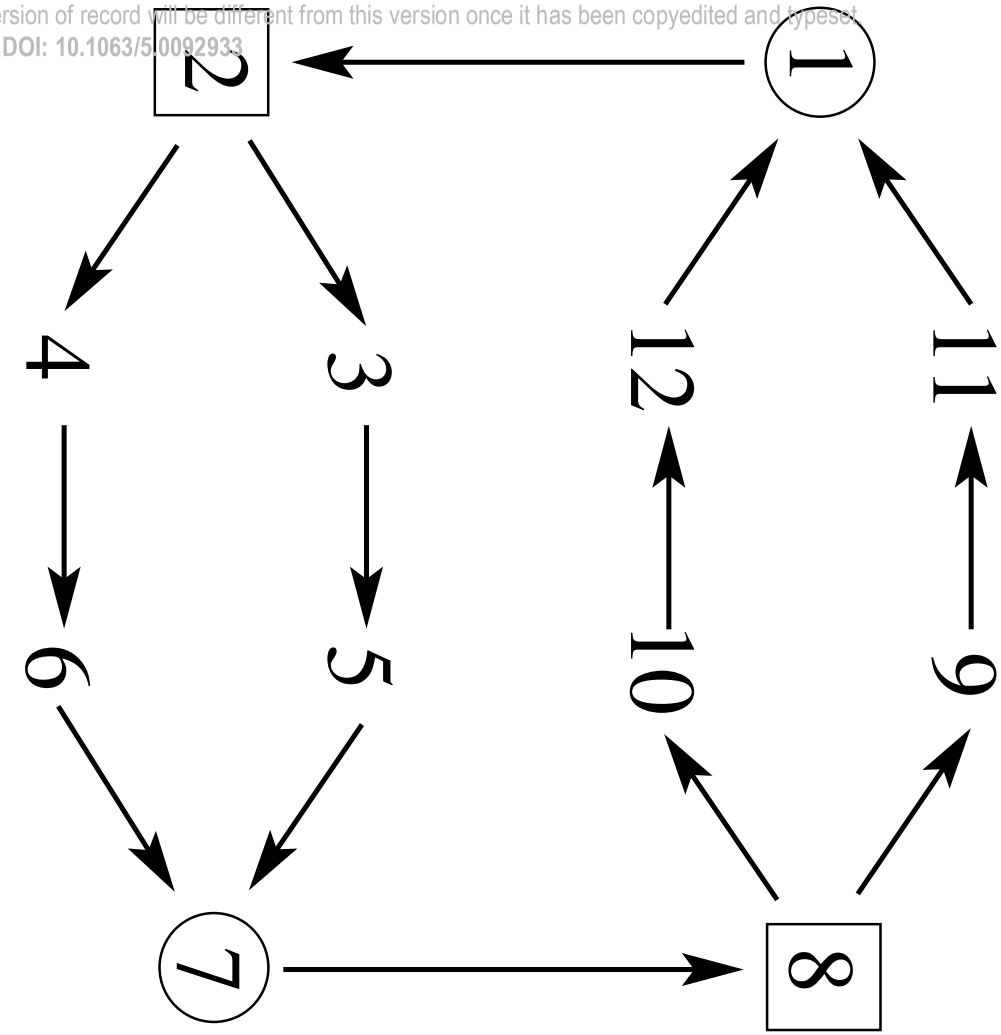

PLEASE CITE THIS ARTICLE AS DOI: 10.1063/5.0092933

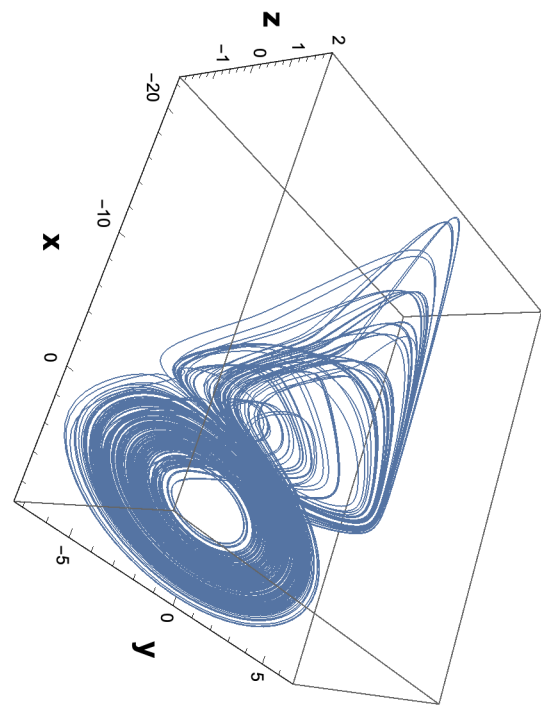

PLEASE CITE THIS ARTICLE AS DOI: 10.1063/5.0092933

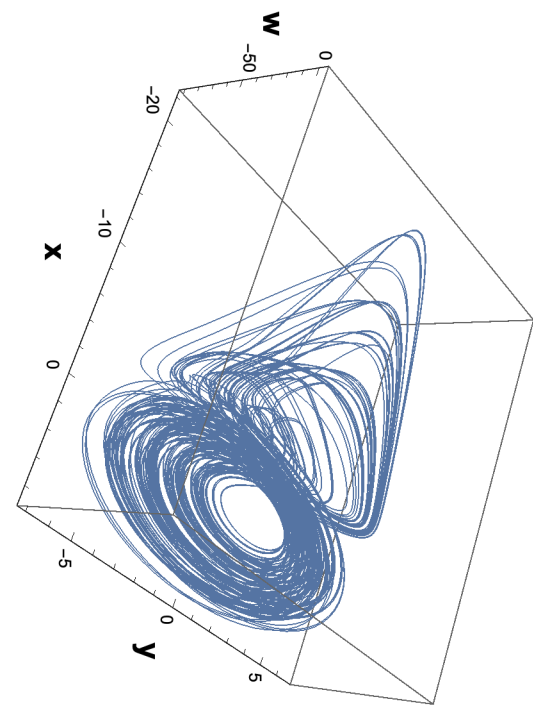

PLEASE CITE THIS ARTICLE AS DOI: 10.1063/5.0092933

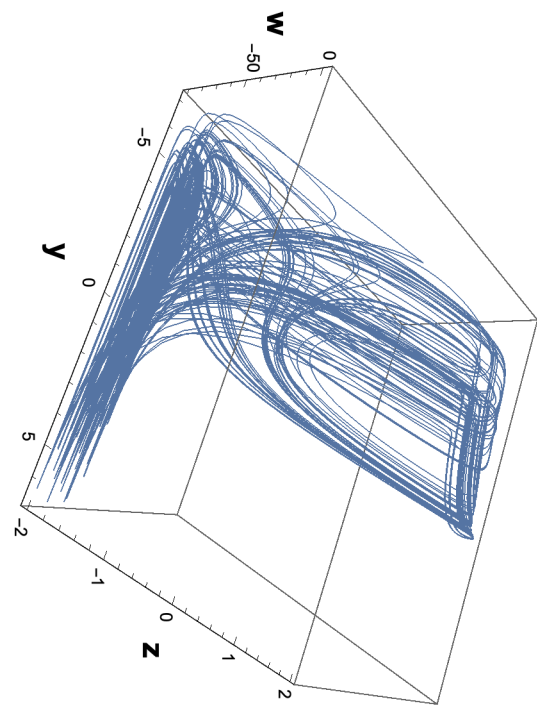

PLEASE CITE THIS ARTICLE AS DOI: 10.1063/5.0092933

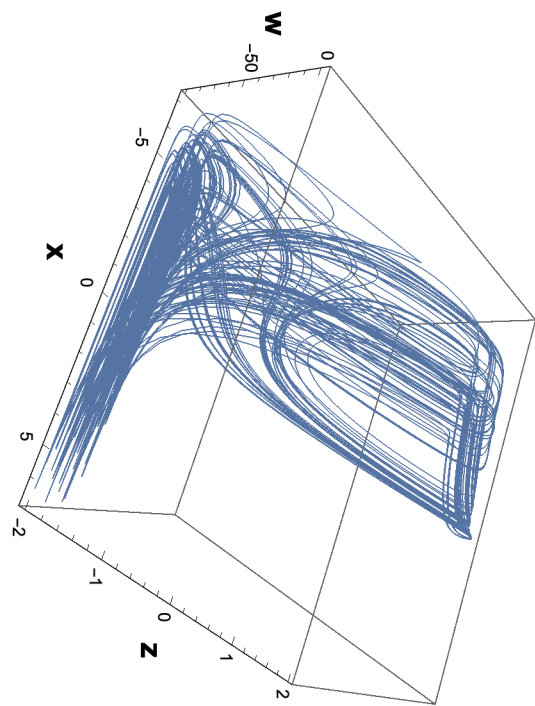

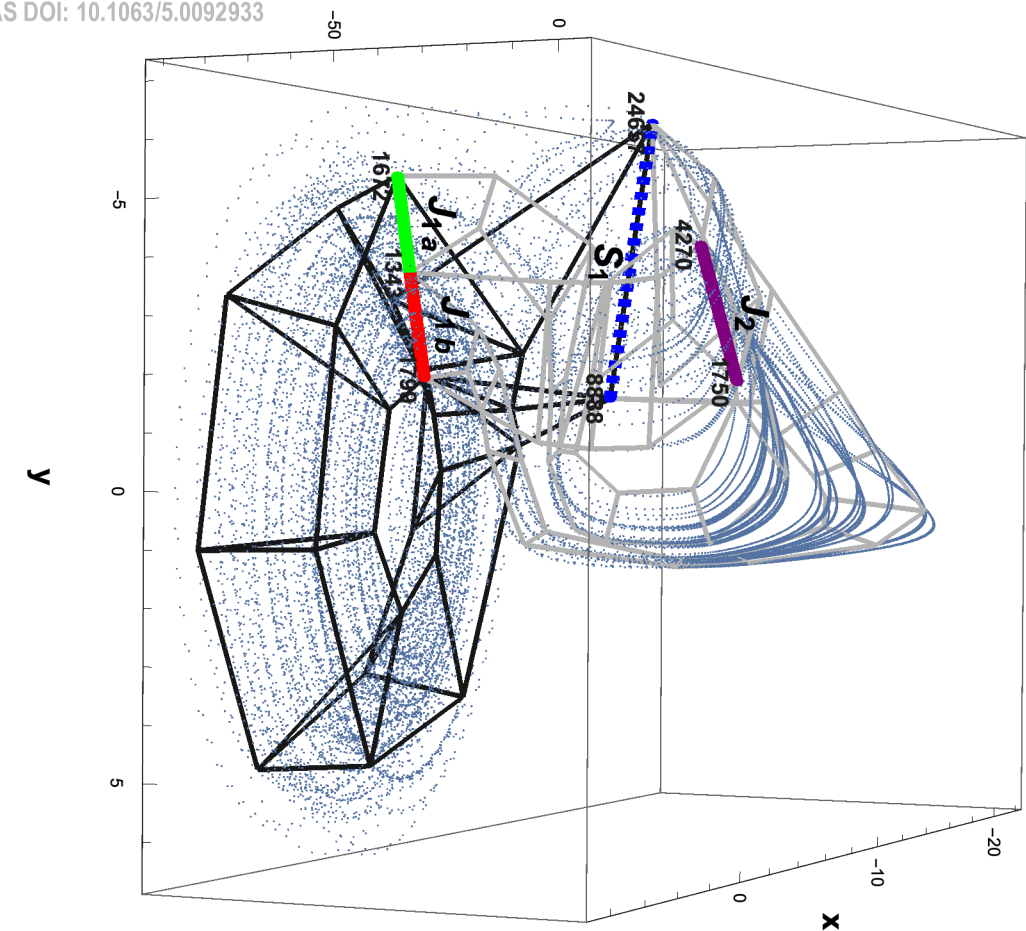

Chaos

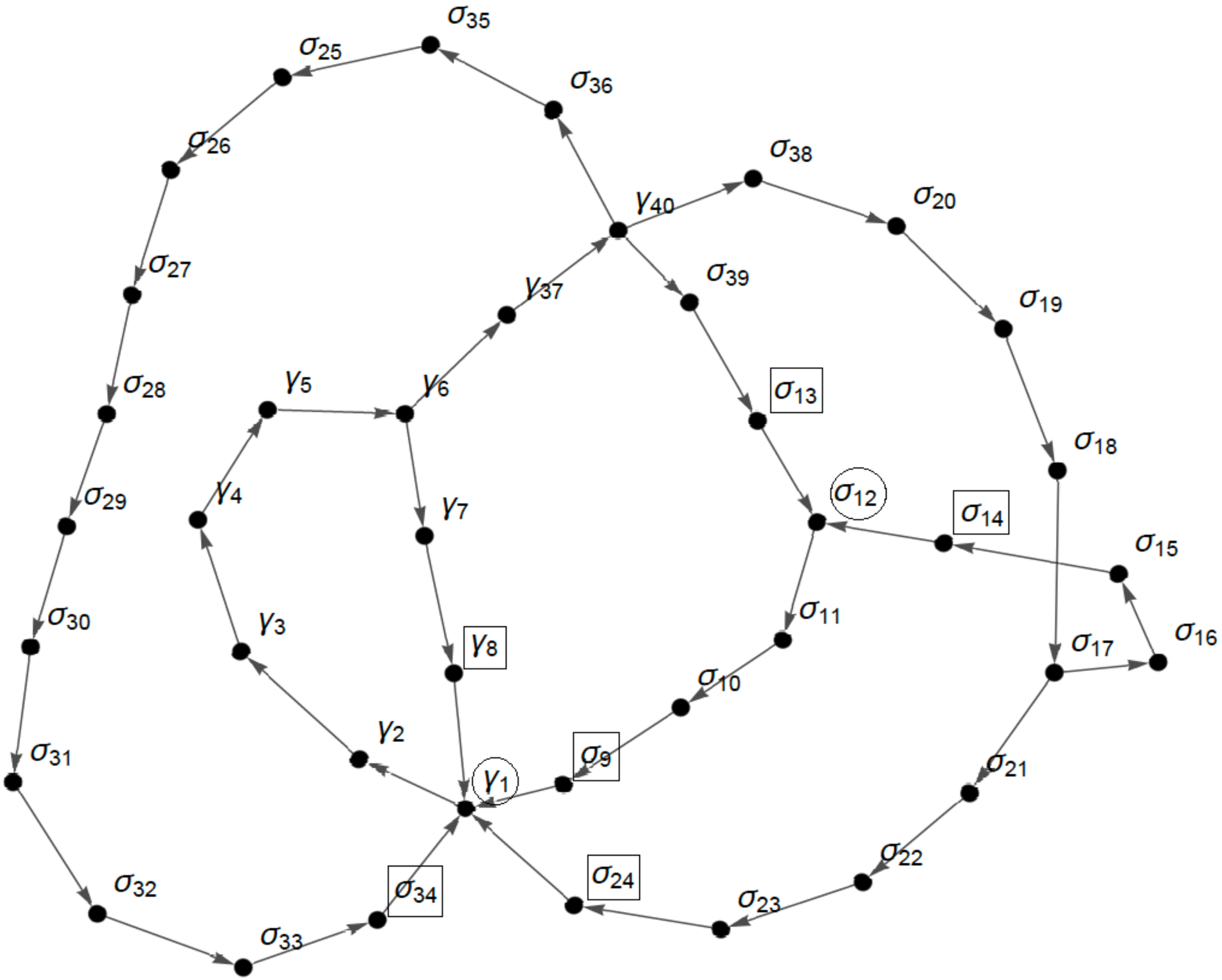

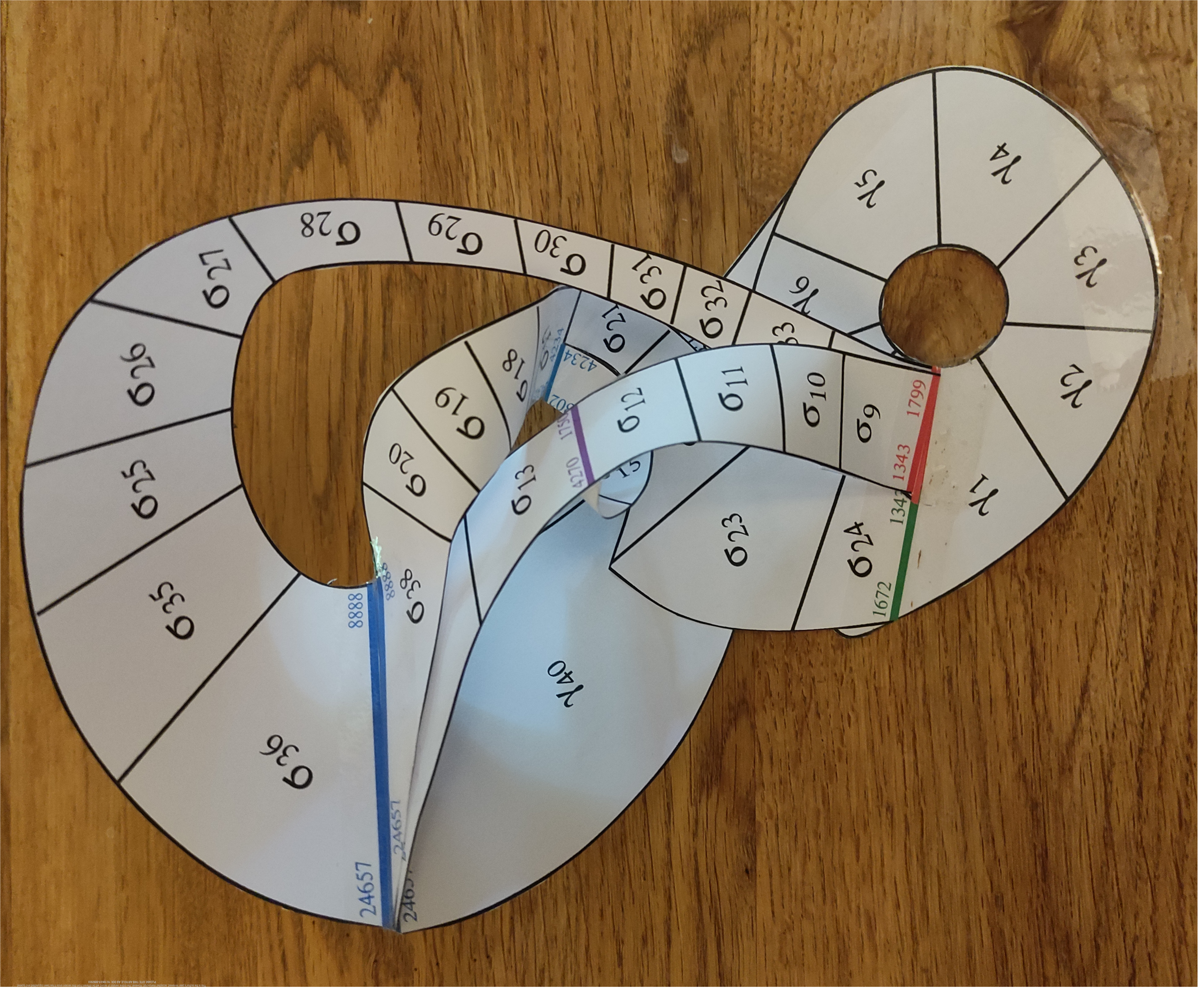

PLEASE CITE THIS ARTICLE AS DOI: 10.1063/5.0092933

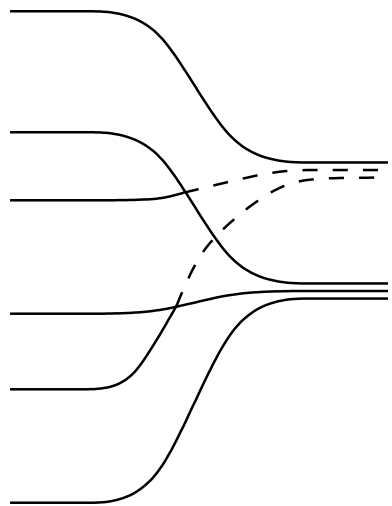

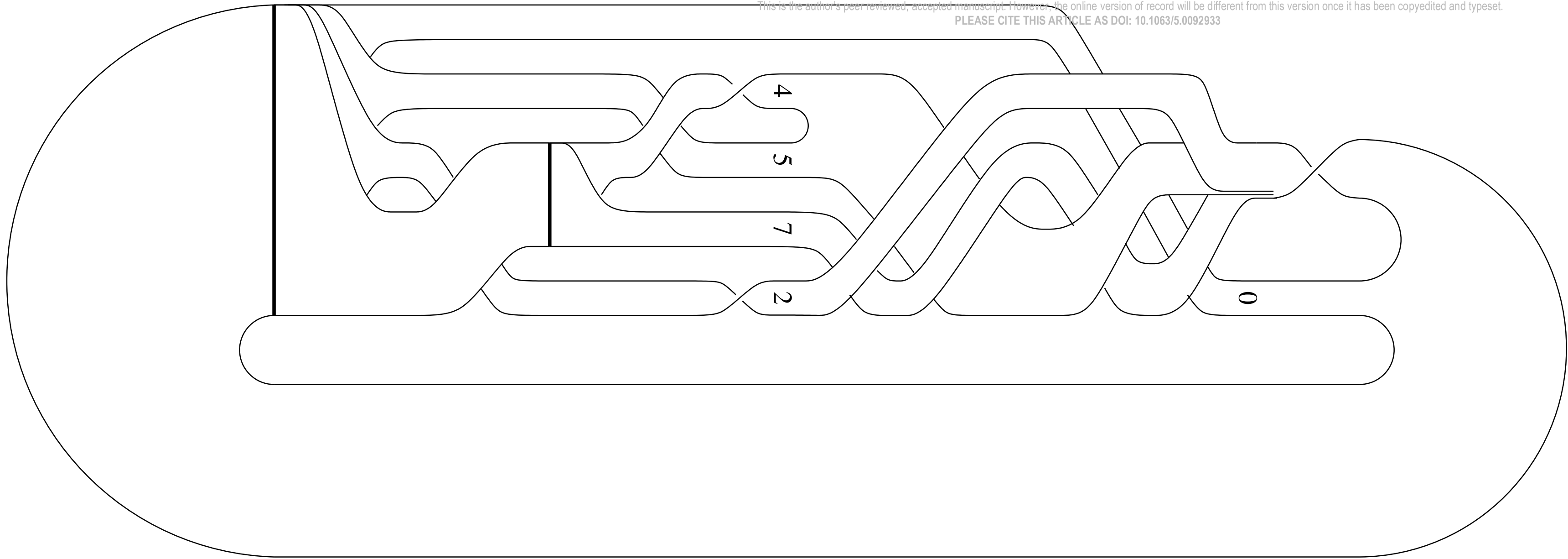

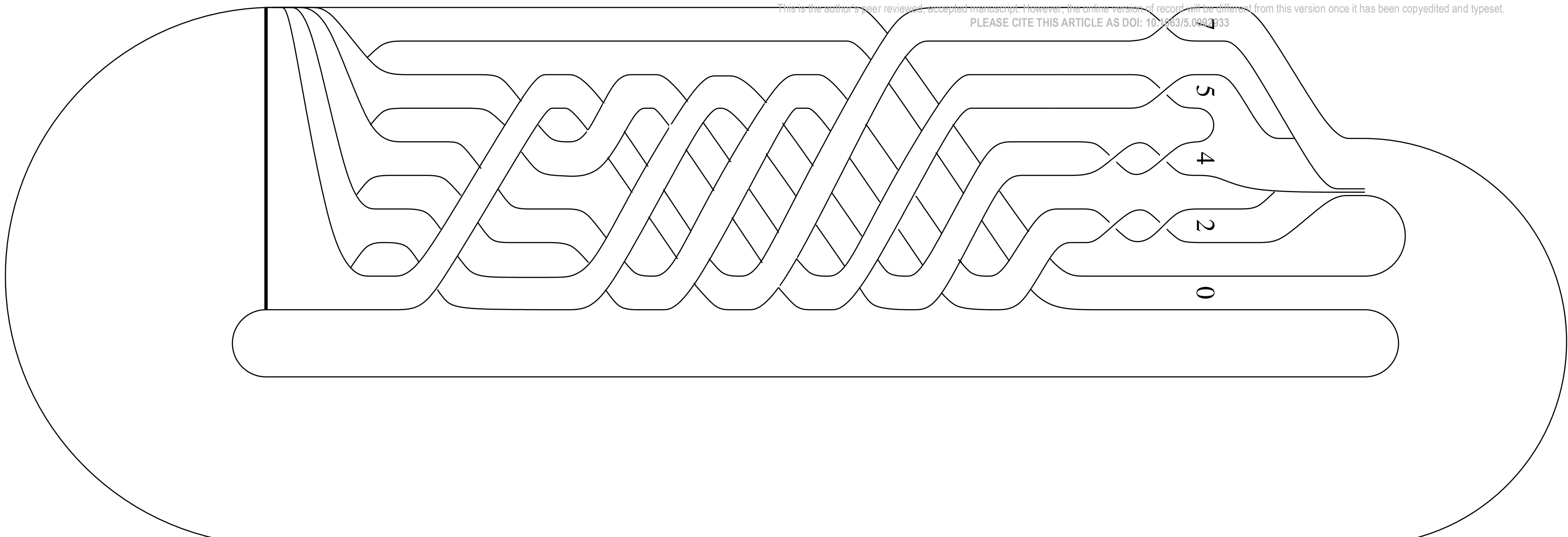

PLEASE CITE THIS ARTICLE AS DOI: 10.1063/5.0092933